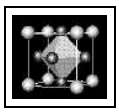

F.H.B. Mertins

Perovskite-type ceramic membranes

Partial oxidation of methane in a catalytic membrane reactor

March 15, 2005

Promotion committee

Chairman:	
Prof.dr. D. Feil	Unversity of Twente
Promotor:	
Prof.dr.ing. D.H.A. Blank	University of Twente
Assistant promotor:	
Dr. H.J.M. Bouwmeester	University of Twente
Referee:	
Dr.ir. R. Bredesen	SINTEF Materials Technology
Ir. P.P.A.C. Pex	Energieonderzoek Centrum Nederland
Members:	
Prof.dr. L. Leffers	University of Twente
Prof.dr. J.A.M. Kuipers	University of Twente
Prof.dr. J. Schoonman	University of Delft

The author would like to thank the *Netherlands Organisation for Scientific research* (NWO), *Shell Global Solutions International* and the *Dutch Ministries of Economic Affairs* (EZ/Senter) and of *Environmental Affairs* for their financial support (Grant No. 99612) in the framework of the research programme **"Towards Sustainable Technologies"**.

Perovskite-type ceramic membranes

Partial oxidation of methane in a catalytic membrane reactor

ISBN 90-365-2167-X

Printed in the Netherlands by **Febodruk BV**

Cover design by Julien Pleis (julienpleis@hotmail.com)

PEROVSKITE-TYPE CERAMIC MEMBRANES

PARTIAL OXIDATION OF METHANE

IN A CATALYTIC MEMBRANE REACTOR

DISSERTATION

to obtain
the doctor's degree at the University of Twente,
under the authority of the rector magnificus,
prof.dr. W.H.M. Zijm,
on account of the decision of the graduation committee,
to be publicly defended
on Thursday, March 17^{th} 2005, at 16.45 hrs.

by

Frédéric Henri Bertrand Mertins
born on September 15^{th}, 1976
in Strasbourg, France

This dissertation is approved by the promotor Prof.dr.ing. D.H.A. Blank

and the assistant promotor Dr. H.J.M.Bouwmeester

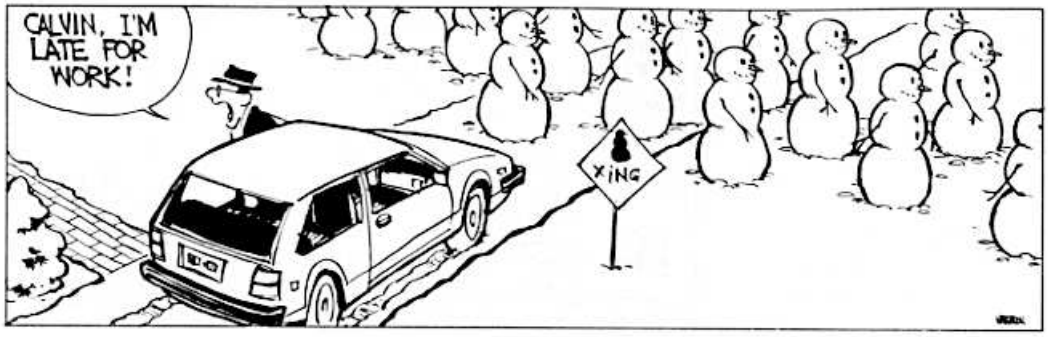
CALVIN, I'M LATE FOR WORK!
XING

Table of Contents

Part I

Preamble

Summary

The application of mixed ionic and electronic conductors as oxygen separating membranes offer an attractive alternative for the production of synthesis gas from methane when compared with traditional reforming. Materials with the perovskite structure are the most promising candidates thanks to the ease of tuning their electro-chemical properties with appropriate doping. A number of issues has to be addressed before any industrial breakthrough. The features of interest when using these materials in membrane reactor technology are the magnitude of the oxygen flux (proportional to the oxygen vacancies concentration) and the thermodynamical stability.
In *Chapter 2*, the ionic conductivity of a series of materials with composition $La_{1-x}Sr_xCoO_{3-\delta}$ with $0.1 \leq x \leq 0.7$ was determined via oxygen permeation measurements as a function of the oxygen partial pressure. It was shown that the ionic conductivity in this series of materials varies almost linearly with the concentration of oxygen vacancies. For small concentration of strontium ($x = 0.1$) the expected values are in good agreement with the theory. At higher doping levels, local discrepancies are found. It is suggested that the presence of a stagnant layer on the permeate side of the membrane is the cause for the local disagreement between the experimental and the expected values. The influence of oxygen vacancies interactions is thought to be significant at lower temperatures.
In *Chapter 3*, different materials with a perovskite composition were tested for syngas generation. The influence of a number of dopants on both the A- and B-site of the ABO_3-perovskite structure was investigated. Substitution with barium and chromium were found to limit the magnitude of the oxygen flux. Some materials exhibit a high oxygen flux but the critical issue of their thermodynamic stability make them unsuitable for industrial applications. The best potential candidate found in this study, namely $La_{0.7}Sr_{0.3}Fe_{0.7}Ga_{0.3}O_{3-\delta}$, exhibits a lower oxygen flux than the best performing materials but its stability under the harsh conditions associated with CPO is better.

The stability of this material was investigated further in *Chapter 4*. X-ray diffraction revealed a second phase after synthesis. This second phase seems to be unstable when placed in an oxygen chemical potential gradient as it disappears from the near surface on the low-P_{O_2} side of the membrane after the CPO experiment. X-ray photoelectron spectroscopy combined with X-ray fluorescence showed the enrichment of strontium on the methane side of the membrane and scanning electron microscopy revealed the presence of a dusty-like layer on the surface exposed to the methane stream. An oxygen flux of 5.1 ml.min^{-1}.cm^{-2} was obtained at 900 °C for a membrane thickness of 0.5 mm with a pure methane feed. Evidence that the oxygen transport is partially controlled by the surface reactions was found.
In *Chapter 5*, dense tubular membranes were produced by centrifugal casting of an aqueous suspension, containing powder particles of the mixed-conducting perovskite $La_{0.5}Sr_{0.5}CoO_{3-\delta}$ and a dispersant. The resulting green bodies were dried and sintered to produce tubes with a maximum length of 12 cm, having a relative density higher than 92 %. The particle morphology, the amount of dispersant and its burnout appeared to be of influence to the quality of the final product. Oxygen permeation measurements were conducted in the temperature range 850-950 °C in air/He gradients. Results are found to be consistent with data reported for flat membranes.
In *Chapter 6*, a dense bi-layered membrane concept is proposed as solution to the problem of membrane stability under reducing conditions of operation. A dense thin film of $La_{0.8}Sr_{0.2}FeO_{3-\delta}$ was successfully grown with pulse laser deposition (PLD) on a dense support of $La_{0.3}Sr_{0.7}CoO_{3-\delta}$ and this system was chosen as a proof-of-principle. Under air/He gradients, the oxygen flux of the bi-layered membrane is half of that obtained with an unmodified $La_{0.3}Sr_{0.7}CoO_{3-\delta}$ dense support. Under CPO conditions, the oxygen flux is almost equivalent to that of an 0.5-mm thick $La_{0.8}Sr_{0.2}FeO_{3-\delta}$ membrane. This example illustrates the fact that by fine-tuning the compositions of the support and the thin film and the relative thickness of both layers, it is possible to protect a high-flux membrane, otherwise non-stable against the severe conditions encountered during syngas generation. It also proves that high oxygen fluxes are achievable.

Sammenvatting

De toepassing van gemengd, zuurstofionen en elektronen, geleidende membranen vormen een aantrekkelijk alternatief voor de productie van synthesegas in vergelijking met traditionele reforming. Materialen met een perovskietstructuur zijn het meest belovend, dankzij het gemak waarmee hun elektrochemische eigenschappen geoptimaliseerd kunnen worden door middel van een geschikte dotering. Een aantal kwesties verdient aandacht voordat een industrile doorbraak mogelijk is. Van belang wanneer deze materialen gebruikt worden in membraanreactortechnologie zijn de grootte van de zuurstofflux (evenredig met de concentratie van zuurstofvacatures in het perovskiet rooster) en hun thermodynamische stabiliteit.
In *Hoofdstuk 2* werd de ionengeleiding van een reeks materialen met samenstelling $La_{1-x}Sr_xCoO_{3-\delta}$ gemeten met behulp van zuurstofpermeatieexperimenten als functie van de partile druk van zuurstof. Voor kleine concentraties van strontium (x = 0.1) zijn de verwachte waarden in goede overeenstemming met de theorie. Bij hogere doteringsconcentraties is er echter een tegenspraak. Aangetoond wordt dat een tweetal processen, te weten de interactie tussen zuurstofvacatures en de aanwezigheid van een stagnante laag aan de lage P_{O_2} zijde van het membraan, een significante invloed heeft en het conflict tussen theorie en experiment kan verklaren.
In *Hoofdstuk 3* werden verschillende materialen met een perovskietsamenstelling getest voor de bereiding van syngas. De invloed van een aantal doteringen op zowel A- en B-plaats van de ABO_3 perovskietstructuur werd onderzocht. Gevonden werd dat de substitutie met barium en strontium de grootte van de zuurstofflux beperkt. Sommige materialen laten een hogere flux zien maar de kritische eis die gesteld wordt aan hun thermodynamische stabiliteit maakt hen onbruikbaar voor industrile toepassing. De meest belovende kandidaat in deze studie, namelijk $La_{0.7}Sr_{0.3}Fe_{0.7}Ga_{0.3}O_{3-\delta}$, laat een lagere flux zien in vergelijking met andere materialen, maar daarentegen beschikt het in vergelijking met andere materialen over een goede stabiliteit onder de extreme omstandigheden van syngasbereiding.

De stabiliteit van dit materiaal werd verder onderzocht in *Hoofdstuk 4*. Rntgendiffractieonderzoek toonde de aanwezigheid aan van een tweede fase na synthese. Deze tweede fase blijkt onstabiel te zijn wanneer het materiaal geplaatst wordt in een gradint van de chemische potentiaal van zuurstof en verdwijnt ter plaatse van het oppervlak aan de lage P_{O_2} zijde van het membraan na het CPO experiment. Rntgen photoelectron spectroscopie in combinatie met Rntgen fluoroscentie spectroscopie toonden een verrijking aan van strontium aan de methaanzijde van het membraan, terwijl scanning elektron microscopie de aanwezigheid van een stofachtige laag liet zien op het oppervlak blootgesteld aan de methaanstroom. Een zuurstofflux van 5.1 ml.min^{-1}.cm^{-2} werd verkregen bij 900 °C bij een membraandikte van 0.5 mm onder omstandigheden van een pure methaanvoeding. Aangetoond werd dat onder deze omstandigheden de zuurstofflux gedeeltelijk gecontroleerd wordt door de oppervlaktereacties.
In *Hoofdstuk 5* werden dichte buisvormige membranen gemaakt met behulp van centrifugale depositie van een waterige suspensie van poederdeeltjes van het gemengdgeleidende perovskiet $La_{0.5}Sr_{0.5}CoO_{3-\delta}$ en een dispersiemiddel. De verkregen groene lichamen werden gedroogd en gesinterd tot buizen met een maximum lengte van 12 cm en een dichtheid hoger dan 92 %. De deeltjesmorfologie, de hoeveelheid dispersiemiddel en de verbranding van organische componenten bleken van invloed te zijn op de kwaliteit van het uiteindelijke product. Zuurstofpermeatiemetingen werden verricht in het temperatuurgebied 850-950 °C in lucht/helium gradinten. De resultaten zijn in overeenstemming met data gerapporteerd voor vlakke membranen.
In *Hoofdstuk 6* wordt een dubbel-gelaagd membraan concept voorgesteld als oplossing voor het probleem van de stabiliteit van het membraan onder reducerende omstandigheden. Een dunne dichte film van $La_{0.8}Sr_{0.2}FeO_{3-\delta}$ werd met succes gegroeid met behulp van 'pulsed laser' depositie (PLD) op een dicht support van $La_{0.3}Sr_{0.7}CoO_{3-\delta}$, en dit systeem werd gekozen als 'proof-of-principle'. Onder lucht/helium gradinten is de zuurstofflux de helft van die verkregen met het ongemodificeerde $La_{0.3}Sr_{0.7}CoO_{3-\delta}$ membraan. Onder CPO omstandigheden is de zuurstofflux vergelijkbaar met die door het ongedragen $La_{0.8}Sr_{0.2}FeO_{3-\delta}$. Hiermee wordt aangetoond dat een afstemming van de samenstellingen van support en dunne film en van de relatieve dikte van beide lagen het mogelijk is een materiaal met enerzijds een hoge zuurstofflux, anderzijds onstabiel materiaal, te beschermen tegen de extreme omstandigheden waaraan het blootgesteld wordt tijdens syngasbereiding. Het laat ook zien dat hoge zuurstoffluxen haalbaar zijn.

Acknowledgements

First and foremost to my supervisor, Henny Bouwmeester, for the help and guidance he constantly provided throughout the last four years.

To my promotor Dave Blank for his encouragements and advice.

To everyone who still puts up with me...
To many who became friends along the way...
To those whose help was truly appreciated.

Special thanks to my cheerful officemates, Monse, Jelena, Mai and Chrisztina, at ease to converse on any subject...and for letting me focus on the writing of this thesis by going shopping in Intratuin... :)

To Riaan and Steve for sharing the peanuts in Molly's
while reshaping the world...

To the "italian team" for making me feel good about myself...

Et enfin mes remerciements émus à ma famille pour son soutien en toute circonstance, et ma reconnaissance profonde à mes parents, ma soeur et mon frère pour leur amour.

Resume

Frédéric Henri Bertrand Mertins was born in Strasbourg (France) on the 15^{th} of September 1976. In 1994, he passed his highschool diploma with honours and went on studying mathematics, physics and chemistry for two years at Fustel de Coulanges in Strasbourg. After a national exam in two parts (written and oral), he was admitted to the "ENSCI" (National Superior Highschool for industrial ceramics) in Limoges, where he studied traditional and technical ceramics and glass for three years. During that period he spent five months at SINTEF Materials Technology (ceramic group) in Oslo (Norway) as a trainee and one exchange-year at the "Gesteinshüttenkunde Institut" in Aachen (Germany), which included a final year project of 5 months for the measurement of the oxygen activity in a tin bath for flat-glass production. For his national service, he went back to SINTEF for 16 months as a *voluntary service overseas*. At the beginning of the year 2001, he started a Ph.D. at the University of Twente in the Inorganic Materials Science Group (IMS) under the supervision of H.J.M. Bouwmeester. The results obtained during this 4-years period are described in this thesis.

Part II

Doctoral Thesis

Chapter One

Introduction

1.1 A special mineral: the perovskite

The parent mineral was first described from samples found in the Ural Mountains in 1839 by the geologist *Gustav Rose*, who named it after the famous Russian mineralogist *Count Lev Aleksevich von Perovski*. It is nowadays regarded as the most abundant solid phase (70-80 %) of the lower earth mantel (670 to 2900 km depth).
The general structure of the perovskite mineral is ABX_3 where A and B are cations and X oxygen anions. One way to visualize the structure is to place the smaller B cation in an oxygen octahedral environment on the corner of a cube which center would be occupied by the larger A cation, as seen on fig. 1.1. In such a cubic structure, the coordination numbers of the A and B

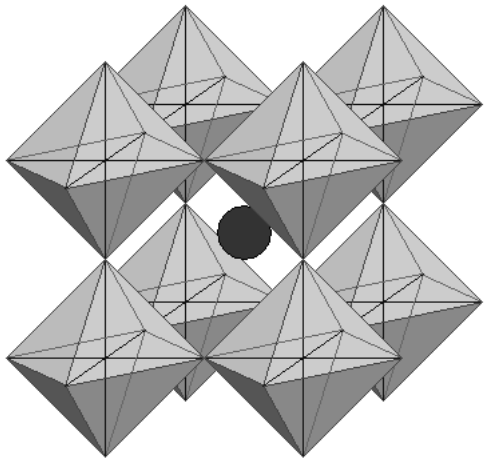

FIGURE 1.1: *Ideal perovskite structure exhibited by $CaTiO_3$.*

cations are 12 and 6, respectively. The A cation is generally an alkali earth metal or a transition metal. The B cation is a transition metal or a rare earth metal but can also be found in the family (Al, Ga, Pb, Bi, Ti, etc). The relative size difference between the two types of cations can lead to the tilting of the BO_6 octahedra, the structure therefore becoming orthorhombic. Goldschmidt introduced a so-called tolerance factor [1] being in essence a measure of the "cubic-ness" of the perovskite structure. The definition of

this factor is:

$$t = \frac{r_A + r_B}{\sqrt{2}\,(r_B + r_O)} \tag{1.1}$$

where r_A, r_B and r_O are the ionic radii of the A-site cation, the B-site cation and the oxygen anion, respectively. When t equals unity, the structure is cubic. Lower values of t correspond to lower symmetry.

Perovskite materials are classified as ceramics and can be doped, i.e. a fraction of the A-site and/or the B-site cations can be replaced by another metal. It is therefore possible to tune the properties of these ceramics for a very wide range of applications. The well-known (undoped) $BaTiO_3$ is used as multilayer capacitor, $(La, Ca, Sr)MnO_3$ for its colossal magnetoresistance, $Li_{0.5-x}La_xTiO_3$ as battery material and $La_{1-x}Sr_xMnO_{3-\delta}$ as cathode material in solid oxide fuel cells (SOFC); to name only a few.

Materials with the perovskite structure can also be **mixed ionic and electronic conductors (MIEC)**. Their use as membrane for oxygen separation will be the core of this thesis. The feature of interest in this case is the **oxygen non-stoichiometry**, refered to as δ, which is a function of composition, temperature and oxygen partial pressure. Using doping, oxygen vacancies (charged defects) are created in the lattice. At low temperature they remain ordered but at high temperature, typically T $>$ 600 °C, they become available for transport, providing a path for the migration of the oxygen anions from one side of the membrane to the other side [2]. A counter-balancing flux of electronic charge carriers is present in the material so that the electroneutrality holds. A typical example of mixed-conduction (MIEC) in a material with the perovskite structure is $La_{1-x}Sr_xCoO_{3-\delta}$. This material is for instance a very promising candidate for oxygen separation from air. Other materials with the general formula $(La, Sr, Ba, Ca)(Fe, Cr, Ga, Co)O_{3-\delta}$ can be used as membranes in membrane reactor technology, e.g. for the conversion of methane into syngas, a mixture of hydrogen and carbon monoxide.

1.2 Theory of transport

1.2.1 Diffusion in the bulk

The mathematical treatment of oxygen transport in mixed-conductors has been presented by several authors [3–5]. The basic assumption of this theory is that the transport of electronic charge carriers (oxygen anions, electrons and electron holes) determines the overall oxygen permeation. Moreover, the driving force is a gradient of oxygen chemical potential across the membrane.

The interaction between the lattice and the oxygen in the gas phase is described by the following equation using the Kröger-Vink notation [6]:

$$\frac{1}{2}O_2 + V_o^{\cdot\cdot} + 2e' \rightleftharpoons O_o^{\times} \tag{1.2}$$

It is implicitly assumed that the oxygen vacancies are fully ionized. The interaction between electrons and electron holes can be described by:

$$nil \rightleftharpoons e' + h^{\cdot} \tag{1.3}$$

Considering equilibrium in eqs. 1.2 and 1.3, the chemical potential of the different species can be related according to the following relations:

$$\frac{1}{2}\nabla\mu_{O_2} + \nabla\mu_{V_o^{\cdot\cdot}} + 2\nabla\mu_{e'} = 0 \tag{1.4}$$

$$\nabla\mu_{e'} + \nabla\mu_{h^{\cdot}} = 0 \tag{1.5}$$

where μ_k denotes the chemical potential of the charge carrier k. The single particle flux of charge carriers, neglecting the cross terms between fluxes, is given by:

$$j_k = -\frac{\sigma_k}{z_k^2 F^2}\nabla\eta_k \tag{1.6}$$

where F is the *Faraday* constant, σ_k denotes the conductivity, z_k the charge number and η_k the gradient of the electrochemical potential of the charge carrier k. The latter includes a gradient in chemical potential μ_k and a gradient in electrical potential ϕ_k according to:

$$\nabla\eta_k = \nabla\mu_k + z_k F\nabla\phi \tag{1.7}$$

At equilibrium, or steady state, no charge accumulation occurs. The flux of ionic and electronic defect are therefore related to each other by the charge balance, given as:

$$2j_{V_o^{\cdot\cdot}} + j_{h^{\cdot}} = j_{e'} \tag{1.8}$$

Combining eqs. 1.4 to 1.8, and taking into account that $j_{O_2} = -\frac{1}{2}j_{V_o^{\cdot\cdot}}$, one can express the oxygen flux as follows:

$$j_{O_2} = -\frac{1}{16F^2}\frac{(\sigma_{e'} + \sigma_{h^{\cdot}})\sigma_{V_o^{\cdot\cdot}}}{(\sigma_{e'} + \sigma_{h^{\cdot}}) + \sigma_{V_o^{\cdot\cdot}}}\nabla\mu_{O_2} \tag{1.9}$$

where $\sigma_{e'} + \sigma_{h^{\cdot}} = \sigma_{el}$ and $\sigma_{V_o^{\cdot\cdot}} = \sigma_{ion}$. Integrating eq. 1.9 with respect to the thickness of the membrane material can be done using the following relation:

$$\nabla\mu_{O_2} = RT\,\frac{\partial lnP_{O_2}}{\partial x} \tag{1.10}$$

where R is the gas constant, T the temperature, P_{O_2} the oxygen partial pressure and x the distance coordinate. The obtained relation is the Wagner equation [7, 8] in its usual form:

$$j_{O_2} = -\frac{RT}{16F^2L}\int_{lnP'_{O_2}}^{lnP''_{O_2}}\frac{\sigma_{el}\sigma_{ion}}{\sigma_{el} + \sigma_{ion}}\,dlnP_{O_2} \tag{1.11}$$

where L is the membrane thickness and P'_{O_2} and P''_{O_2} represent the oxygen partial pressure at the high- and the low-PO_2 side of the membrane, respectively.

1.2.2 Surface processes

The oxygen exchange reaction between the gas phase and the oxide surface involves a number of reaction steps, each of which may be rate determining. Possible steps are the oxygen adsorption on the oxide surface, oxygen dissociation, (surface) diffusion of intermediate species, charge transfer and incorporation into the lattice. It is generally assumed that this sequence of

reactions applies for both membrane surfaces, in reverse directions. In the presence of a reactive gas, for instance methane, the rate-limiting step may be different than in the case of an argon sweep. It is therefore difficult to derive an appropriate expression for the interfacial oxygen flux.
The Onsager equation [2] gives a general expression for the oxygen flux through the solid/gas interface at conditions near to equilibrium:

$$j_{O_2} = -j^o_{ex} \frac{\Delta\mu^{int}_{O_2}}{RT} \tag{1.12}$$

where $\Delta\mu^{int}_{O_2}$ is the oxygen chemical potential difference across the interface and j^o_{ex} denotes the exchange rate in the absence of an oxygen chemical potential gradient. The later parameter is related to the surface exchange coefficient k_s accessible from data of $^{18}O - ^{16}O$ isotopic exchange:

$$j^o_{ex} = \frac{1}{4} k_s c_o \tag{1.13}$$

where c_o is the volume concentration of oxygen anions at equilibrium.

The oxygen chemical potential gradient applied across a MIEC is in practice consumed in two ways:

- loss of driving force at either one or both interfaces
- loss of driving force for the bulk diffusion

Decreasing the thickness of the membrane material can enhance the oxygen flux (see eq. 1.11 on page 21) as long as the interface processes play a negligible role. It is pointless to reduce the thickness further if the limiting mechanism is the surface oxygen exchange. Bouwmeester *et al.* [2] introduced the concept of characteristic membrane thickness in order to distinguish between surface exchange and bulk diffusion controlled kinetics. When the total driving force is shared between these two processes, the membrane has a thickness L_c, defined as:

$$L_c = \frac{RT}{16F^2} \frac{\overline{t_{el}\sigma_{ion}}}{j^o_{ex}} \tag{1.14}$$

where t_{el} is the electronic transference number.

Combining eqs. 1.14 and 1.12 with an equation mathematically equivalent to 1.11, one obtains the overall flux equation:

$$j_{O_2} = -\frac{1}{1 + 2L_c/L} \frac{\overline{t_{el}\sigma_{ion}}}{16F^2} \frac{\Delta\mu_{O_2}^{total}}{L} \tag{1.15}$$

A factor 2 is introduced in the denominator to take into account the fact that for a symmetrical membrane the exchange processes at both interface can be rate-limiting. For large membrane thicknesses, eq. 1.15 is equivalent to eq. 1.11 on page 21 (Wagner's equation). For thicknesses much smaller than $2L_c$, the oxygen flux is independent of the thickness L.

1.3 Syngas production with MIEC membranes

The price of crude oil is high due to the limited reserves which are estimated to last for only another few decades. In addition, the constantly rising requirements for clean fuels are driving industrials to use natural gas, which offers an interesting energy source when upgraded to higher-value chemicals. This process is commonly known as gas-to-liquid or GTL-technology.

Synthesis gas, or syngas (CO + H_2), is an intermediate chemical feedstock obtained from methane, the main component of natural gas. It can be further processed to value-added chemicals via methanol synthesis or the well-known Fischer-Tropsch synthesis, a process developed in 1923 by the German chemists Franz Fischer and Hans Tropsch to obtain synthetic fuel from coal. Thanks to the constant development of this process, the produced fuel has a high octane index and is very clean since it contains no metals or sulfur. Last year ExxonMobil, Shell, ChevronTexaco and Sasol have announced their plan to invest more than 20 billion dollars to build large GTL-facilities in Katar, on the shore of the Persian Golf.

Another possible use for syngas is the production of hydrogen. The elimination of the CO present in the syngas is usually accomplished in a two-step process, the first of which being the water gas-shift reaction:

$$CO + H_2O \rightleftharpoons CO_2 + H_2 \quad \Delta H^0_{25\ ^\circ C} = -41.2 \text{ kJ.mol}^{-1} \tag{1.16}$$

The second step is the separation of carbon dioxide and hydrogen, which is accomplished thanks to a palladium/silver membrane. A large consumer of hydrogen is the ammonia production but hydrogen can also power a fuel cell, as depicted in fig. 1.2 on page 25. This utilization of the hydrogen (produced from natural gas) has great potential when one considers the enormous amount of natural gas stranded in remote locations, estimated to be circa $75 \cdot 10^{12}\,\text{m}^3$, which corresponds to approximately 250 billion barrels of synthetic oil.

The production of syngas from methane is predominantly achieved via steam reforming, according to the following reaction:

$$CH_4 + H_2O \rightleftharpoons CO + 3H_2 \quad \Delta H^0_{25\ ^\circ C} = 206 \text{ kJ.mol}^{-1} \tag{1.17}$$

This reaction is energy consuming since it is very endothermic. In addition, a natural gas desulphurization unit precedes the actual steam reformer because the metal catalysts used for this reaction are easily poisoned by sulphur. Coke formation, especially in the case of a nickel catalyst, is also a major concern. Noble metal catalysts, such as Pd, Pt or Rh, are less sensitive to carbon deposition and have a higher tolerance towards sulphur but they cannot be favored for obvious economical reasons. A remedy to these problems lies in the slightly exothermic **catalytic partial oxidation (CPO) reaction**:

$$CH_4 + \frac{1}{2}O_2 \rightleftharpoons CO + 2H_2 \quad \Delta H^0_{25\ ^\circ C} = -71 \text{ kJ.mol}^{-1} \tag{1.18}$$

The main challenge in this case is to produce pure oxygen. It is nowadays achieved in a cryogenic plant but the associated investment costs are very high, therefore limiting the use of this process. Air can be used in place of oxygen but there is a risk of producing harmful NO_x compounds and handling large quantities of nitrogen is costly.

In the last decades, researchers have developed MIEC membranes suitable for the **partial oxidation of methane into syngas (so-called membrane CPO)**. Combined with the earlier mentioned shift reaction and the hydrogen separation step, this process can supply hydrogen to a fuel cell. An overview of this scheme is proposed in fig. 1.2.

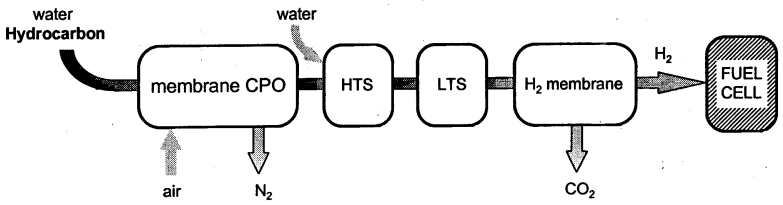

FIGURE 1.2: *A fuel cell is powered by hydrogen produced via the catalytic partial oxidation (CPO) of natural gas. HTS and LTS stand for the high- and low-temperature shift reactions, respectively.*

The advantages of this approach are as follows:

- Economically attractive process
- Elimination of NO_x compounds
- Avoids the premixing of CH_4 and O_2 (safety)
- Air can be used as oxygen supply
- Oxygen separation and partial oxidation are combined in a single reactor
- Application in remote locations possible

Although the principle has been proven by many authors [9–15] over the last decade, there are a number of issues related to the use of MIEC with the perovskite structure [16–18]. Such membrane materials are exposed to very reducing environments and large oxygen chemical potential gradients at relatively high temperatures.

A number of requirements, listed below, have to be fulfilled before any real industrial breakthrough:

- Low production costs
- Ease of processing (tubular geometry favored)
- High oxygen permeation
- Mechanical, chemical and structural stability

1.4 Scope of the thesis

This thesis focuses on the preparation and characterization of ceramic materials with the perovskite structure for oxygen separation and the conversion of methane to syngas. *Chapter 2* presents a study of the ionic conductivity in $La_{1-x}Sr_xCoO_{3-\delta}$. Relevant parameters such as the ordering of the oxygen vacancies are investigated. In *Chapter 3*, a number of membrane materials are tested for the catalytic partial oxidation (CPO) of methane. Results are discussed in relation with the composition of the materials. In *Chapter 4*, further investigations on a specific material are presented with special attention to the stability and the magnitude of the oxygen flux. *Chapter 5* deals with the preparation of dense tubular membrane (perovskite structure) using a centrifugal casting technique. In *Chapter 6*, knowledge from *Chapter 2-4* is used to produce a bi-layered system suitable for CPO.

Bibliography

[1] V.M. Goldschmidt, Skrifer Norske Videnskaps-Akad. Oslo, I. Mat.-Nat. Kl. 8 (1926).

[2] H.J.M. Bouwmeester and A.J. Burggraaf, *Dense ceramic membranes for oxygen separation*, in: CRC Handbook of Solid State Electrochemistry, Eds. P.J. Gellings and H.J.M. Bouwmeester, CRC Press, Boca Raton 1997.

[3] H. Schmalzried, *Solid State Reactions*, Verlag Chemie, Weinheim, 1981.

[4] H. Rickert, *Electrochemistry of solids, an introduction*, Springer Verlag Berlin, 1982.

[5] L. Heyne, *Electrochemistry of mixed-ionic electronic conductors*, in Solid Electrolytes, Topics in Applied Physics, S. Geller, Ed., Springer-Verlag, Berlin, 1977, 167-221.

[6] F.A. Kröger and H.J. Vink, *Relations between the concentrations of imperfections in crystalline solids*, Solid State Physics, Vol. 3, F. Seitz and D. Turnbull, Eds., Academic Press, New York, 1956, 307.

[7] C. Wagner and W. Schottky, *Beitrag zur Theorie des Anlaufvorganges*, Z. Phys. Chem., 1930, B11, 25-41.

[8] C. Wagner, *Equations for transport in solid oxides and sulfides of transition metals*, Prog. Solid State Chem. 10 (1975) 3-16.

[9] X. Gu, W. Jin, C. Chen, N. Xu, J. Shi and Y.H. Ma, *YSZ-$SrCo_{0.4}Fe_{0.6}O_{3-\delta}$ membranes for the partial oxidation of methane to syngas*, AIChE J. 48 (2002) 2051-2060.

[10] J.T. Ritchie, J.T. Richardson and Dan Luss, *Ceramic membrane reactor for synthesis gas production*, AIChE J. 47 (2001) 2092-2101.

[11] H. Dong, Z. Shao, G. Xiong, J. Tong, S. Sheng and W. Yang, *Investigation on POM reaction in a new perovskite membrane reactor*, Catal. Today 67 (2001) 3-13.

[12] Z. Shao, G. Xiong, H. Dong, W. Yang and L. Lin, *Synthesis, oxygen permeation study and membrane performance of a $Ba_{0.5}Sr_{0.5}Co_{0.8}Fe_{0.2}O_{3-\delta}$ oxygen-permeable dense ceramic reactor for partial oxidation of methane to syngas*, Sep. Purif. Technol. 25 (2001) 97-116.

[13] W. Jin, S. Li, P. Huang, N. Xu, J. Shi and Y.S. Lin, *Tubular lanthanum cobaltite perovskite-type membrane reactors for partial oxidation of methane to syngas*, J. Membrane Sci. 166 (2000) 13-22.

[14] W.T. Stephens, T.J. Mazanec and H.U. Anderson, *Influence of gas flow rate on oxygen flux measurements for dense oxygen conducting ceramic membranes*, Solid State Ionics 129 (2000) 271-284.

[15] T. Ishihara and Y. Takita, *Partial oxidation of methane into syngas with oxygen permeating ceramic membrane reactors*, Catal. Surv. JPN 4 (2000) 125-133.

[16] A. Petric, P. Huang and F. Tietz, *Evaluation of La-Sr-Co-Fe-O perovskites for solid oxide fuel cells and gas separation membranes*, Solid State Ionics 135 (2000) 719-725.

[17] P.V. Hendriksen, P.H. Larsen, M. Mogensen, F.W. Poulsen and K. Wiik, *Prospects and Problems of dense oxygen permeable membranes*, Catal. Today 56 (2000) 283-295.

[18] H.J.M. Bouwmeester, *Dense ceramic membranes for methane conversion*, Catal. Today 82 (2003) 141-150.

Chapter Two

Ionic conductivity of $La_{1-x}Sr_xCoO_{3-\delta}$

2.1 Introduction

Perovskite materials with the composition $La_{1-x}Sr_xCoO_{3-\delta}$ exhibit high oxygen fluxes at temperatures typically higher than ∼800 °C thanks to their ionic conductivity reaching values 1-2 orders of magnitude higher than that of yttria-stabilized zirconia (YSZ) [1, 2]. These materials are therefore of interest for applications such as oxygen separation membranes, novel catalytic reactors, oxygen sensors or as cathode materials for solid oxide fuel cells (SOFC). The transport properties of these materials are strongly dependent on the level of strontium doping, the temperature and the oxygen partial pressure in the surrounding gas [3–5]. Increasing the concentration of strontium on the A-site of the perovskite structure increases both the number of oxygen vacancies and the concentration of Co^{4+}, as a result of the charge compensation mechanism, maintaining the overall electro-neutrality [6]. Misuzaki *et al.* [4] measured the oxygen non-stoichiometry in the series $La_{1-x}Sr_xCoO_{3-\delta}$. For all compositions investigated, the oxygen vacancy concentration increases profoundly with decreasing oxygen partial pressure. Since ionic conductivity in these perovskites is proportional to the concentration of oxygen vacancies, it is expected to increase with strontium doping and/or decreasing oxygen partial pressure. However, direct measurement of the ionic conductivity, for instance by using electron-blocking electrodes, is experimentally difficult. In this study, the ambipolar conductivity in this type of materials [7] was determined as a function of the oxygen partial pressure by means of oxygen permeation measurements. Since the ionic transference numbers in these materials are much smaller than unity [8], the ambipolar conductivity is equal to the ionic conductivity.

2.2 Theory

The theory of oxygen permeation through mixed-conducting materials has been described by Wagner [9,10] and the following relation applies in the case

of a steady-state, diffusion-limited and one-dimensional oxygen transport:

$$j_{O_2} = -\frac{RT}{16F^2L}\int_{lnP'_{O_2}}^{lnP''_{O_2}} \sigma_{amb}\, dlnP_{O_2} \tag{2.1}$$

where σ_{amb}, R, T, F and L are the ambipolar conductivity, the gas constant, the temperature, the $Faraday$ constant and the thickness of the membrane material, respectively. The oxygen partial pressures on both sides of the membrane material are represented by P'_{O_2} (high-P_{O_2}) and P''_{O_2} (low-P_{O_2}). The ambipolar conductivity is defined as follows:

$$\sigma_{amb} = \frac{\sigma_{el}\,.\,\sigma_{ion}}{\sigma_{tot}} = t_{el}\,.\,\sigma_{ion} \tag{2.2}$$

where σ_{ion}, σ_{el}, σ_{tot} and t_{el} are the ionic conductivity, the electronic conductivity, the total conductivity and the electronic transference number, respectively. Since the electronic conductivity is much larger than the ionic conductivity in these types of materials, the electronic transference number is often approximated to be equal to unity. If the oxygen partial pressure at one side of the membrane is fixed, for instance P'_{O_2}, one can obtain $\sigma_{ion}(P''_{O_2})$ by measuring the isothermal oxygen permeation as a function of P''_{O_2} according to:

$$\sigma_{ion}(P''_{O_2}) = -\frac{4^2F^2L}{RT}\left(\frac{\partial j_{O_2}}{\partial lnP''_{O_2}}\right)_{P'_{O_2}} \tag{2.3}$$

Reciprocally, $\sigma_{ion}(P'_{O_2})$ can be obtained by fixing P''_{O_2} and measuring the isothermal oxygen permeation as function of P'_{O_2}.

2.2.1 Slope of the curve $\log(\sigma_{ion})$ versus $\log(\delta)$

The ionic conductivity can be expressed using the Nernst-Einstein equation:

$$\sigma_{ion} = \frac{4F^2[V_o^{\cdot\cdot}]D_v}{RTV_m} \tag{2.4}$$

where $[V_o^{\cdot\cdot}]$, D_v and V_m are the concentration of oxygen vacancies (Kröger-Vink notation), the vacancy diffusion coefficient and the perovskite molar volume. It should be noted that this relation holds in the case of fully

ionized and non-interacting oxygen vacancies. The oxygen vacancy diffusion coefficient [11] can be written as follows:

$$D_v = D_v^{\circ}\left(1 - \frac{\delta}{3}\right) \tag{2.5}$$

where δ is the concentration of oxygen vacancies (written $[V_o^{\cdot\cdot}]$ in Kröger-Vink notation) and the factor

$$\left(1 - \frac{\delta}{3}\right)$$

represents the fraction of sites in the oxygen sublattice of the perovskite structure (ABO_3) to which an oxygen vacancy can jump. Combining eqs. 2.4 and 2.5 gives:

$$\sigma_{ion} = \frac{4F^2 D_v^{\circ}}{RTV_m} \,.\, \delta \,.\, \left(1 - \frac{\delta}{3}\right) \tag{2.6}$$

from which follows:

$$log(\sigma_{ion}) = log\left(\frac{4F^2 D_v^{\circ}}{RTV_m}\right) + log(\delta) + log\left(1 - \frac{\delta}{3}\right) \tag{2.7}$$

Assuming that D_v° is independent of the oxygen non-stoichiometry, the partial derivative of eq. 2.7 with respect to log(δ) is given by:

$$\frac{\partial log(\sigma_{ion})}{\partial log(\delta)} = \frac{\partial K}{\partial log(\delta)} + \frac{\partial log(\delta)}{\partial log(\delta)} + \frac{\partial log(\left(1 - \frac{\delta}{3}\right)}{\partial log(\delta)} \tag{2.8}$$

where

$$K = log\left[\frac{4F^2 D_v^{\circ}}{RTV_m}\right] \tag{2.9}$$

Since K is, to a first approximation, independent of δ, the first term on the right-hand side of eq. 2.8 is equal to zero. Therefore:

$$\frac{\partial log(\sigma_{ion})}{\partial log(\delta)} = 0 + 1 + \left(\frac{-\delta}{3 - \delta}\right) = \frac{3 - 2\delta}{3 - \delta} \tag{2.10}$$

For small values of δ, the slope of the curve $log(\sigma_{ion})$ versus $log(\delta)$ is almost unity, whereas for larger values of δ, it is smaller than 1.

2.3 Experimental

The powders were prepared by thermal decomposition of metal-EDTA (ethylene-diamine-tetra-acetic acid) complexes, a method developed by van Doorn *et al.* [12]. Commercially available metal nitrates[1,2] were dissolved in a minimum amount of water according to the stoichiometry of $La_{1-x}Sr_xCoO_{3-\delta}$ (x = 0.1, 0.2, 0.5 and 0.7). This metal nitrate solution was added to a solution of EDTA and ammonium hydroxide in a molar ratio of 1:3 (perovskite:EDTA). The pH of the solution was maintained between 8.5 and 9 by addition of ammonia for a period of 4 h. The solution was heated and kept under air flow to help the evaporation process. The solution was then poured in a porcelain dish and put in a furnace at 230 °C. After evaporation of the remaining water, the pyrolysis took place. The resulting powder was calcined for 3 h at 950 °C with heating and cooling rates of 2 °C.min^{-1}. The powder was then ball-milled for 6 h in ethanol using zirconia milling balls of 1 and 10 mm in diameter. After milling, the suspension was separated from the milling balls and dried overnight in air. Ceramic samples were prepared by pressing (uniaxially and subsequently isostatically at 400 MPa) powder batches into disc-shaped membranes, which were sintered at 1150 °C for 10 h with heating and cooling rates of 1 °C.min^{-1}. The density of these materials was checked with the Archimedes' method using mercury. The ceramics were polished with SiC paper (1000 mesh). The final diameter of the membranes was 15 mm and the thickness ranged from 1 to 2.58 mm. The oxygen permeation experiments were performed using a quartz glass reactor at a temperature between 850 °C and 1000 °C. The samples were sealed into the reactor by means of a glass ring[3]. Two types of measurements were conducted. In *method A*, one side of the membrane was exposed to air (f_{air} = 116.4 ml.min^{-1}) and the other side to different helium flowrates (f_{helium} = 16.6-152 ml.min^{-1}) to vary the oxygen partial pressure. In *method*

[1] $La(NO_3)_2$ and $Co(NO_3)_2$, Merck, purity > 99 %
[2] $Sr(NO_3)_2$, Fluka-Acr, purity > 99 %
[3] SCHOTT AG, model 8252

B, various oxygen partial pressures were obtained with a mixture of oxygen (f_{oxygen} = 5.8-99.8 ml.min^{-1}) and nitrogen ($f_{nitrogen}$ = 11.2-100 ml.min^{-1}) and fed to one side of the membrane while, on the other side, the flowrate of helium was adjusted in such a way as to keep the oxygen partial pressure at the outlet of the reactor constant. The outlet gas on the permeate side of the membrane was directed to a gas chromatograph[1] for quantitative analysis of both oxygen and nitrogen.

2.4 Results

In fig. 2.1, the oxygen flux as a function of the logarithm of the oxygen partial pressure on the permeate side of the membrane is shown for the composition $La_{0.9}Sr_{0.1}CoO_{3-\delta}$.

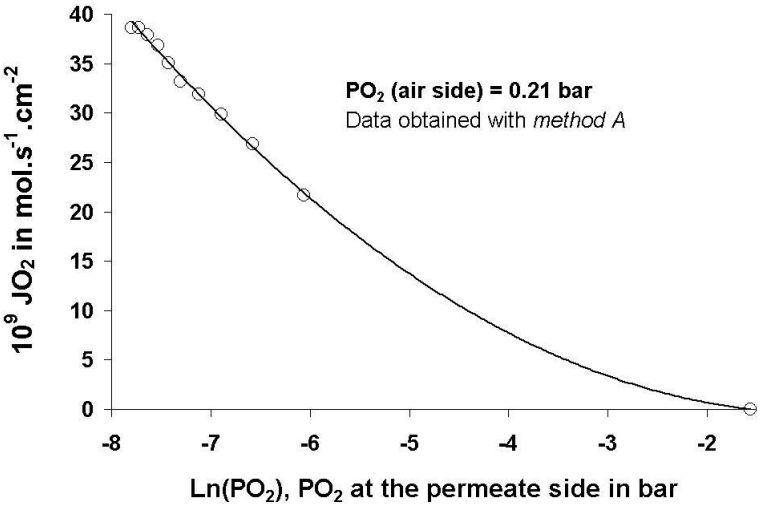

FIGURE 2.1: *Oxygen flux through a $La_{0.9}Sr_{0.1}CoO_{3-\delta}$ membrane as a function of the logarithm of the oxygen partial pressure on the permeate side obtained at 1000 °C.*

These data points were obtained with *method A*. The point where the oxygen flux is equal to zero corresponds to the situation where air is fed to both sides

[1]GC 4600 Micro Gas Chromatograph Varian

of the membrane. The black line is a least-squares fit with a third degree polynomial. As the oxygen partial pressure decreases on the permeate side of the membrane, the oxygen flux increases almost a factor 2. The same type of measurements were conducted according to *method B*, i.e. by maintaining the oxygen partial pressure on the permeate side constant. The results are presented in fig. 2.2.

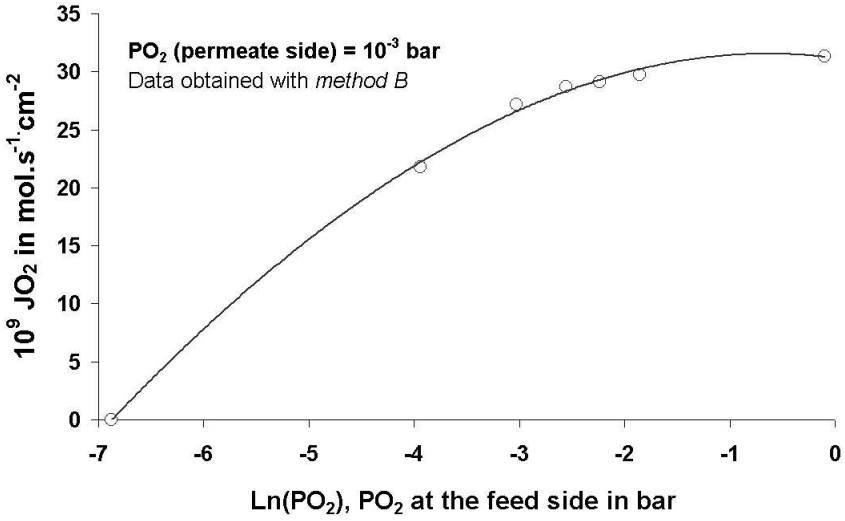

FIGURE 2.2: *Oxygen flux through a $La_{0.9}Sr_{0.1}CoO_{3-\delta}$ membrane as a function of the logarithm of the oxygen partial pressure on the air side obtained at 1000 °C.*

Similarly to fig. 2.1, the point where the oxygen flux is equal to zero is not an actual measurement point but corresponds to the situation where the same oxygen partial pressure is applied on both sides of the membrane. The black line is again a least-squares fit with a third degree polynomial.

Based on these results, the ionic conductivity was determined according to eq. 2.3. The results are presented in fig. 2.3. In the temperature range under consideration, the ionic conductivity of $La_{0.9}Sr_{0.1}CoO_{3-\delta}$ is constantly increasing with decreasing oxygen partial pressure. The slope of the curves obtained at relatively high oxygen partial pressure appears to be slightly

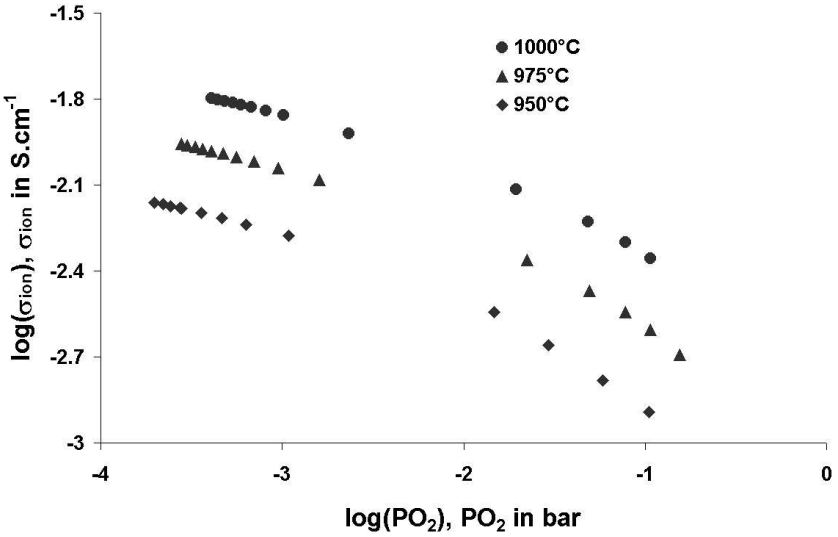

FIGURE 2.3: *Logarithm of the ionic conductivity of $La_{0.9}Sr_{0.1}CoO_{3-\delta}$ versus the logarithm of the oxygen partial pressure at different temperatures.*

higher than that at lower oxygen partial pressure. Similar measurements were conducted with the other members of the series $La_{1-x}Sr_xCoO_{3-\delta}$.

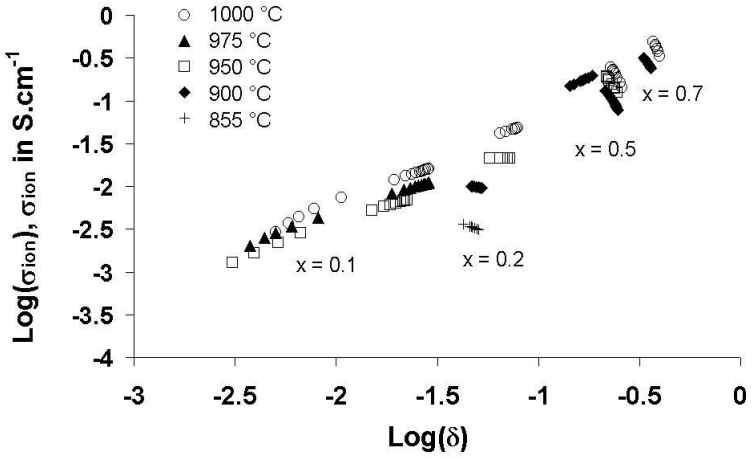

FIGURE 2.4: *Ionic conductivity of different $La_{1-x}Sr_xCoO_{3-\delta}$ compositions determined according to eq. 2.3 at different temperatures.*

The same procedure was then applied to determine the ionic conductivity of these materials with eq. 2.3. The data of the non-stoichiometry as a function of the oxygen partial pressure obtained by Misuzaki *et al.* [4] were used to plot the ionic conductivity versus the logarithm of the non-stoichiometry, as presented in fig. 2.4. For the composition with $x = 0.1$, the ionic conductivity is found to increase with oxygen non-stoichiometry for every temperature under consideration. For $x = 0.2$ the slope of the curve $log(\sigma_{ion})$ versus $log(\delta)$ decreases with the temperature from a positive value (1000 °C) to a negative value (T < 1000 °C). For the measurements where $x = 0.5$ and $x = 0.7$, the ionic conductivity decreases sharply with increasing non-stoichiometry (data obtained with *method A*) except for one set of data ($x = 0.5$) obtained with *method B* at 900 °C.

2.5 Discussion

The critical length in the series $La_{1-x}Sr_xCoO_{3-\delta}$ varies between 50 and 150 μm [13]. Chen *et al.* [1] have for instance estimated the critical length of $La_{0.3}Sr_{0.7}CoO_{3-\delta}$ to be in the order of 80 μm. The thickness of the $La_{0.9}Sr_{0.1}CoO_{3-\delta}$ membranes in this study was 1 mm. Membranes of other compositions were thicker than 2 mm, sometimes as thick as 2.58 mm. Under these conditions, the influence of the surface exchange process can be considered to be negligible for all compositions investigated.

According to eq. 2.10, a slope close to unity is expected for all values of δ for the curve $log(\sigma_{ion})$ versus $log(\delta)$ ($\delta < 0.5$ in the series under consideration according to [4]). The results presented in fig. 2.4 clearly show a linear relation (with a slope close to unity) between the ionic conductivity and the oxygen non-stoichiometry. However, some discrepancies are found. For instance, strongly negative slopes are obtained with *method A* for the materials where $x = 0.5$ and $x = 0.7$ at different temperatures. This suggests a dominating process linked to the experimental procedure. In addition, the slopes seem not to be influenced by the temperature, which points into the direc-

tion of a gas diffusion based process. The authors suggest the presence of a stagnant layer on the low-P_{O_2} side of the membrane as depicted in fig. 2.5. A satisfactory modeling of the influence of this stagnant layer has not yet been found; it is therefore not possible at this stage to give reliable quantitative analysis of the different processes involved.

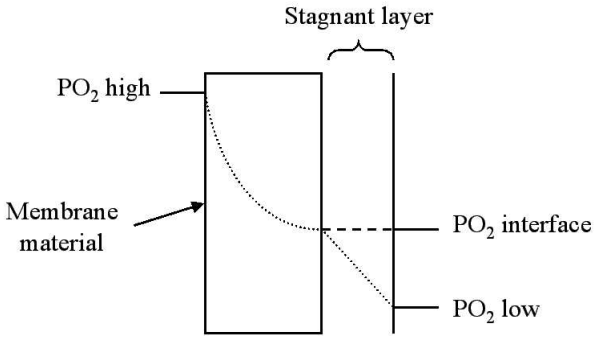

FIGURE 2.5: *Schematic representation of the influence of a stagnant layer on the low-P_{O_2} side of a perovskite membrane. The gradients are chosen arbitrarily.*

To be able to apply eq. 2.3 in the case where a stagnant layer is present on the permeate side of the membrane, the oxygen flux should be plotted as a function of the $P_{O_2\,interface}$ instead of as a function of $P_{O_2\,low}$. For the sake of illustration, some values are derived from the set of data obtained for $La_{0.5}Sr_{0.5}CoO_{3-\delta}$ at 900 °C and presented in fig. 2.6. The values of $P_{O_2\,interface}$ were obtained from a simple model where the oxygen flux relates to the oxygen partial pressures on both sides of the membrane with a power law dependence. This example clearly shows the difference in slope between the two curves, leading to a higher value of the ionic conductivity for the data set plotted against $P_{O_2\,interface}$. This strongly supports the hypothesis of the presence of a stagnant layer on the permeate side of the membrane during the permeation experiments.

The influence of such a stagnant layer will be more pronounced as the oxygen flux through the membrane material increases. The oxygen flux through $La_{0.8}Sr_{0.2}CoO_{3-\delta}$ is a factor 3-8 smaller than the ones obtained with the

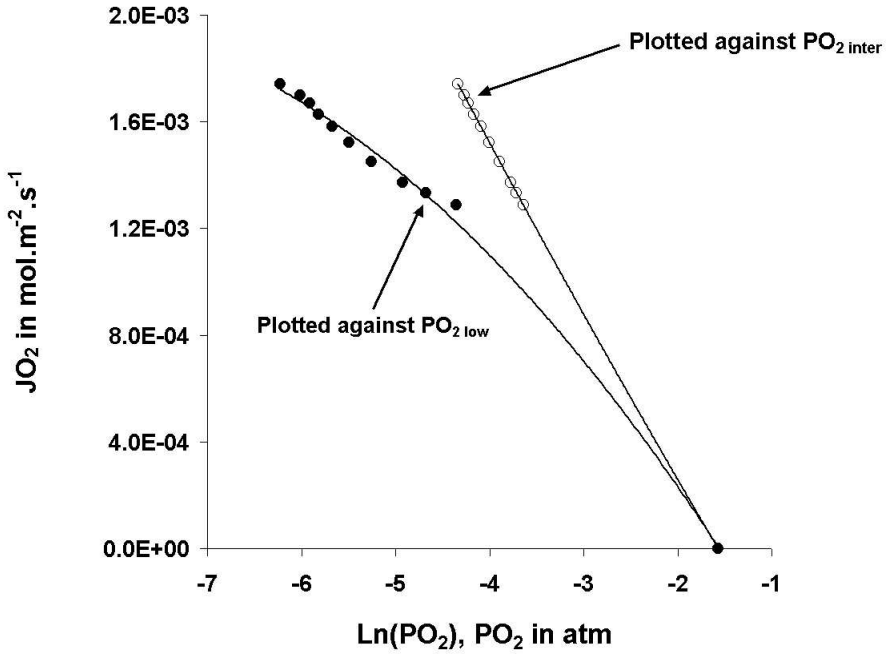

FIGURE 2.6: *Oxygen flux plotted versus $P_{O_2\,low}$ and $P_{O_2\,interface}$ for the composition $La_{0.5}Sr_{0.5}CoO_{3-\delta}$ at 900 °C.*

materials where $x = 0.5$ and $x = 0.7$. The effect of a stagnant layer with the composition $La_{0.8}Sr_{0.2}CoO_{3-\delta}$ will therefore be limited. This assumption is supported by the fact that at 1000 °C the experimental slope for $La_{0.8}Sr_{0.2}CoO_{3-\delta}$, obtained with *method A*, is positive; whereas for the materials where $x = 0.5$ and $x = 0.7$ the slopes are strongly negative for each temperature. This suggests a different predominant process in the case of $La_{0.8}Sr_{0.2}CoO_{3-\delta}$. The effect of the temperature is significant and the authors believed that ordering of the oxygen vacancies at lower temperature might be a possible explanation.

2.6 Conclusions

Data from oxygen permeation experiments on a series of materials with composition $La_{1-x}Sr_xCoO_{3-\delta}$ (x = 0.1, 0.2, 0.5 and 0.7) were used to determine the ionic conductivity as a function of the oxygen partial pressure. An overall

linear relation was found with a slope close to unity between the ionic conductivity and the non-stoichiometry. Local discrepancies were observed. For the composition where $x = 0.1$, good agreement is found with the expected behavior. The difference between experimental findings and expected values for the other compositions was attributed to the presence of a stagnant layer on the permeate side of the membrane during the permeation experiments. Efforts to develop an adequate model are on their way but as yet it is not possible to quantify this process with good accuracy. For the composition where $x = 0.2$, ordering of the oxygen vacancies might be an explanation for the obtained results.

Bibliography

[1] C.H. Chen, H.J.M. Bouwmeester, R.H.E. van Doorn, H. Kruidhof and A.J. Burggraaf, *Oxygen permeation of* $La_{0.3}Sr_{0.7}CoO_{3-\delta}$, Solid State Ionics 98 (1997) 7-13.

[2] W. Sitte, E. Bucher and W. Preis, *Nonstoichiometry and transport properties of strontium-substituted lanthanum cobaltites*, Solid State Ionics 154-155 (2002) 517-522.

[3] M.H.R. Lankhorst, H.J.M. Bouwmeester and H. Verweij, *High-Temperature Coulometric Titration of* $La_{1-x}Sr_xCoO_{3-\delta}$*: Evidence for the Effect of Electronic Band Structure on Nonstoichiometry behavior*, J. Solid State Chem. 133 (1997) 555-567.

[4] J. Mizusaki, Y. Mima, S. Yamauchi and K. Fueki, *Nonstoichiometry of the Perovskite-Type Oxides* $La_{1-x}Sr_xCoO_{3-\delta}$, J. Solid State Chem. 80 (1989) 102-111.

[5] A.N. Petrov, V.A. Cherepanov, O.F. Kononchuk and L.Ya. Gagrilova, *Oxygen Nonstiochiometry of* $La_{1-x}Sr_xCoO_{3-\delta}$ $(0 < x \leq 0.6)$, J. of Solid State Chem. 87 (1990) 69-76.

[6] J. Mizusaki, *Nonstoichiometry, diffusion, and electrical properties of perovskite-type oxide electrode materials*, Solid State Ionics 52 (1992) 79-91.

[7] C.H. Chen, H. Kruidhof, H.J.M. Bouwmeester and A.J. Burggraaf, *Ionic conductivity of perovskite $LaCoO_3$ measured by oxygen permeation technique*, J. Appl. Electrochem. 27 (1997) 71-75.

[8] V.V. Kharton, E.N. Naumovich and A.V. Nilolaev, *A method to investigate oxide ionic transport for materials with high electronic conductivity*, Solid State Ionics 83 (1996) 301-307.

[9] C. Wagner and W. Schottky, *Beitrag zur Theorie des Anlaufvorganges*, Z. Phys. Chem., 1930, B11, 25-41.

[10] C. Wagner, *Equations for transport in solid oxides and sulfides of transition metals*, Prog. Solid State Chem., 1975, 10(1), 3-16.

[11] J.B. Goodenough, *Fast ionic conduction in solids*, Proc. R. Soc. Lond. A, 393 (1984) 215-234.

[12] R.H.E. van Doorn, H. Kruidhof, A. Nijmeijer, L. Winnubst and A.J. Burggraaf, *Preparation of $La_{0.3}Sr_{0.7}CoO_{3-\delta}$ perovskite by thermal decomposition of metal-EDTA complexes*, J. Mater. Chem. 8 [9] (1998) 2109-2112.

[13] L.M. van der Haar, M.W. den Otter, M. Morskate, H.J.M. Bouwmeester and H. Verweij, *Chemical diffusion and oxygen surface transfer of $La_{1-x}Sr_xCoO_{3-\delta}$ studied with electrical conductivity relaxation*, J. Electrochem. Soc. 149(3) 41-46 (2002).

Chapter Three

Catalytic Partial Oxidation (CPO) of methane: material screening/investigation

3.1 Introduction

The materials $SrCo_{0.8}Fe_{0.2}O_{3-\delta}$ and $SrCo_{0.5}FeO_{3.25}$ were used by Balachandran *et al.* [1–3] for the partial oxidation of methane. The former material exhibits a high oxygen flux in air/helium gradient but is unstable in a syngas atmosphere [2]. Pei *et al.* [4] studied the failure mechanism of this material. Two types of fractures occured, the first shortly after the reaction started and the second a few days later. The first failure was caused by a lattice mismatch across the membrane due to the imposed oxygen partial pressure gradient. The second failure was due to the large lattice expansion after partial decomposition of the $SrCo_{0.8}Fe_{0.2}O_{3-\delta}$ phase to $SrCO_3$, Co and Fe. The material $SrCo_{0.5}FeO_{3.25}$ is stable under syngas conditions and an oxygen flux of 3 ml.min^{-1}.cm^{-2} was reported at 900 °C [1]. Materials from the serie (La,Sr)(Fe,Co)$O_{3-\delta}$ have been extensively studied and their permeation behavior are well-known [5–9]. Strontium- and cobalt-rich materials in this serie often lead to a superior oxygen flux [10, 11] but their chemical stability and their stability towards reduction are relatively poor. Phase segregation occurs, leading to the formation of compounds such as $SrCO_3$, SrO, Co_2O_3 or La_2O_3. This degradation reduces the oxygen flux and can ultimately result in membrane failure [4, 12–16]. In several patents, Mazanec *et al.* [17–19] referred to the composition $La_{0.2}Sr_{0.8}Fe_{0.8}Co_{0.1}Cr_{0.1}O_{3-\delta}$ as one of the materials used by British Petroleum in their pilot plant for CPO. It was suggested that a small amount of chromium on the B-site of the perovskite structure is sufficient to both enhance the chemical stability of the parent $(La, Sr)(Fe, Co)O_{3-\delta}$ material and retain its high oxygen flux.

The literature also hints at the possibility of replacing strontium by barium on the A-site of the perovskite structure to enhance the chemical stability of the materials. The barium anions are larger than the strontium ones, respectively 161 pm and 144 pm in a 12-coordinated environment [20], therefore stabilizing the structure. Shao *et al.* [21] have investigated the material $Ba_{0.5}Sr_{0.5}Co_{0.8}Fe_{0.2}O_{3-\delta}$ in CPO conditions. At 900 °C, it exhibited an oxygen flux of 10.8 ml.min^{-1}.cm^{-2} with a $LiLaNiO_x/\gamma$-Al_2O_3 catalyst packed

on to the surface[1]. H_2-TPR experiments proved this material to be unstable in reducing atmosphere but it possessed good phase reversibility [22]. Tsai *et al.* [12,23] used the material $La_{0.2}Ba_{0.8}Co_{0.2}Fe_{0.8}O_{3-\delta}$ in a membrane reactor for syngas generation. It was successfully operated at 850 °C for more than 850 h with an oxygen flux of 4 ml.min^{-1}.cm^{-2}.
Schwartz *et al.* [24] reported in a patent the use of a brownmillerite material of composition $Sr_{1.7}La_{0.3}Ga_{0.6}Fe_{1.4}O_{5.15}$ for syngas generation. The reactor was operated for one year after which it was voluntarily terminated.
It is difficult to combine a high thermodynamical stability with a high oxygen permeability in one single material. The most stable materials reported in literature usually offers a too low oxygen flux in order to compete with the traditional autothermal reforming route. Bredesen and Sogge [25] reported in an economical analysis that for a membrane material cost of \$1600/m^2, an oxygen flux of around 10 ml.min^{-1}.cm^{-2} is needed to compete with the traditional route.
This chapter reports data on high-flux materials selected from literature, exposes a study on the influence of different dopants on the oxygen flux and the stability of related materials and presents results obtained with novel materials.

3.2 Experimental

3.2.1 Membrane synthesis

The powders were prepared by thermal decomposition of metal-EDTA (ethylene-diamine-tetra-acetic acid) complexes, a method developed by van Doorn *et al.* [26]. Commercially available metal nitrates[2,3,4] were dissolved in a mini-

[1]The membrane thickness was not explicitly mentioned.
[2]$La(NO_3)_2$, $Ba(NO_3)_2$, $Ca(NO_3)_2$ and $Co(NO_3)_2$, Merck, purity > 99 %
[3]$Fe(NO_3)_2$ and $Cr(NO_3)_2$, Merck, purity > 99.5 %
[4]$Sr(NO_3)_2$, Fluka-Acr, purity > 99 %

mum amount of water according to the stoichiometry of the targeted compositions. A range of materials was prepared, from $Ba_{0.5}Sr_{0.5}Co_{0.8}Fe_{0.2}O_{3-\delta}$ and $(La_{0.8}Ca_{0.2})_{1.01}FeO_{3-\delta}$ to $La_{0.2}A_{0.8}Fe_{1-y-z}Co_yCr_zO_{3-\delta}$ with $A = Ba$ *or* Sr, $y = 0.1$ *or* 0.2 and $z = 0$ *or* 0.1. This metal nitrates solution was added to a solution of EDTA and ammonium hydroxide in a molar ratio of 1:3 (mole perovskite : mole EDTA). The pH of the solution was maintained between 8.5 and 9 by addition of ammonia for a period of 4 h. The solution was heated and kept under airflow to help the evaporation process. It was then poured in a porcelain dish and placed in a furnace at 230 °C for at least 3 h. After evaporation of the remaining water, the pyrolysis took place. The resulting powders were calcined for 3-5 h at 900-950 °C with heating and cooling rates of 2 °C.min^{-1}. The powders were then ball-milled for 6 h in ethanol using zirconia milling balls of 1 and 10 mm in diameter. After milling, the suspension was separated from the milling balls and dried overnight in ambient air. Ceramic samples were prepared by pressing (uniaxially and subsequently isostatically at 400 MPa) powder batches into disc-shaped membranes, which were sintered at 1150-1300 °C for 10 h with heating and cooling rates of 1 °C.min^{-1}. The density of these materials was checked with the Archimedes' method using mercury. The ceramics were polished with SiC paper (1000 mesh). The final diameter of the membranes was 15 mm and the thickness ranged from 1.5 to 2 mm.

The perovskite materials containing gallium, namely $La_{1-x}Sr_xFe_{1-y}Ga_yO_{3-\delta}$ with $x = 0.2$ *or* 0.3 and $y = 0.3$ *or* 0.6, were prepared via the solid state reaction synthesis, which is, for the sake of clarity, described in detail in 4.2 on page 75.

3.2.2 Catalyst synthesis

A solution of $Ni(NO_3)_2$[1] was impregnated on α-Al_2O_3[2] and slowly dried. The resulting powder was calcinated at 900 °C for 5 h in stagnant air. It was then annealed at 700 °C for several hours in a N_2:H_2 mixture containing a few volume percent of nitrogen. The obtained catalyst has a nickel loading of 5 wt%.

3.2.3 CPO set-up

The catalytic partial oxidation of methane into syngas was performed in a quartz glass reactor at a temperature of 900 °C. A schematic drawing of this arrangement is presented in fig. 3.1.

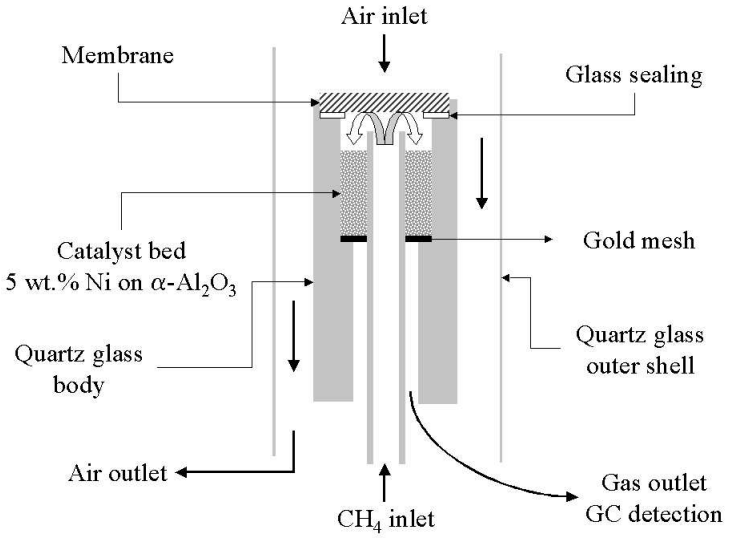

FIGURE 3.1: *Schematic representation of the quartz glass reactor.*

The samples were sealed to the reactor by means of a glass ring. The catalyst was placed downstream, at a distance of a few millimeters from the membrane surface on top of a gold mesh. One side of the membrane was exposed to air (f_{air} = 98.3 ml.min^{-1}) and the other side to either a mixture

[1]Merck, KGaA, Darmstadt, Germany
[2]AKP15, Sumimoto Chemical, Japan

of argon and methane or pure methane at various flowrates. The outlet gas on the permeate side of the membrane was directed to a gas chromatograph[1] for quantitative analysis of the reaction products. A schematic representation of the setup is presented in fig. 3.2.

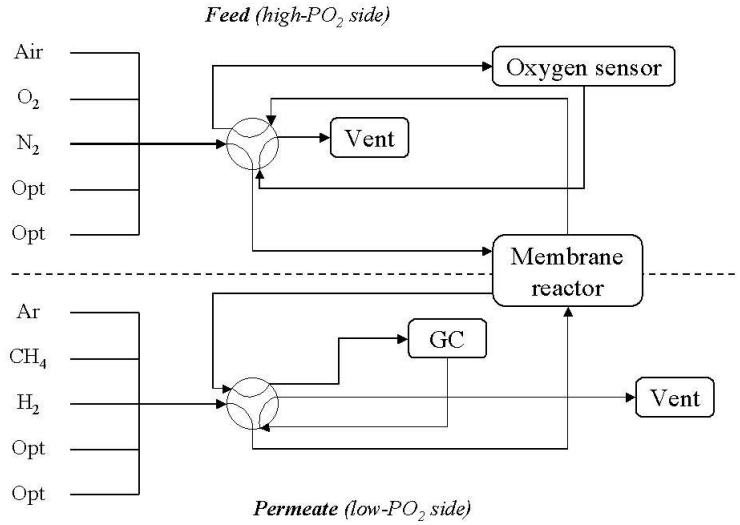

FIGURE 3.2: *Schematic representation of the CPO set-up.*

3.2.4 Calculation of the oxygen flux

The calculations presented in this section are based on a feed gas containing a mixture of methane and argon but remain valid in the case of a pure methane feed. The gas chromatograph is not equipped to detect water, which would be most harmful for the molsieve column. A backflush is therefore programmed in the detection method to get rid of any traces of water before the gas reaches the columns. A schematic representation of the flow of the different gases is shown in fig. 3.3.
The total flowrate entering the gas chromatograph, F_{GC}, can be writen as:

$$F_{GC} = F_{CO}^{out} + F_{CO_2}^{out} + F_{H_2}^{out} + F_{CH_4}^{out} + F_{ar}^{out} + F_{O_2}^{out} + F_{N_2}^{out} + F_{C_2H_4}^{out} + F_{C_2H_6}^{out} \quad (3.1)$$

[1]CP-4600 Micro Gas Chromatograph Varian

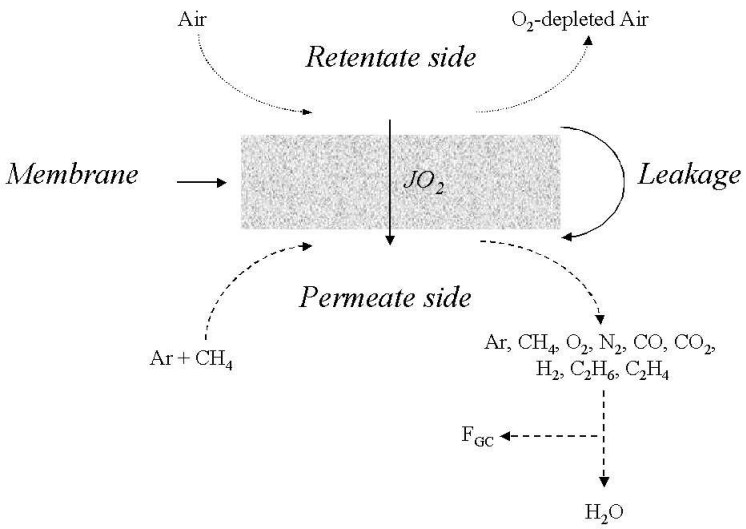

FIGURE 3.3: *Schematic representation of the different gas flows.*

Using the assumption that no carbon is formed in the reaction zone, the carbon balance gives the following relation:

$$F_{CH_4}^{in} = F_{CH_4}^{out} + F_{CO}^{out} + F_{CO_2}^{out} + 2F_{C_2H_4}^{out} + 2F_{C_2H_6}^{out} \tag{3.2}$$

Inserting eq. 3.2 into eq. 3.1, one obtains the following relation:

$$F_{GC} = F_{H_2}^{out} + F_{CH_4}^{in} + F_{ar}^{out} + F_{O_2}^{out} + F_{N_2}^{out} - (F_{C_2H_4}^{out} + F_{C_2H_6}^{out}) \tag{3.3}$$

Since argon is a sweep gas and does not participate to the reaction:

$$F_{ar}^{out} = F_{ar}^{in} \tag{3.4}$$

In addition, the flowrates of the other gases can be expressed as a function of the detected amounts, in ppm, as:

$$F_i^{out} = (ppm_i \times 10^{-6}).F_{GC} \tag{3.5}$$

where F_i^{out} and ppm_i are the flowrate and the detected amount of the gas i.

Eq. 3.3 can then be rewritten as:

$$F_{GC} = \frac{10^6(F_{CH_4}^{in} + F_{ar}^{in})}{(10^6 + ppm_{C_2H_4} + ppm_{C_2H_6}) - (ppm_{H_2} + ppm_{O_2} + ppm_{N_2})} \tag{3.6}$$

It is therefore possible to calculate the flowrate of the gas entering the gas chromatograph in each case. The flowrate of the other gases can be determined according to eq. 3.5. The flowrate of water is found using the hydrogen balance:

$$F_{H_2O}^{out} = 2F_{CH_4}^{in} - (F_{H_2}^{out} + 2F_{CH_4}^{out} + 2F_{C_2H_4}^{out} + 3F_{C_2H_6}^{out}) \tag{3.7}$$

Finally the oxygen flux through the membrane material is calculated according to the following relation:

$$J_{O_2} = \left(\frac{F_{CO}^{out}}{2} + F_{CO_2}^{out} + \frac{F_{H_2O}^{out}}{2} + F_{O_2}^{out}\right) - \left[\left(\frac{0.20986}{0.79014}\right).F_{N_2}^{out}\right] \tag{3.8}$$

It should be here noted that the different flowrates calculated above have the following unit: $ml.min^{-1}$. The permeating surface area of the membrane material is determined after the measurement and a correction factor[1] is applied to obtain the effective permeating surface area. The different fluxes can then be converted to: $mol.s^{-1}.cm^{-2}$.

3.3 Results

3.3.1 High-flux materials selected from literature

$\mathbf{Ba_{0.5}Sr_{0.5}Co_{0.8}Fe_{0.2}O_{3-\delta}}$

The catalytic partial oxidation experiment was conducted with a 2 mm-thick membrane at a temperature of 927 °C. The first part of the measurement was dedicated to obtain a stable oxygen flux with fixed gas flowrates on both sides of the membrane. The results are presented in fig. 3.4.

[1] *Calculated from a numerical solution of the steady-state diffusion equation based on Fick's second law, assuming a constant diffusion coefficient*

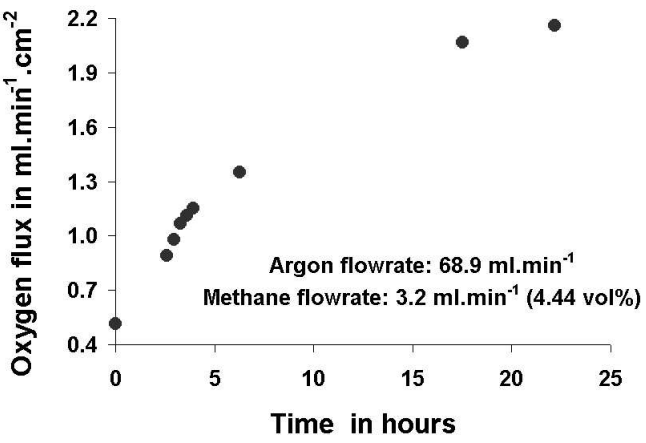

FIGURE 3.4: *Oxygen flux through a* $Ba_{0.5}Sr_{0.5}Co_{0.8}Fe_{0.2}O_{3-\delta}$ *membrane at 927 °C as a function of time.*

The oxygen flux increases continuously during the first 17 h of experiment. It then stabilizes at a value of 2.16 ml.min^{-1}.cm^{-2}. The corresponding methane conversion, H_2 and CO selectivities are shown together with the H_2:CO ratio in fig. 3.5.

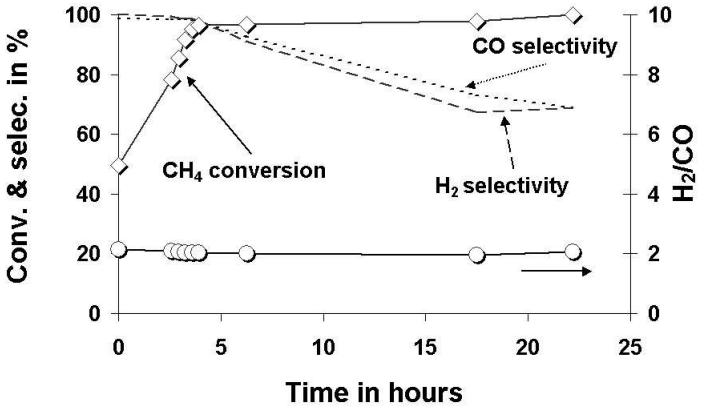

FIGURE 3.5: *Methane conversion,* H_2 *and CO selectivities and* H_2*:CO ratio as a function of time.*

In the first 5 h, the conversion of methane increases from 50 to 97 %. The corresponding H_2 and CO selectivities are close to 100 %. After 5 h of experiment, the conversion of methane is close to 100 % and remains stable. The H_2:CO ratio follows a similar trend but both the H_2 and CO selectivities are dropping to a value close to 70 %.
The second part of the measurement consisted in increasing the concentration of methane in the feed gas and measuring the corresponding oxygen flux. The results are presented in fig. 3.6.

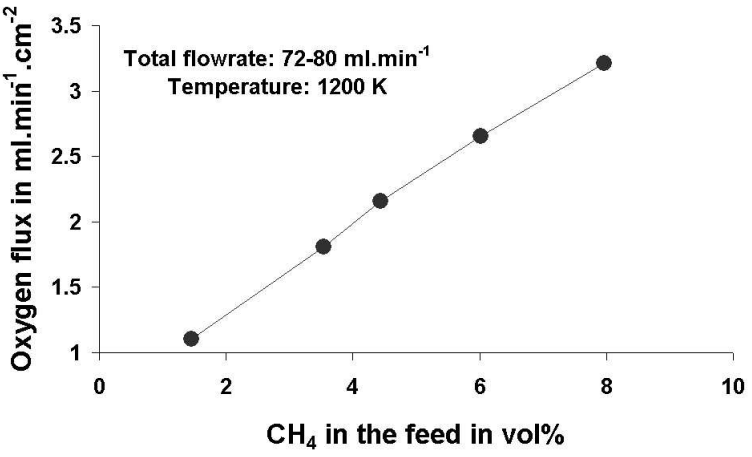

FIGURE 3.6: *Oxygen flux through a $Ba_{0.5}Sr_{0.5}Co_{0.8}Fe_{0.2}O_{3-\delta}$ membrane at 900 °C as a function of the methane content in the feed gas.*

The concentration of methane in the feed gas was brought from 1.4 to 8 vol% by increasing the methane flowrate while keeping the argon flowrate constant. The total flowrate increased accordingly from 72 to 80 ml.min^{-1}. The oxygen flux increases almost linearly from 1.1 to 3.2 ml.min^{-1}.cm^{-2}. The conversion of methane, the H_2 and CO selectivities are shown together with the H_2:CO ratio in fig. 3.7. The conversion of methane rapidly reaches 100 % and the H_2:CO ratio a value close to 2. The H_2 and CO selectivities are less than 20 % for a concentration of methane in the feed gas lower than 2 vol%, but they both increase to reach 83 % and 73 %, respectively, when the concentration of methane in the feed gas reaches 8 %.

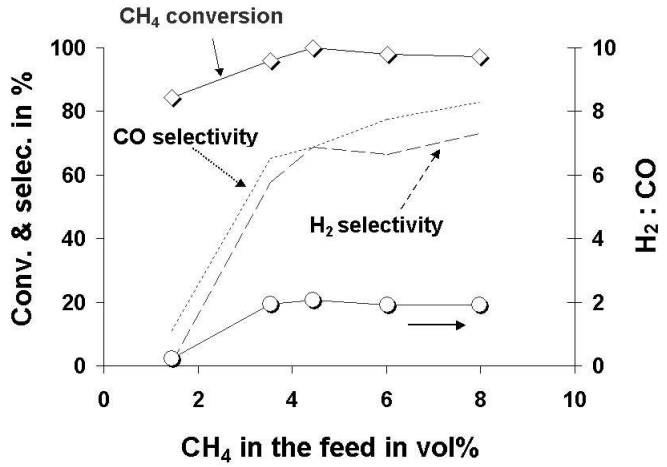

FIGURE 3.7: *Methane conversion, H_2 and CO selectivities and H_2:CO ratio as a function of the methane content in the feed gas at 900 °C.*

$\mathbf{La_{0.2}Sr_{0.8}Fe_{0.8}Co_{0.1}Cr_{0.1}O_{3-\delta}}$

The experiment was conducted with a 1.98 mm-thick membrane at 900 °C. A mixture of argon and methane was fed to the permeate side of the membrane. The argon flowrate was decreased step by step. The results are presented in fig. 3.8.

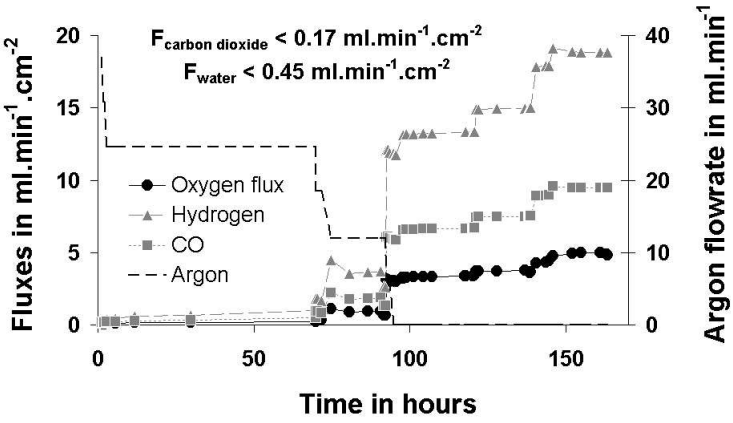

FIGURE 3.8: *Oxygen flux as a function of time obtained at 900 °C with a $La_{0.2}Sr_{0.8}Fe_{0.8}Co_{0.1}Cr_{0.1}O_{3-\delta}$ membrane.*

In the first 70 h of experiment the oxygen flux and the methane conversion are both very low. Upon decreasing the argon flowrate the oxygen flux reaches a value of 0.9 ml.min^{-1}.cm^{-2} and the conversion of methane increases to ∼60 % with CO and H_2 selectivities both in the range of 97-98 %. The methane flowrate was then increased (around 90 h). The oxygen flux increased to almost 5 ml.min^{-1}.cm^{-2} leading to a conversion of methane of almost 100 %.

3.3.2 Barium and chromium substitution

Perovskite materials doped with barium and/or chromium were investigated under different conditions for the partial oxidation of methane into syngas. A 2.2 mm-thick $La_{0.2}Ba_{0.8}Fe_{0.8}Co_{0.1}Cr_{0.1}O_{3-\delta}$ membrane was tested at 900 °C and the results are presented in fig. 3.9.

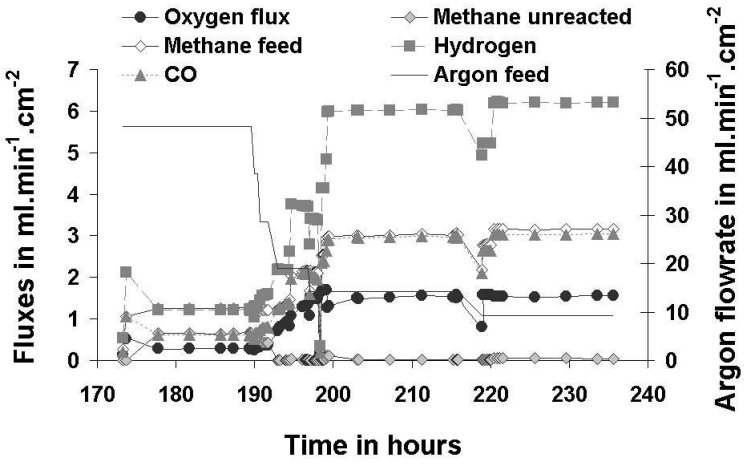

FIGURE 3.9: *$La_{0.2}Ba_{0.8}Fe_{0.8}Co_{0.1}Cr_{0.1}O_{3-\delta}$ material tested at 900 °C for syngas generation.*

The argon flow was continuously decreased while the methane flow was doubled once. When the methane content in the feed reaches a value of 4 vol% (for a total inlet flowrate of 40 ml.min^{-1}) the oxygen flux starts to increase, leading to the production of H_2 and CO in larger quantities. In the meantime, the conversion of methane increased. For a concentration of methane in the

feed gas of 23 vol%, the oxygen flux reaches a value of 1.6 ml.min^{-1}.cm^{-2}. The corresponding conversion of methane is higher than 98 % and the H_2 and CO selectivities are higher than 99 % and 97 %, respectively. The H_2:CO ratio is slightly above the expected value of 2.

Two other materials, $La_{0.2}Sr_{0.8}Fe_{0.9}Co_{0.1}O_{3-\delta}$ and $La_{0.2}Ba_{0.8}Fe_{0.9}Co_{0.1}O_{3-\delta}$, were tested under similar conditions. The results are presented in table 3.1. The oxygen fluxes presented in table 3.1 were obtained for a methane content in the feed gas of 20 vol%. After correcting for the difference in thickness, assuming that bulk diffusion is the limiting process for the transport of oxygen, the strontium-containing material exhibits an oxygen flux ∼1.5 times higher than the barium-containing material.

Composition	$\mathbf{La_{0.2}Ba_{0.8}Fe_{0.9}Co_{0.1}O_{3-\delta}}$	$\mathbf{La_{0.2}Sr_{0.8}Fe_{0.9}Co_{0.1}O_{3-\delta}}$
Temperature	900°C	900°C
Catalyst	Ni on alumina	Ni on alumina
Thickness	2.2 mm	1.6 mm
Maximum oxygen flux	2.76 ml.min^{-1}.cm^2 (CH_4 ~ 20 vol%)	5.5 ml.min^{-1}.cm^2 (CH_4 ~ 20 vol%)
CH_4 conversion	> 99 %	> 99 %
CO selectivity	93 %	74 %
H_2 selectivity	94 %	86 %
Remarks	Stopped due to leakage	Leakage after 100 h

TABLE 3.1: *Influence of the type of dopant on the A-sublattice of a perovskite material in CPO experiments.*

The composition $La_{0.2}Sr_{0.8}Fe_{0.8}Co_{0.2}O_{3-\delta}$ was also investigated. The results are presented in figs. 3.10 and 3.11. The experiment was started with a mixture of argon and methane on the permeate side of the membrane. The argon flow was decreased step by step until it reached a value of 41.5 ml.min^{-1}, while the methane flow was kept constant at a value of 6.8 ml.min^{-1}. The oxygen flux started to increase when the methane content in the feed gas reached a value of 11 vol%, for a total flowrate of 62 ml.min^{-1}. The maximum oxy-

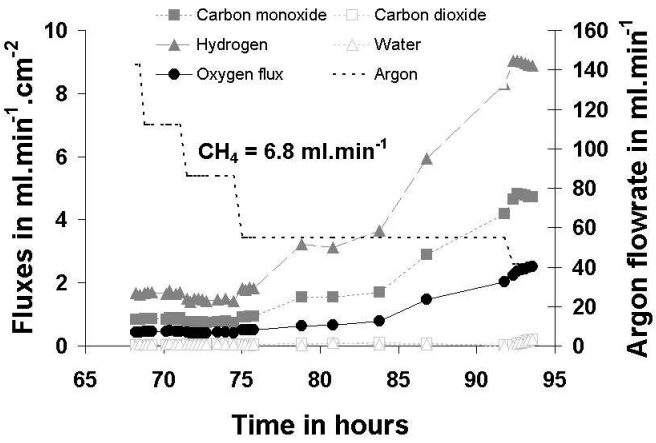

FIGURE 3.10: *$La_{0.2}Sr_{0.8}Fe_{0.8}Co_{0.2}O_{3-\delta}$ material tested at* 900 °*C for CPO.*

gen flux, 2.5 ml.min^{-1}.cm^{-2}, was obtained for a concentration of methane of 14 vol% (total flowrate of 48 ml.min^{-1}) before the membrane cracked.

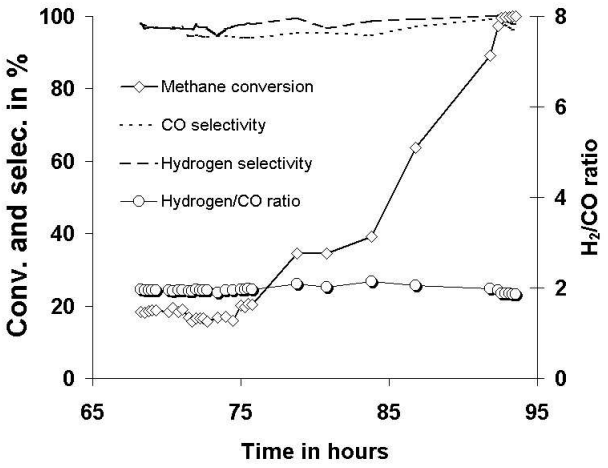

FIGURE 3.11: *Conversion of methane, H_2 and CO selectivities and H_2:CO ratio as a function of time for a $La_{0.2}Sr_{0.8}Fe_{0.8}Co_{0.2}O_{3-\delta}$ membrane tested at* 900 °*C for CPO.*

The H_2:CO ratio was close to the value of 2 and the H_2 and CO selectivities were equal to 97 % and 95 %, respectively. The conversion of methane is constantly increasing from 18 % to a value close to 100 %.

3.3.3 New materials

Other types of perovskite compositions were also investigated. The material $(La_{0.8}Ca_{0.2})_{1.01}FeO_{3-\delta}$ was tested for CPO at a temperature of 900 °C. The results obtained are presented in fig. 3.12.

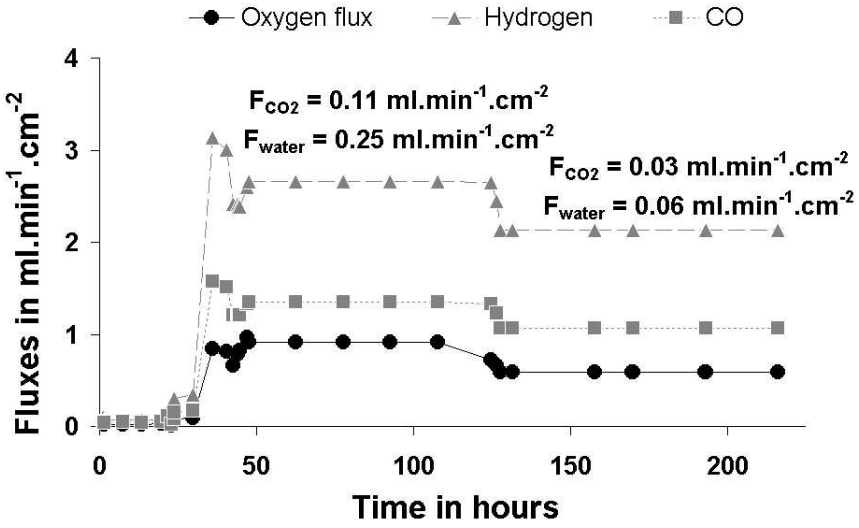

FIGURE 3.12: *Oxygen flux through a* $(La_{0.8}Ca_{0.2})_{1.01}FeO_{3-\delta}$ *membrane at 900 °C as a function of time.*

A mixture of argon and methane was fed on the permeate side of the membrane. The flowrate of argon was decreased in a stepwise fashion until the feed gas was exclusively composed of methane. A constant oxygen flux of 0.6 ml.min^{-1}.cm^{-2} was obtained for a membrane thickness of 1.51 mm. The conversion of methane was 94 % and the selectivities of CO and H_2 were 98 % and 97 %, respectively.

Materials containing gallium on the B-site, such as $La_{0.8}Sr_{0.2}Ga_{0.6}Fe_{0.4}O_{3-\delta}$ and $La_{0.7}Sr_{0.3}Fe_{0.7}Ga_{0.3}O_{3-\delta}$, were also investigated and the results are presented in figs. 3.13 and 3.14, respectively. A mixture of argon and methane was fed to the low-P_{O_2} side of the $La_{0.8}Sr_{0.2}Ga_{0.6}Fe_{0.4}O_{3-\delta}$ membrane. The argon flow was decreased step by step and the methane flow increased with time. The oxygen flux increases slightly and the H_2 and CO selectivities are

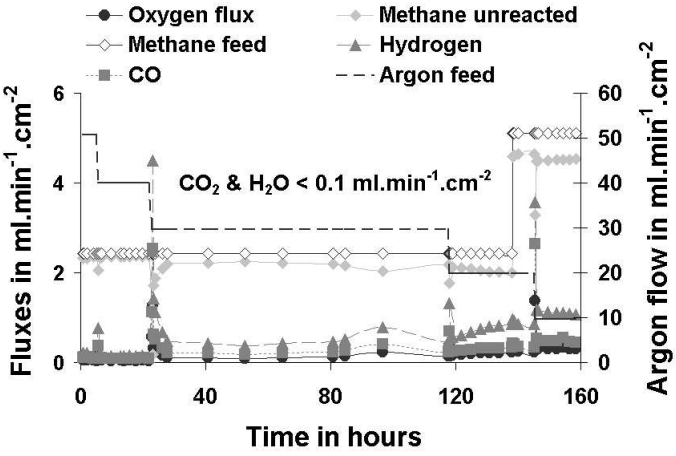

FIGURE 3.13: *$La_{0.8}Sr_{0.2}Ga_{0.6}Fe_{0.4}O_{3-\delta}$ material tested at 900 °C for CPO.*

both in the range of 95 %, but the conversion of methane remains below 30 %. The maximum oxygen flux obtained was 1.6 ml.min^{-1}.cm^{-2} at 900 °C for a membrane thickness of 1.8 mm. An identical procedure was applied to a

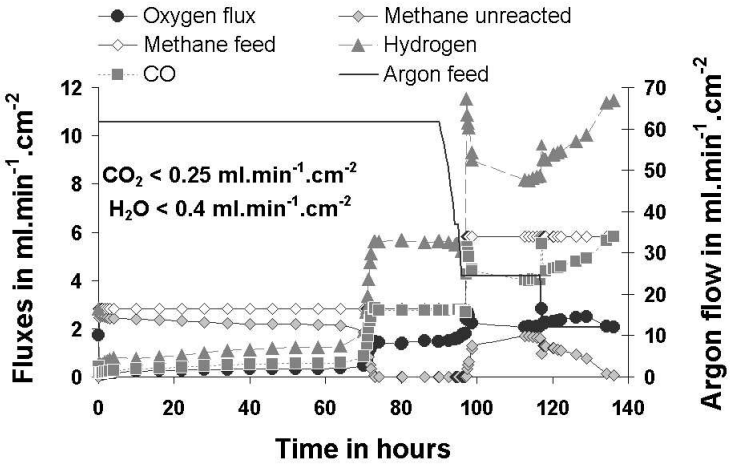

FIGURE 3.14: *$La_{0.7}Sr_{0.3}Fe_{0.7}Ga_{0.3}O_{3-\delta}$ material tested at 900 °C for CPO.*

1.45 mm-thick membrane with the composition $La_{0.7}Sr_{0.3}Fe_{0.7}Ga_{0.3}O_{3-\delta}$ (cf. fig. 3.14). An oxygen flux of 2.5 ml.min^{-1}.cm^{-2} was obtained with a methane content in the feed gas of 33 vol% (total flowrate: 20 ml.min^{-1}). The H_2 and CO selectivities were both around 99 % and the H_2:CO ratio was 2.

3.4 Discussion

3.4.1 Membrane and catalyst activation

As can be seen from figs. 3.4 and 3.8, a certain amount of time is needed before the system reaches equilibrium. This behaviour is due to two mechanisms, the activation of the catalyst on one hand and the response time of the material to a new gas environment with a different oxygen partial pressure on the other hand.

At the beginning of the experiment the catalyst will be in its oxidized state because of the sealing procedure, which involves heating the reactor to a pre-defined temperature (depending on the type of glass sealing used) and subsequently cooling to the measurement temperature. During this procedure the membrane is exposed to ambient air to avoid any additional stress due to the presence of an oxygen chemical potential gradient. The nickel oxide has to be reduced to act as a catalyst in the partial oxidation of methane. This can be done by feeding hydrogen but it could prove to be too reducing an atmosphere for the membrane material to withstand. The preferred strategy is to feed a mixture of argon and methane and then to slowly decrease the argon flow, thus decreasing the total flowrate (i.e. increasing the residence time) and increasing the concentration of methane in the feed gas. The oxygen partial pressure on the permeate side of the membrane will decrease and the nickel oxide will be reduced. The conversion of methane to syngas will thus increase, reducing the partial pressure of oxygen even further. The oxygen flux through the membrane will then increase as depicted in fig. 3.8 between 50 h and 100 h.

In fig. 3.4 the time to reach equilibrium is more than 20 h. Shao *et al.* [22] reported a value of less than 21 h for the same material under similar conditions. The membrane performances are compared in table 3.2. The oxygen flux reported in literature is twice as large as the one obtained in this study. This could nevertheless be explained by a higher concentration of methane in the feed gas, a different flowrate of the feed gas, the use of a thinner material

or a different positioning of the catalyst in the reactor. Under the assumption that the transport of oxygen is mainly determined by the bulk diffusion, the expected oxygen flux for a 1 mm-thick membrane is 10.1 $ml.min^{-1}.cm^{-2}$ based on the results obtained in this study.

	Literature	***This study***
Temperature	850 °C	900 °C
Thickness	-	2 mm
Catalyst	LiLaNiO/γ-Al_2O_3	Ni/α-Al_2O_3
Feed	Diluted methane	35 vol% of CH_4
CH_4 conversion	98.5 %	99.5 %
CO selecectivity	93 %	73 %
H_2 selecectivity	-	66 %
H_2/CO	-	1.84
JO_2 max.	10.45 $ml.min^{-1}.cm^{-2}$	5.05 $ml.min^{-1}.cm^{-2}$

TABLE 3.2: *Comparison of the performances of a $Ba_{0.5}Sr_{0.5}Co_{0.8}Fe_{0.2}O_{3-\delta}$ membrane used for CPO.*

Four time coordinates were chosen in fig. 3.5 to thermodynamically calculate the equilibrium compositions of the gas mixtures obtained with the experimental CH_4:O_2 ratios. The results are presented in table 3.3.

Time in hours	**0**	**2.5**	**3.9**	**17.5**
CH_4 feed in $ml.min^{-1}$	3.2	3.2	3.2	3.2
JO_2 in $ml.min^{-1}$	0.72	1.25	1.62	2.9
CH_4 conversion	45 %	78 %	97.6 %	99 %
CO selectivity	99.9 %	99.9 %	98.9 %	76 %
H_2 selectivity	99.9 %	99.9 %	98.7 %	71.4 %
H_2/CO	2	2.03	2	1.87

TABLE 3.3: *Determination of the thermodynamic equilibrium composition of different CH_4:O_2 experimental mixtures at 900 °C. Time coordinates chosen from fig. 3.5.*

Good agreement is found between the experimental values of the conversion of methane, the H_2 and CO selectivities and the H_2:CO ratio from fig. 3.5

and the thermodynamically predicted values in table 3.3. This also indicates that a sufficient amount of catalyst was used during this experiment. In the first few hours of reaction, there is an excess of methane when compared with the stoichiometry of the partial oxidation reaction, which explains the low conversion. Since the oxygen flux keeps increasing (cf. fig. 3.4), the system eventually reaches the point where all the methane is converted to syngas (time coordinate of 3.9 h in table 3.3). But the still increasing oxygen flux leads to the formation of CO_2 and H_2O, therefore decreasing both the H_2 and CO selectivities.

In fig. 3.6, the oxygen flux increases almost linearly with the concentration of methane in the feed gas, at least in the range investigated, i.e. from 1.4 to 8 vol%. The conversion of methane is indeed found increasing, together with the H_2 and CO selectivities (cf. fig 3.7). The oxygen flux through this material is proportional to the concentration of methane in the feed gas in a linear relation for methane loading smaller than 10 vol%.
The maximum oxygen flux obtained with $La_{0.2}Sr_{0.8}Fe_{0.8}Co_{0.1}Cr_{0.1}O_{3-\delta}$ with a conversion of methane of around 100 % is 5 ml.min^{-1}.cm^{-2} at 900 °C for a membrane thickness of 1.98 mm. This value is three times smaller than that reported by Mazanec *et al.* [17]. In this case as well, the details of the rector design and catalyst type are not explicitely given in the patent. It is therefore not possible to compare directly the magnitude of the oxygen fluxes. After the CPO experiment, the membrane was brought back to a milder oxygen chemical potential gradient consisting of air and helium, keeping the operating temperature constant at 900°C. The magnitude of the obtained oxygen flux was identical to the one obtained before the CPO experiment when the gas-thighness was checked. This indicates that the membrane did not suffer irreversible changes in its structure (membrane degradation) during the syngas generation experiment.

3.4.2 Influence of barium

The performance of two similar materials, $La_{0.2}Sr_{0.8}Fe_{0.8}Co_{0.1}Cr_{0.1}O_{3-\delta}$ and $La_{0.2}Ba_{0.8}Fe_{0.8}Co_{0.1}Cr_{0.1}O_{3-\delta}$, are compared in table 3.4.

Composition	$La_{0.2}Sr_{0.8}Fe_{0.8}Co_{0.1}Cr_{0.1}O_{3-\delta}$	$La_{0.2}Ba_{0.8}Fe_{0.8}Co_{0.1}Cr_{0.1}O_{3-\delta}$
Temperature	900 °C	900 °C
Catalyst	Ni on α-Al_2O_3	Ni on α-Al_2O_3
Thickness	1.85 mm	1.95 mm
Oxygen flux	3.5 ml.min^{-1}.cm^2 (CH_4 ~ 33%)	1.6 ml.min^{-1}.cm^2 (CH_4 ~ 25%)
CH_4 conversion	> 98 %	> 98 %
CO selectivity	> 99 %	97 %
H_2 selectivity	> 99 %	98 %
H_2/CO	~2	~2
Remarks	350 h on duty	Leakage after 240 h

TABLE 3.4: *Influence of the substitution of barium for strontium on the performance of a membrane in CPO experiments at 900 °C.*

Despite the small difference in membrane thickness and concentration of methane in the feed gas, it is clear that, under similar conditions, the barium-containing material exhibits a lower oxygen flux. This could be attributed to the relative size of the strontium and barium ions, as mentionned in the introduction. It is indeed known from literature [27] that the oxygen ions transport occurs via a curved route around the BO_6 octahedron edge through a saddle-point, or critical radius [28], defined by two A-site ions and one B-site ion. The larger the A-site ions the smaller the opening of this triangle and the more difficult it is for the oxygen anions to pass through it. The larger barium ions will therefore hinder the transport of oxygen. After correcting for the difference of thickness, and assuming a linear relation between the magnitude of the oxygen flux and the concentation of methane in the feed gas, the oxygen flux obtained for $La_{0.2}Ba_{0.8}Fe_{0.8}Co_{0.1}Cr_{0.1}O_{3-\delta}$ is roughly 1.6 times smaller than with $La_{0.2}Sr_{0.8}Fe_{0.8}Co_{0.1}Cr_{0.1}O_{3-\delta}$. This value is very close to the one derived from the results presented in table 3.1, where a similar effect can be seen.

3.4.3 Influence of chromium

By comparing the following compositions, i.e. $La_{0.2}Sr_{0.8}Fe_{0.8}Co_{0.1}Cr_{0.1}O_{3-\delta}$, $La_{0.2}Sr_{0.8}Fe_{0.8}Co_{0.2}O_{3-\delta}$ and $La_{0.2}Sr_{0.8}Fe_{0.9}Co_{0.1}O_{3-\delta}$, it is possible to evaluate the influence of chromium doping on the B-site of the perovskite structure. The results obtained with the three above mentionned compositions are presented in table 3.5.

Composition	*LSFCCr*	*LSFC I*	*LSFC II*
Temperature	900 °C	900 °C	900 °C
Catalyst	Ni on α-Al_2O_3	Ni on α-Al_2O_3	Ni on α-Al_2O_3
Thickness	1.85 mm	1.6 mm	1.95 mm
Oxygen flux	5.2 ml.min^{-1}.cm^{-2} (pure methane)	5.5 ml.min^{-1}.cm^{-2} (CH_4 ~ 20 %)	2.52 ml.min^{-1}.cm^{-2} (CH_4 ~ 7.8 %)
CH_4 conversion	> 98 %	> 99 %	> 99 %
CO selectivity	> 99 %	74 %	96 %
H_2 selectivity	> 99 %	86 %	98 %
Remarks	350 h on duty	Leakage after 100 h	Cracked after 95 h

TABLE 3.5: *Influence of the substitution of chromium by iron or cobalt on the performance of a membrane in CPO experiments at 900°C. LSFCCr stands for $La_{0.2}Sr_{0.8}Fe_{0.8}Co_{0.1}Cr_{0.1}O_{3-\delta}$, LSFC I for $La_{0.2}Sr_{0.8}Fe_{0.9}Co_{0.1}O_{3-\delta}$ and LSFC II for $La_{0.2}Sr_{0.8}Fe_{0.8}Co_{0.2}O_{3-\delta}$.*

When chromium is replaced by iron (*LSFC I*), the same oxygen flux is obtained with a concentration of methane in the feed of only 20 vol%. For the same methane loading the chromium-containing material exhibits an oxygen flux of around 1 ml.min^{-1}.cm^{-2}, about 5 times lower than *LSFC I*. In this case, the conversion of methane was about 60 %, meaning that the equilibrium may not have been reached although these conditions were maintained for as long as 15 h. The material containing 20 % of cobalt on the B-site (*LSFC II*) has an oxygen flux of 2.52 ml.min^{-1}.cm^{-2}, half of the values presented for the other two materials in table 3.5. But this value is obtained with only 7.8 vol% of methane in the feed gas. It is reasonable to expect that

this cobalt-rich material would exhibit the highest oxygen flux in the serie under consideration. Unfortunately, this material is not stable under syngas conditions and repeatedly cracked during the experiments.

3.4.4 New materials

The calcium-containing material exhibits a low oxygen flux when compared with other types of membranes presented in this work (cf. fig. 3.12). Similar compositions were mentioned in a patent from Dyer *et al.* [29]. For the specific composition $(La_{0.8}Ca_{0.2})_{1.01}FeO_{3-\delta}$, they report an oxygen flux slightly larger than 1 ml.min^{-1}.cm^{-2} for a membrane thickness of 0.5 mm at the most. Considering the difference of operating conditions (gas flowrates, reactor design, type and position of the catalyst), the value reported in this study is in the same range of magnitude. Compositions with higher calcium contents were doped with cobalt and tested for the production of syngas [30]. The oxygen flux was found to increase with the cobalt doping but the stability of the membrane varied in the opposite direction. A stable oxygen flux of 1.2 ml.min^{-1}.cm^{-2} was obtained with the composition $La_{0.4}Ca_{0.6}Fe_{0.75}Co_{0.25}O_{3-\delta}$ at 900 °C under conditions similar to those of syngas production. A possible explanation for this low oxygen flux is the lattice stress introduced by the calcium cation. In the cubic closest packing of the ideal perovskite structure, the A-site cation and the oxygen anion should be equal in size, i.e. the radius of the A-site cation should be around 140 pm or slightly higher [31]. The Ca^{2+} cation has a radius of 134 pm (coordination 12) according to Shannon *et al.* [20] (144 pm for the Sr^{2+}). Since this difference is small, other parameters are certainly playing an important role. Nevertheless higher oxygen fluxes were obtained with other membrane compositions and the calcium-containing material was not selected for further investigations.

An oxygen flux of 1 ml.min^{-1}.cm^{-2} was reported [32] for the composition $La_{0.8}Sr_{0.2}Ga_{0.6}Fe_{0.4}O_{3-\delta}$ at 1000 °C. Under similar conditions (membrane

thickness, concentration of methane in the feed gas), the results obtained in this study are in the same range of magnitude (see fig. 3.13). In this case as well, the oxygen flux appears limited, even though a pure methane feed was used in the CPO experiment. This could be due to a too small concentration of dopant on the A-site. Increasing the concentration of strontium would increase the concentration of oxygen vacancy and therefore the ionic conductivity. Since Ga^{3+} has a fixed oxidation number, increasing the iron content would be beneficial for the concentration of electronic charge carriers.
The results obtained with $La_{0.7}Sr_{0.3}Fe_{0.7}Ga_{0.3}O_{3-\delta}$ confirm this line of reasonning. The oxygen flux obtained is much higher, as can be seen in fig. 3.14. Such a high oxygen flux, obtained with only 30 % of strontium on the A-site of the perovskite structure, could be (partly) explained by the near-zero value found for the binding energy of the strontium-vacancy pair in $LaGaO_3$ [27]. This material was observed visually after the CPO experiments and seems more stable (less color change) than many of the materials under consideration. The two parent compositions, $LaGaO_3$ and $LaFeO_3$ are very stable under reduced oxygen partial pressure. This $La_{0.7}Sr_{0.3}Fe_{0.7}Ga_{0.3}O_{3-\delta}$ composition is therefore seen as the best candidate material for industrial applications and its stability will be investigated in the next chapter in more detail.

3.5 Conclusions

A number of different perovskite materials were investigated for the partial oxidation of methane to syngas. A majority of them are potential candidates for industrial applications based on a flux threshold of 10 $ml.min^{-1}.cm^{-2}$ [25] because of the range of thicknesses used in this study, making it reasonable to expect a significant increase in the magnitude of the oxygen flux when the membrane thickness is reduced by a factor two or more.
Nevertheless a number of materials have proven to be unstable under the reducing conditions associated with CPO. It is indeed difficult to evaluate

quantitatively the stability of a material. H_2-TPR experiments have been conducted by a number of research groups to evaluate the stability of materials. Unfortunately, this does not mimic the actual situation where a material is experiencing an oxygen chemical potential gradient, i.e. oxygen is being transported through it. Based only on the magnitude of the oxygen flux, the most promising candidates have the following compositions:

- $La_{0.2}Sr_{0.8}Fe_{0.8}Co_{0.1}Cr_{0.1}O_{3-\delta}$
- $La_{0.2}Sr_{0.8}Fe_{0.9}Co_{0.1}O_{3-\delta}$
- $Ba_{0.5}Sr_{0.5}Co_{0.8}Fe_{0.2}O_{3-\delta}$
- $La_{0.7}Sr_{0.3}Fe_{0.7}Ga_{0.3}O_{3-\delta}$

With stability considerations in mind, the gallium-containing material seems the most suited for the production of syngas from natural gas. The other materials could be used if protected, as described later in *Chapter 6*.

Bibliography

[1] U. Balachandran, J.T. Dusek, S.M. Sweeney, R.B. Poeppel, R.L. Mieville, P.S. Mayia, M.S. Kleefish, S.Pei, T.P. Kobylinski, C.A. Udovich and A. Bose, *Methane to Syngas via Ceramic Membranes*,Am. Ceram. Soc. Bull. 74 (1995) 71.

[2] U. Balachandran, J.T. Dusek, R.L. Mieville, R.B. Poeppel, M.S. Kleefish, S. Pei, T.P. Kobylinski, C.A. Udovich and A.C. Bose, *Dense ceramic membranes for partial oxidation of methane to syngas*, Appl. Catal. A-Gen. 133 (1995) 19.

[3] U. Balachandran, J.T. Dusek, P.S. Mayia, B. Ma, R.L. Mieville, M.S. Kleefish and C.A. Udovich, *Ceramic membrane reactor for converting methane to syngas*, Catal. Today 36 (1997) 265.

[4] S. Pei, M.S. Kleefisch, T.P. Kobylinski, J. Faber, C.A. Udovich, V. Zhang-McCoy, B Dabrowski, U. Balachandran, R.L. Mieville and R.B. Poeppel, *Failure mechanisms of ceramic membrane reactors in partial oxidation of methane to synthesis gas*, Catal. Lett. 30 (1995) 201.

[5] G. Ch. Kostogloudis and Ch. Ftikos, *Properties of A-site defficient* $La_{0.6}Sr_{0.4}Co_{0.2}Fe_{0.8}O_{3-\delta}$*-based perovskite oxides*, Solid State Ionics 126 (1999) 143.

[6] P.S. Mayia and U. Balachandran, *Oxygen transport by oxygen potential gradient in dense ceramic oxidic membranes*, Solid State Ionics 99 (1999) 1.

[7] A.G. Dixon and Y.H. Ma, *Waste reduction and recovery using* O_2-permeable *membrane reactors*, Ind. Eng. Chem. Res. 33 (1994) 3015.

[8] S. Li, W. Jin, N. Xu and J. Shi, *Synthesis and permeation properties of* $La_{0.2}Sr_{0.8}Co_{0.2}Fe_{0.8}O_{3-\delta}$ *membranes*, Solid State Ionics 124 (1999) 161.

[9] W.L. Warren, K. Vanheusdan, D. Dimos and B.A. Tuttle, *Oxygen vacancy motion in perovskite oxides*, J. Am. Ceram. Soc. 79 (1996) 536.

[10] Y. Teraoka, T. Nobunaga and N. Yamazoe, *Effect of cation substitution on the oxygen semipermeability of perovskite-type oxides*, Chem. Let. 3 (1988) 503.

[11] A.N. Ezin, E.Kh. Kurumchin, I.V. Murygin, V.I. Tsidilkovski and G.K. Vdovin, *The types of surface exchange and diffusion of oxygen in* $La_{0.7}Sr_{0.3}CoO_{3-\delta}$, Solid State Ionics 112 (1998) 117.

[12] C.Y. Tsai, A.G. Dixon and Y.H. Ma, *Dense perovskite* $La_{1-x}A_xFe_{1-y}Co_yO_{3-\delta}$ *(A=Ba,Sr,Ca) Membrane Synthesis, Application and Characterization*, J. Am. Ceram. Soc. 81 (1998) 1437.

[13] S.J. Xu and N. Li, *Perovskite type oxide materials for the oxidative coupling of methane*, AIChE J. 43 (1997) 2731.

[14] A.A. Yaremchenko and V.V. Kharton, *Oxygen permeability of perovskite type* $BaBi_{1-x}La_xO_{3-\delta}$, Mater. Res. Bull. 33 (1999) 1027.

[15] V.V. Kharton, A. Yaremchenko, A. Kovalevsky, A. Viskup and P. Kerko, *Perovskite-type oxides for high temperature oxygen separation membranes*, J. Membrane Sci. 163 (1999) 307.

[16] N. Xu, S. Li, W. Jin, J. Shi and Y.S. Lin, *Experimental and modeling study on tubular dense membranes for oxygen permeation*, AIChE J. 45 (1999) 2519.

[17] T. Cable and T. Mazanec, *Process for the partial oxidation of hydrocarbons*, U.S. Patent 5,714,091 (1998).

[18] T. Cable, J. Frye, W. Kliewer and T. Mazanec, *Solid multi-components membranes, electrochemical reactor components, electrochemical reactors and use of membranes, reactor components, and reactor for oxidation reactions*, U.S. Patent 5,744,015 (1998).

[19] T. Cable and T. Mazanec, *Oxygen mixed conduction membranes*, U.S. Patent 5,788,748 (1998).

[20] R.D. Shannon, *Revised Effective Ionic Radii and Systematic Studies of Interatomic Distances in Halides and Chalcogenides*, Acta Crystallogr. A32 (1976) 751.

[21] Z. Shao, G. Xiong, H. Dong, W. Yang and L. Lin, *Synthesis, oxygen permeation study and membrane performance of a $Ba_{0.5}Sr_{0.5}Co_{0.8}Fe_{0.2}O_{3-\delta}$ oxygen-permeable dense ceramic reactor for partial oxidation of methane to syngas*, Sep. Purif. Technol. 25 (2001) 97-116.

[22] Z. Shao, H. Dong, G. Xiong, Y. Cong and W. Yang, *Performance of a mixed-conducting ceramic membrane reactor with high oxygen permeability for methane conversion*, J. Membrane Sci. 183 (2000) 181-192.

[23] C.Y. Tsai, A.G. Dixon, W.R. Moser and Y.H. Ma, *Dense perovskite membrane reactors for partial oxidation of methane to syngas*, AIChE J. 43 (1997) 2741.

[24] J.H. White, A.F. Sammells and M. Schwartz, *Catalytic membrane reactor with two components three-dimensional catalysis*, International patent WO9921649 (1999).

[25] R. Bredesen and J. Sogge, Paper presented at: The United Nations Economic Commission for Europe Seminar on Ecological Applications of Innovative Membrane Technology in Chemical Industry, Chem./Sem. 21/R.12, 1-4 May 1996, Cetaro, Calabria, Italy.

[26] R.H.E. van Doorn, H. Kruidhof, A. Nijmeijer, L. Winnubst and A.J. Burggraaf, *Preparation of $La_{0.3}Sr_{0.7}CoO_{3-\delta}$ perovskite by thermal decomposition of metal-EDTA complexes*, J. Mater. Chem. 8 [9] (1998) 2109-2112.

[27] M.S. Islam, *Computer modelling of defects and transport in perovskite oxides*, Solis State Ionics 154-155 (2002) 75-85.

[28] J.A. Kilner and R.J. Brook, , Solid State Ionics 6 (1982) 237.

[29] Dyer *et al.*, *Mixed Conducting Membranes for Syngas Production*, U.S. Patent 6,492,290 (2002).

[30] S. Diethelm, J. van Herle, P.H. Middleton and D. Favrat, *Oxygen permeation and stability of $La_{0.4}Ca_{0.6}Fe_{1-x}Co_xO_{3-\delta}$ (x = 0, 0.25, 0.5) membranes*, J. Power Sources 5229 (2003) 1-6.

[31] M. Mogensen, D. LyBye, N. Bonanos, P.V. Hendriksen and F.W. Poulsen, *Factors controlling the oxide ion conductivity of fluorite and perovskite structured oxides*, Solid State Ionics 174 (2004) 279-286.

[32] T. Ishihara and Y. Takita, *Partial oxidation of methane into syngas with oxygen permeating ceramic membrane reactors*, Catal. Surv. JPN 4 (2000) No. 2.

Chapter Four

Investigation of the stability and performance of $La_{0.7}Sr_{0.3}Fe_{0.7}Ga_{0.3}O_{3-\delta}$

4.1 Introduction

A major concern for the application of perovskite membranes for the catalytic partial oxidation of methane is their thermodynamic stability [1–4]. The large oxygen chemical potential gradients combined with high temperatures are favorable conditions for the degradation of the membrane material. Reduction of the perovskite material, phase transformation or kinetic demixing are examples of the different processes that can lead to membrane degradation and ultimately failure of operation [5–7].

New materials withstanding these harsh conditions and exhibiting a reasonably high oxygen flux, i.e. economically enabling the CPO technology [8], are therefore needed. The quest for such materials has recently taken a new course. While the first attempts were based on the stabilization of well-known high-flux materials, such as barium or chromium doping in the serie (La,Sr)(Fe,Co)$O_{3-\delta}$ as discussed in the previous chapter, a different approach is to introduce electronic conductivity in a (stable) ionic conductor [9–14]. This type of materials is used as electrolyte in Solid Oxide Fuel Cells (SOFC). Improving the long-term performances of such devices can be achieved by reducing their operating temperature, which involves new electrolyte materials with improved oxygen transport properties. The operating conditions and requirements associated with the electrolyte materials in SOFC are very similar to the ones faced by a MIEC membrane for syngas generation. The materials used as electrolytes in SOFC are therefore of interest for the partial oxidation of methane.

The perovskite composition $LaGaO_{3-\delta}$ is a pure ionic conductor and it is possible to enhance its conduction properties by doping the B-sublattice with magnesium. The electron transference number of $LaGa_{0.85}Mg_{0.15}O_{3-\delta}$ at oxygen partial pressures ranging from 10 to 1.01×10^5 Pa does not exceed 0.08 [9]. Increasing the number of oxygen vacancies, which in turn would increase the ionic conductivity of such materials, is achieved by doping with strontium on the A-sublattice. The highest (mainly ionic) conductivity for $La_{0.8}Sr_{0.2}Ga_{0.83}Mg_{0.17}O_{3-\delta}$ at 800 °C was found to be 0.17 S.cm^{-1} [15].

This level of ionic conductivity is sufficient to compete with state-of-the-art yttria-stabilized zirconia (8YSZ) and these materials are thus potentially applicable for the partial oxidation of methane into syngas, on the condition that their electronic conduction is enhanced. A number of authors have followed this direction of research by doping these mainly ionic conductors with late transition metals on the B-sublattice, such as Co, Ni, Cr or Fe [16–18]. It was found that the total conductivity was dependent on the type of dopant according to the following order: Co > Ni > Fe > Cr [14, 17]. The conductivity of the chromium doped material was too low for it to be used in syngas generation experiments [17]. The nickel and cobalt doped materials both show signs of poor stability at reduced oxygen partial pressures [14]. The iron doped material was therefore chosen for an extensive study of its behavior and performances under CPO conditions.

4.2 Experimental

The powder was prepared via the solid state reaction. $La_2(CO_3)_3,\ x\,H_2O$[1] and $Sr(CO_3),\ x\,H_2O$[2] were first annealed in stagnant air at 900 °C with heating and cooling rates of 2 °C.min^{-1}. Stoichiometric amounts of Fe_2O_3[1], Ga_2O_3[1] and the previously obtained La_2O_3 and SrO were ball-milled in ethanol at 200 rpm for 30 min in a planetary ball-miller[3]. The mixture was dried overnight in ambient air. It was then calcined at 1100 °C in stagnant air for 5 h with heating and cooling rates of 2 °C.min^{-1}. The obtained powder was then ball-milled on a roller-bench[4] for 6 h in ethanol using zirconia milling balls of 1 and 10 mm in diameter. After milling, the suspension was separated from the milling balls and dried overnight in ambient air. The powder was calcined a second time at 1150 °C in stagnant air for 5 h with

[1]Aldrich, purity: > 99.9 %

[2]Merck, purity: > 99 %

[3]Pulverisette 5, FRITSCH GmbH, Idar-Oberstein, Germany

[4]Leroy Somer, Toulouse, France

heating and cooling rates of 1 °C.min^{-1}. The milling procedure was repeated once more before the powder could be processed. Ceramic samples were prepared by pressing (uniaxially and subsequently isostatically at 400 MPa) the obtained powder into disc-shaped membranes, which were sintered at 1300 °C for 10 h with heating and cooling rates of 1 °C.min^{-1}. The density of these materials was checked with the Archimedes' method using mercury. The ceramics were polished with SiC paper (1000 mesh). The final diameter of the membranes was 15 mm and the thickness ranged from 0.5 to 1.6 mm. The experimental set-up used for the partial oxidation experiments is described in the previous chapter.

4.3 Results

4.3.1 Reproducibility and activity

The performances of the membrane material were tested in syngas generation experiments. The results obtained with different membranes are presented in table 4.1.

Catalyst	Thickness (mm)	CH_4 (ml.min^{-1})	Argon (ml.min^{-1})	JO_2 (ml.min^{-1}.cm^{-2})	X_{CH_4}	S_{CO}	S_{H_2}	C_2H_6 (ml.min^{-1})	C_2H_4 (ml.min^{-1})
Ni	1.6	6.9	0	3.7	> 99 %	> 90 %	88 %	0	0
Ni	1.45	6.3	12.9	2.5	87 %	98 %	> 99 %	0	0
Ni	0.5	12.1	0	5.1	94 %	99.5 %	99 %	0	0
NONE !	1.45	6.8	0	0.06	1.2 %	47 %	24 %	0.01	0.01

TABLE 4.1: *Results of partial oxidation experiments obtained with different $La_{0.7}Sr_{0.3}Fe_{0.7}Ga_{0.3}O_{3-\delta}$ membranes at 900 °C.*

Three membranes with different thicknesses were tested in the presence of the catalyst. In the first experiment, the H_2 and CO selectivities are both around 90 %. This is due to the excess of oxygen compared to the amount of methane, when the stoichiometry of the partial oxidation reaction is taken into account. In the second experiment the conversion of methane is less than 100 % because of the excess of methane. In the the third experiment, the thickness of the membrane was approximately reduced by a factor 3. The maximum oxygen flux obtained with an almost total conversion of methane was 5.1 $ml.min^{-1}.cm^{-2}$.
Another experiment was conducted without catalyst to test the activity of the membrane material towards the partial oxidation reaction. The results clearly show that the $La_{0.7}Sr_{0.3}Fe_{0.7}Ga_{0.3}O_{3-\delta}$ material has no catalytic activity towards any of the following reactions: partial oxidation, total oxidation and methane coupling.

4.3.2 X-ray analysis

Catalyst after reaction

After the CPO experiment, the reactor was cooled down rapidly to room temperature. The flow of methane was kept constant but the flow of air was stopped. The catalyst was extracted and directly analyzed with X-ray diffraction. The result is shown in fig. 4.1. Most of the detected reflections belong to the α-Al_2O_3 phase which is the support material of the catalyst. It is possible to identify nickel in the metallic state with the reflections at $2\,\theta = 44.5\,^\circ$ and $2\,\theta = 51.5\,^\circ$. The reflections of nickel oxide are overlapping with others except for the position $2\,\theta = 62.5\,^\circ$.

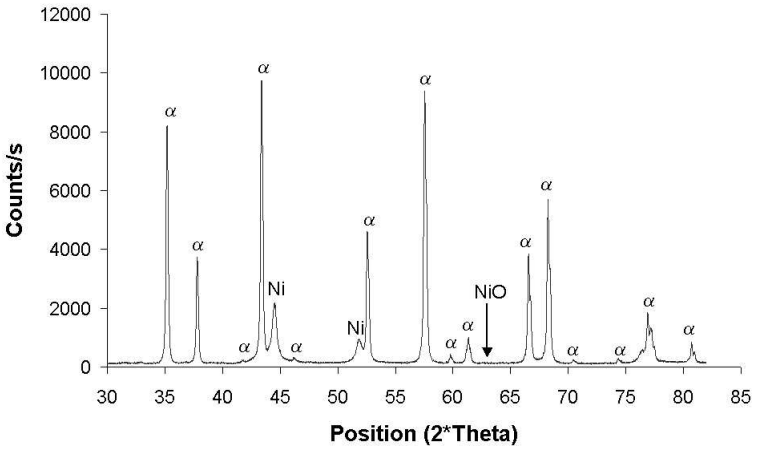

FIGURE 4.1: *Diffractogram of the catalyst used in CPO experiments. The reflections are labeled 'α' for α-Al_2O_3 and 'Ni' for nickel in the metallic state. The position of a reflection of nickel oxide is marked 'NiO'.*

Powder

The $La_{0.7}Sr_{0.3}Fe_{0.7}Ga_{0.3}O_{3-\delta}$ powder was analyzed after the second calcination step. The result is presented in fig. 4.2.

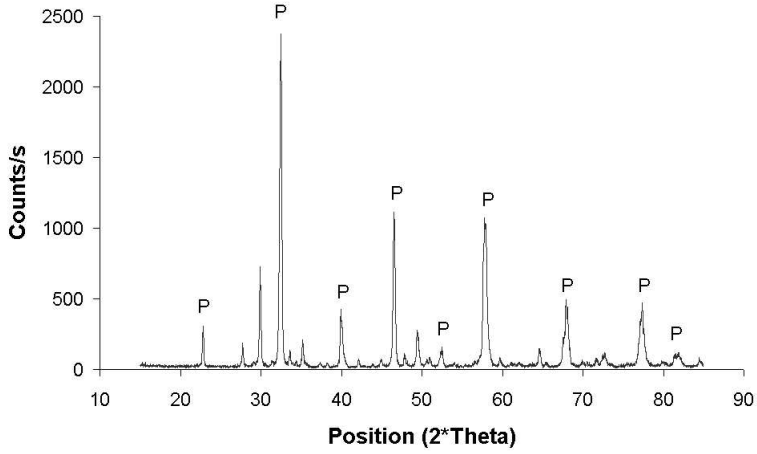

FIGURE 4.2: *Diffractogram of the $La_{0.7}Sr_{0.3}Fe_{0.7}Ga_{0.3}O_{3-\delta}$ powder. The reflections labeled 'P' belong to a cubic perovskite structure.*

The characteristic reflections of a cubic perovskite structure are present but a number of other minor reflections indicates the presence of one or more second phases. It was unfortunately not possible to identify any of the potential additional phases present in this material.

Post-mortem analysis of the membrane

Both sides of the $La_{0.7}Sr_{0.3}Fe_{0.7}Ga_{0.3}O_{3-\delta}$ membrane were analyzed with X-ray diffraction after the CPO experiment. The reactor was cooled down rapidly with the methane gas still flowing to preserve the structure of the material. The air flowrate was stopped during this procedure. The results are shown in fig. 4.3.

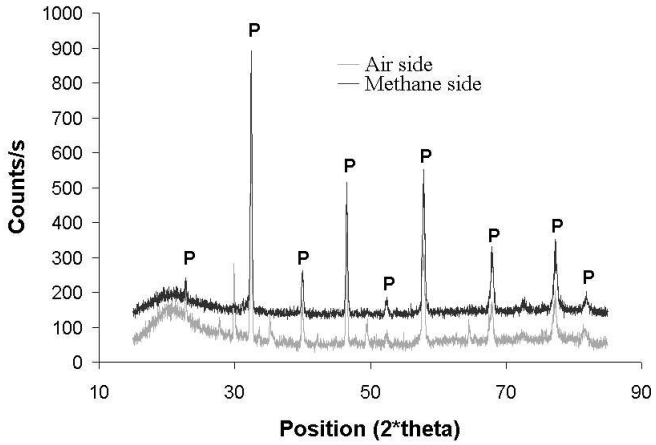

FIGURE 4.3: *Diffractogram of both sides of a $La_{0.7}Sr_{0.3}Fe_{0.7}Ga_{0.3}O_{3-\delta}$ membrane after the CPO experiment. The reflections labeled 'P' belong to a cubic perovskite structure.*

A factor of 100 was added to the 'Counts/s' of the methane side measurement for the sake of clarity. This type of measurement was repeated three times with the same results, i.e. the additional reflections (not belonging to the perovskite structure) were not present on the methane side after the experiment.

4.3.3 SEM-EDX

After the CPO experiment, the cross-section of the membrane was examined with SEM, as shown in fig. 4.4.

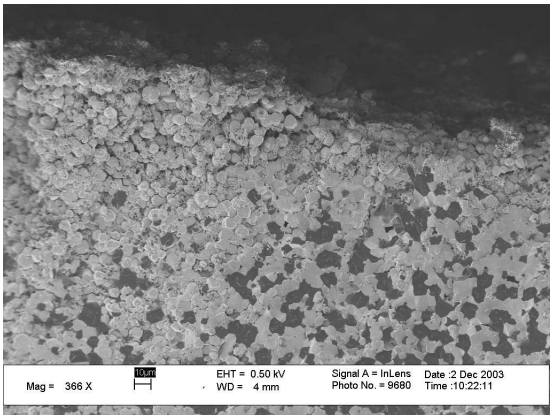

FIGURE 4.4: *SEM micrograph of the cross-section (methane side) of a* $La_{0.7}Sr_{0.3}Fe_{0.7}Ga_{0.3}O_{3-\delta}$ *membrane after CPO experiment.*

Two different types of grains can be observed, i.e. grey and black, and the membrane surface seems to be degraded slightly. The darker grains are not present close to the surface. A closer view of the surface is shown in fig. 4.5.

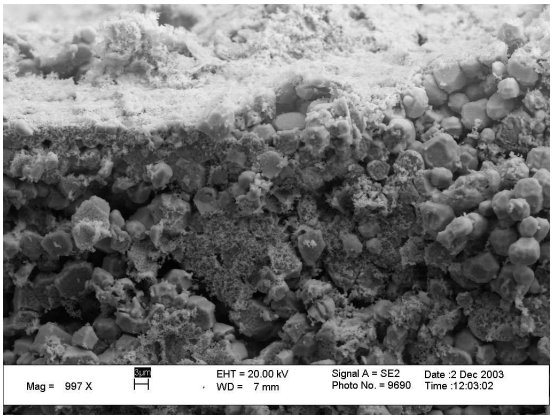

FIGURE 4.5: *SEM picture of the cross-section (close-up view) of a* $La_{0.7}Sr_{0.3}Fe_{0.7}Ga_{0.3}O_{3-\delta}$ *membrane after CPO experiment.*

The grains near the surface look polished, almost spherical with no sharp edges. The surface is covered with a dust-like layer. This highly porous material appears to run deeper into the bulk of the membrane.
Elemental analysis on the two types of grains was performed by means of EDX. The same analysis was applied on two different reference samples, i.e. membranes which were not used for CPO. The results are presented in table 4.2.

Atomic %	Expected values	Ref.	Ref.	Grain type 1	Grain type 2
La	14	11	11	11	8
Sr	6	6	6	6	8
Fe	14	19	19	19	9
Ga	6	5	4	4	15
O	60	59	59	59	58

TABLE 4.2: *Results of the EDX analysis on fresh (reference) and used (CPO) samples with the composition* $La_{0.7}Sr_{0.3}Fe_{0.7}Ga_{0.3}O_{3-\delta}$.

The results obtained with both reference samples are very close to the expected values, with error estimates in the range of a few percent. Nevertheless, the material seems to be slightly lanthanum deficient and iron rich. The analysis on the grain type 1, which are grey in fig. 4.4, reveals the same composition as in the reference material, i.e. the grey grains have the perovskite structure. The grain type 2, which are dark in fig. 4.4, are lanthanum and iron poor, slightly rich in strontium and strongly enriched with gallium.

The EDX-mapping technique was used to analyze an area of 5 μm $\times$ 5 μm. The results are shown in fig. 4.6. The areas with a different composition (color coded in fig. 4.6) correspond to the grain type 2, which are gallium and strontium rich and lanthanum and iron poor.

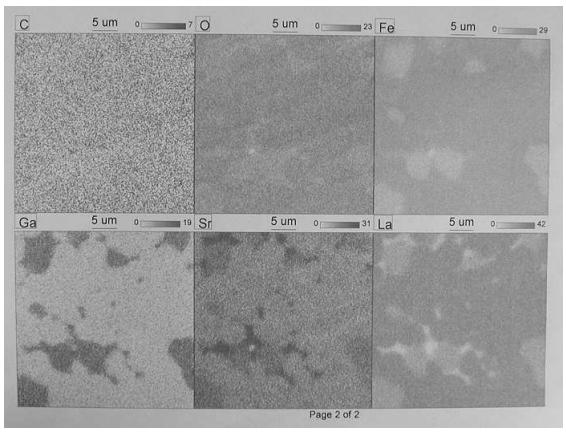

FIGURE 4.6: *EDX-mapping of an area close to the $La_{0.7}Sr_{0.3}Fe_{0.7}Ga_{0.3}O_{3-\delta}$ membrane surface after the CPO experiment.*

A SEM micrograph of the cross-section (air side) of the membrane after the CPO experiment is shown in fig. 4.7. Both type of grains are present and distributed randomly, as in the fresh membrane material.

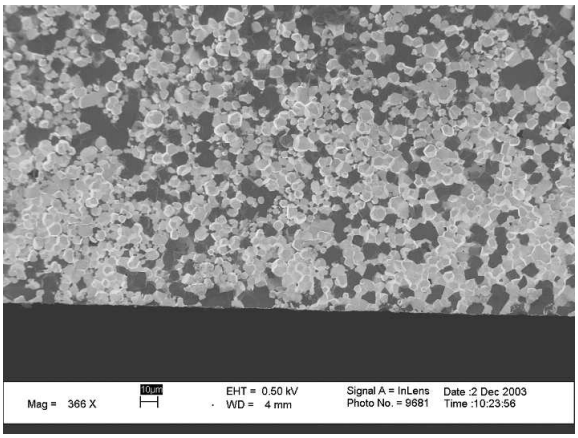

FIGURE 4.7: *SEM micrograph of the cross-section of a $La_{0.7}Sr_{0.3}Fe_{0.7}Ga_{0.3}O_{3-\delta}$ membrane after CPO experiment (air side).*

4.3.4 XPS

X-Ray photon spectroscopy was used to analyze the methane side of the $La_{0.7}Sr_{0.3}Fe_{0.7}Ga_{0.3}O_{3-\delta}$ membrane after the synthesis gas generation experiments. Once again the reactor was rapidly cooled down, keeping a methane flow and stopping the air flow. The measurements were conducted on three membranes tested in the reactor for different periods of time. The depth of measurement was 100 nm for the results given in table 4.3.

Atomic %	Expected values	After 136 h	After 180 h	After more than 200 h
La	15	12	7	5
Sr	6	16	24	27
Fe	15	7	6	3
O	64	65	63	65

TABLE 4.3: *Results of the XPS analysis on the methane side of* $La_{0.7}Sr_{0.3}Fe_{0.7}Ga_{0.3}O_{3-\delta}$ *membranes after CPO experiments.*

Gallium is not present in this table because the only gallium peak which was not overlapping with others was too small to be trusted for quantitative analysis. The expected values are therefore recalculated for their sum to be equal to 100. The oxygen content is fairly constant. The lanthanum and iron concentration are dropping rapidly with time whereas the amount of strontium is increasing sharply.

4.3.5 XRF

X-Ray fluorescence was used to determine the chemical composition of a fresh $La_{0.7}Sr_{0.3}Fe_{0.7}Ga_{0.3}O_{3-\delta}$ membrane and the composition of the methane side of such a membrane after the partial oxidation experiment. The results are given in table 4.4.

Wt%	Fe_2O_3	Ga_2O_3	SrO	La_2O_3
Expected values	24	12	14	50
Fresh sample	27	15	14	44
Used sample	28	10	17	45

TABLE 4.4: *Results of the XRF analysis on a fresh $La_{0.7}Sr_{0.3}Fe_{0.7}Ga_{0.3}O_{3-\delta}$ membrane and on the methane side after CPO.*

In both analysis the samples are slightly iron rich and lanthanum poor. The strontium concentration is larger on the methane side of the used membrane whereas the gallium content is smaller.

4.4 Discussion

4.4.1 Membrane performance

The experiment conducted without catalyst demonstrates that the material $La_{0.7}Sr_{0.3}Fe_{0.7}Ga_{0.3}O_{3-\delta}$ has no preferential activity towards partial oxidation, total oxidation or methane coupling. In addition, the oxygen flux is very low compared with the experiments including catalyst. This is explained by the fact that methane acts mostly as a sweep gas, i.e. similarly to helium or argon because of its poor activation due to a high C-H bond strength [19]. The oxygen partial pressure near the surface of the membrane therefore remains relatively high, in the order of 10^{-6} to 10^{-8} bar, and the magnitude of the oxygen flux is restrained to values barely twice as large as in the case of an inert gas sweep.

On the contrary, during the experiments involving the catalyst, the oxygen flux reaches much higher values. The conversion of methane is enhanced, ensuring a high syngas production rate. This decreases the oxygen partial

pressure and consequently increases the oxygen flux further. For a concentration of methane in the feed gas of 33 vol%, the 1.45 mm-thick membrane exhibits an oxygen flux of 2.5 ml.min^{-1}.cm^{-2} and the 1.6 mm-thick membrane an oxygen flux of 2.4 ml.min^{-1}.cm^{-2}, confirming that, under these conditions, bulk diffusion is the predominant transport mechanism. Based on this assumption, the expected oxygen flux for the 0.5 mm thick membrane is approximately 7.5 ml.min^{-1}.cm^{-2} (see eq. 1.11 on page 21). The experimental oxygen flux found for a concentration of methane in the feed gas of 33 vol% is 4 ml.min^{-1}.cm^{-2}, a merely 53 % of the expected value. Other processes, such as the surface exchange, may play a role in the transport of oxygen in this material at reduced thicknesses. This observation is confirmed by taking the value of the oxygen flux from the 1.6 mm-thick membrane with pure methane feed as a reference point. The expected oxygen flux for the 0.5 mm-thick membrane, under the same conditions, is 11 ml.min^{-1}.cm^{-2}. The obtained experimental oxygen flux is 5.1 ml.min^{-1}.cm^{-2}, which is only 46 % of the extrapolated value.

When comparing oxygen fluxes as a function of the thickness, one assumes that the oxygen partial pressure on both side of the membrane are the same. This assumption does not hold rigourously in the present case due to the difference in oxygen fluxes, which inevitably generates different syngas production rates and consequently different oxygen partial pressures on the methane side of the membrane. The extent of the influence of the surface processes can therefore not be estimated quantitatively but the qualitative discussion remains valid.

4.4.2 The catalyst

The state of the catalyst after the CPO experiment revealed in fig. 4.1, i.e. metallic nickel, shows that a low oxygen partial pressure is present during the experiment on the methane side of the membrane. The carbon mass balance calculated from the detected gases was found to be correct within a

few percent, thus supporting the assumption that no carbon is formed in the reaction chamber, i.e. there is no carbon deposition on the catalyst material. The performance of the catalyst was checked in a standard catalytic test. The results show that at high temperature, typically 900 °C and above, the conversion of methane is higher than 98 % and the CO and H_2 selectivities are higher than 96 %.

4.4.3 X-Ray analysis

The results of fig. 4.2 shows the presence of at least one additional phase in the $La_{0.7}Sr_{0.3}Fe_{0.7}Ga_{0.3}O_{3-\delta}$ powder. It is common to find second phase products in powders prepared via the solid state reaction technique due to contaminations or inhomogeneous mixing conditions. In addition Kharton *et al.* [16] show that with a strontium content higher than 10 %, increasing the amount of gallium dopant leads to segregation of a second phase: $SrLaGa_3O_7$. Another impurity phase often encountered in ceramic materials based on $LaGaO_3$ is $SrLaGaO_4$ [20–22]. No second phase could clearly be identified from the diffractogram presented in fig. 4.2 because of the too low intensity of the additional reflections.

A similar diffraction pattern is found when analyzing the membrane material after CPO on the air side. This shows that the membrane has not suffered any major structural changes on the air side during the syngas generation experiment. On the contrary, the analysis on the methane side does not reveal any traces of additional phases anymore. This suggests that when placed in an oxygen chemical potential gradient at high temperature, the second phase material is not stable.

It should also be noted that the difference in thermal expansion coefficient between the two phases contained in the material did not lead to any difficulties during testing. This is attributed to the low expansion coefficient of these gallium based materials compared with other perovskites [23].

4.4.4 Stability investigation

SEM-EDX was successful at proving that the material actually contains two different phases,which is clearly seen on fig. 4.4. The elemental analysis also reveals that the second phase is strongly enriched with gallium whereas the composition of the perovskite phase is close to the expected one. The EDX mapping confirms this findings on a larger scale. Comparing fig. 4.4 and 4.7 shows that the darker grains from the second phase are not present near the surface on the methane side of the membrane material after the CPO experiment. This could explain why the XRD analysis was unable to reveal its presence. The disappearance of this oxide phase is certainly linked to the gradient in the chemical potential of oxygen across the membrane during the experiment.

Fig. 4.5 shows that a dust-like layer is present on the membrane surface after CPO. Some decomposition also appears in the first few micrometers into the membrane material. The perovskite grains seems eroded or polished. This is the result of a deterioration of the material, which is probably the cause of the disappearance of the second phase in this region of the material. The presence of the second phase in the early stage of the experiment could lead to slower deterioration of the perovskite phase in the membrane.

The XPS results show a strong strontium enrichment of the membrane surface during the experiment. This could be attributed to kinetic demixing for a part, but to a larger extent to the partial decomposition of the membrane material on the methane side. It is shown that strontium has a tendency to react with carbon containing species to form strontium carbonates.

The results obtained with XRF confirms the trends and ideas exposed above. The iron content of both the fresh and the used samples is higher than expected, whereas it is the opposite for lanthanum. The increase in strontium content is minor because X-ray fluorescence is a bulk technique. The decrease in gallium content from the fresh sample to the used one can be explained by the fact that the gallium-rich second phase has disappeared from the near surface, at least as far as XRD-depth. The information depth of XRF is

very similar to the one of XRD and the content of gallium in the used sample is thus lower than on a fresh sample containing both phase randomly distributed.

4.5 Conclusions

The perovskite with composition $La_{0.7}Sr_{0.3}Fe_{0.7}Ga_{0.3}O_{3-\delta}$ has been successfully used for the partial oxidation of methane into synthesis gas at 900 °C. With a thickness of 0.5 mm, an oxygen flux of 5.1 ml.min^{-1}.cm^{-2} was achieved. It was found that this material is not catalytically active for either partial oxidation, combustion or methane coupling in our reactor design at 900 °C. Partial decomposition of the material occurred with strontium enrichment on the methane side. Surprisingly, the second phase present after synthesis seems to disappear near the surface on the methane side of the membrane during experiment. This behavior was attributed to the instability of this phase in an oxygen chemical potential gradient at high temperature.

Bibliography

[1] A. Petric, P. Huang and F. Tietz, *Evaluation of La-Sr-Co-Fe-O perovskites for solid oxide fuel cells and gas separation membranes*, Solid State Ionics 135 (2000) 719-725.

[2] P.V. Hendriksen, P.H. Larsen, M. Mogensen, F.W. Poulsen and K. Wiik, *Prospects and Problems of dense oxygen permeable membranes*, Catal. Today 56 (2000) 283-295.

[3] H.J.M. Bouwmeester, *Dense ceramic membranes for methane conversion*, Catal. Today 82 (2003) 141-150.

[4] H. Ullmann, U. Guth, V.V. Vashook, M. Bulow, W. Burckhardt and R. Gotz, *Ceramic oxides with high oxygen transport*, Recent Res. Devel. Solid State Ionics, 2 (2004): ISBN: 81-7895-145-2.

[5] S. Pei, M.S. Kleefisch, T.P. Kobylinski, J. Faber, C.A. Udovich, V. Zhang-McCoy, B Dabrowski, U. Balachandran, R.L. Mieville and R.B. Poeppel, *Failure mechanisms of ceramic membrane reactors in partial oxidation of methane to synthesis gas*, Catal. Lett. 30 (1995) 201.

[6] I.V. Belova, M.J. Brown and G.E. Murch, *Analysis of kinetic demixing in a mixed oxide (A,B)O in an oxygen potential gradient*, Acta Mater. 51 (2003) 1821-1826.

[7] M. Martin, *Materials in thermodynamic potential gradients*, J. Chem. Thermodyn. 35 (2003) 1291-1308.

[8] R. Bredesen and J. Sogge, Paper presented at: The United Nations Economic Commission for Europe Seminar on Ecological Applications of Innovative Membrane Technology in Chemical Industry, Chem./Sem. 21/R.12, 1-4 May 1996, Cetaro, Calabria, Italy.

[9] V.V. Kharton, A.A. Yaremchenko, A.P. Viskup, G.C. Mather, E.N. Naumovich and F.M.B. Marques, *Ionic and p-type electronic conduction in* $LaGa(Mg, Nb)O_{3-\delta}$ *perovskites*, Solid State Ionics 128 (2000) 79-90.

[10] M. Schwartz, J.H. White and A.F. Sammells, *Solid State Oxygen anion and electron mediating membrane and catalytic membrane reactors containing them*, International Patent Application PCT WO 97/14060, 1997.

[11] R.T. Baker, B. Gharbage and F.M.B. Marques, *Ionic and Electronic Conduction in Fe and Cr Doped* $(La, Sr)GaO_{3-\delta}$, J. Electrochem. Soc. 144 (1997) 3130.

[12] N. Trofimenko and H. Ullmann, *Transition metal doped lanthanum gallates*, Solid State Ionics 118 (1999) 215.

[13] A.A. Yaremchenko, V.V. Kharton, A.P. Viskup, E.N. Naumovich, V.N. Tikhonovich and N.M. Lapchuk, *Mixed electronic and ionic conductivity of* $LaCo(M)O_3$ *(M=Ga, Cr, Fe or Ni): V. Oxygen permeability of Mg-doped* $La(Ga, Co)O_{3-\delta}$ *perovskites*, Solid State Ionics 120 (1999) 65.

[14] T. Ishihara and Y. Takita, *Partial oxidation of methane into syngas with oxygen permeating ceramic membrane reactors*, Catal. Surv. Jpn 4 (2000) No.2.

[15] A. Ahmad-Khanlou, F Tietz and D. Stover, *Material properties of* $La_{0.8}Sr_{0.2}Ga_{0.9+x}Mg_{0.1}O_{3-\delta}$ *as a function of Ga content*, Solid State Ionics 135 (2000) 543-547.

[16] V.V. Kharton, A.L. Shaulo, A.P. Viskup, M. Avdeev, A.A. Yaremchenko, M.V. Patrakeev, A.I. Kurbakov, E.N. Naumovich and F.M.B. Marques, *Perovskite-like system (Sr,La)(Fe,Ga)$O_{3-\delta}$:structure and ionic transport under oxidizing conditions*, Solid State Ionics 150 (2002) 229-243.

[17] D. Westphal, G.C. Mather, F.M.B. Marques, S. Jakobs and U. Guth, *Ionic and electronic conduction in stoichiometric and sub-stoichiometric perovskites*, Solid State Ionics 136-137 (2000) 19-24.

[18] A.A. Yaremchenko, A.L. Shaula, D.I. Logvinovich, V.V. Kharton, A.V. Kovalevsky, E.N. Naumovich, J.R. Frade and F.M.B. Marques, *Oxygen-ionic conductivity of perovskite-type $La_{1-x}Sr_xGa_{1-y}Mg_yM_{0.2}O_{3-\delta}$ (M=Fe, Co, Ni)*, Mater. Chem. Phys. 82 (2003) 684-690.

[19] A. Thursfield and I.S. Metcalfe, *The use of dense mixed ionic and electronic conducting membranes for chemical production*, J. Mater. Chem. 14 (2004) 2475-2485.

[20] K. Huang, R.S. Tichy and J.B. Goodenough, *Superior Perovskite Oxide-Ion Conductor; Strontium- and Magnesium-Doped $LaGaO_3$: I, Phase Relationships and Electrical Properties*, J. Am. Ceram. Soc. 81(10) (1998) 2565.

[21] N.M. Sammes, G.A. Tompsett, R.J. Phillips and A.M. Cartner, *Characterisation of doped-lanthanum gallates by X-ray diffraction and Raman spectroscopy*, Solid State Ionics 111 (1998) 1.

[22] G.Ch. Kostogloudis, Ch. Ftikos, A. Ahmad-Khanlou, A. Naoumidis and D. Stoever, *Chemical compatibility of alternative perovskite oxide SOFC cathodes with doped lanthanum gallate solid electrolyte*, Solid State Ionics 134 (2000) 127.

[23] V.V. Kharton, A.A. Yaremchenko, M.V. Patrakeev, E.N. Naumovich and F.M.B. Marques, *Thermal and chemical induced expansion of*

$La_{0.3}Sr_{0.7}(Fe, Ga)O_{3-\delta}$ *ceramics*, J. Eur. Ceram. Soc. 23 (2003) 1417-1426.

Chapter Five

Centrifugal casting of tubular perovskite membranes

5.1 Introduction

The essential feature of centrifugal consolidation is the introduction of a liquid suspension or slurry, containing the particles (ceramic and/or metallic) and a proper dispersant, into a mould, which is rotated to form a cylindrically shaped, relatively dense green body. The centrifugal force field drives the solid-liquid separation. During the last decade, centrifugal casting has attracted considerable interest for the fabrication of high-quality massive [1–4] and porous ceramic tubes [5, 6]. Being in essence restricted to the production of cylindrical geometric shapes, centrifugal casting greatly improves the roundness of the tubes compared to those prepared by conventional slip casting or extrusion, and allows for tailoring of the microstructure and texture of the ceramics (unlike pressing techniques). It also requires fewer additives than extrusion and it is easier to work with on the laboratory scale. Distinguishing features in the centrifugal casting process are the particle size distribution and the colloidal state of the suspension. Typical consolidation behavior for a dispersed suspension includes high particle packing densities and segregation by size or density. The dispersant concentration is chosen high enough to keep the particles from agglomerating (flocculation or coagulation), but not too high as to avoid redispersion when the centrifugation stops. During centrifugation, particles within the suspension move towards the mould wall at a rate dependent upon the centrifugal force and particle drag. As a consequence, the largest particles move faster and accumulate at the mould wall. The inner surface will therefore be mainly made up from the smallest particles and, after sintering, this surface appears much smoother than the outer surface. Advantageous use can be made from this feature if the material needs to be coated with a functional layer, such as in membrane applications [7]. The segregation effect can be used on purpose to fabricate a material with a continuous, gradual change of the porosity and/or composition over its thickness [5, 8]. Segregation can be prevented by taking those measures that decrease the particle rearrangements during centrifugation, such as using flocculated or coagulated suspensions with a high degree of

agglomeration, a high solid loading or a high consolidation rate (i.e. high rotation speed). Previous work has focused on the consolidation behavior of Al_2O_3 and Al_2O_3/ZrO_2 composite suspensions [6]. In the present work, we demonstrate for the first time the fabrication by centrifugal casting of dense tubular membranes of the mixed-conducting perovskite $La_{0.5}Sr_{0.5}CoO_{3-\delta}$ (50-LSC). This composition can be considered as a prototype of a family of mixed-conducting perovskites, showing selective oxygen permeation properties at elevated temperature (800-1000 °C). The present work is part of a larger project with a twofold aim, which includes both the production of tubular perovskite membranes with a graded porosity, i.e. terminated with a dense thin film of appropriate composition, and the production of membranes with a graded composition, such as $La_{0.5}Sr_{0.5}CoO_{3-\delta}$-$La_{0.5}Sr_{0.5}FeO_{3-\delta}$. The general objective is to optimize the performance of mixed-conducting membranes, in terms of stability and magnitude of the oxygen flux, for usage in membrane reactors for the partial oxidation of methane to syngas [9–12].

5.2 Experimental procedure

The starting $La_{0.5}Sr_{0.5}CoO_{3-\delta}$ powder for the tube manufacture was prepared by two different techniques, namely (1) by spray-pyrolysis[1] and (2) home-made, by thermal decomposition of precursor complexes derived from metal nitrate solutions using ethylene-diaminetetraacetic acid (EDTA) as a complexing agent [12]. X-Ray powder diffraction[2] was use to confirm the presence of a single-phase perovskite structure. For both powders, no evidence of second phase formation was found. Powders were ball-milled with isopropanol in a plastic container on a roller-bench[3] rotating at 55 rpm. Zirconium oxide balls of 1 and 15 mm, with a weight ratio of 5:1, were used for milling. The weight ratio of powder to milling balls was 1:12, whereas

[1]Praxair Specialty Ceramics, Woodinville, USA
[2]X'Pert-1, Philips, Almelo, The Netherlands
[3]Leroy Somer, Toulouse, France

isopropanol was added in a 1:1 volume ratio with the powder. The milling time varied from 3 to 24 h. Particle size distributions were determined by laser (λ = 782 nm) scattering[1] using water as solvent. The refractive index of the powder material was not needed since the perovskite materials under consideration are absorbent.

A sedimentation test was designed to evaluate the efficiency of two types of stabilizer. The first set of suspensions was prepared with water, powder and addition of acid or base to set the pH to different values. The second set of suspensions contained water, powder and Darvan C© (ammonium polymethacrylate) [14]. These suspensions were all ultrasonically treated before being poured in test tubes. When sedimentation occurs, a transparent liquid layer appears in the top part of the test tubes. The height variation of this layer was observed as a function of time.

For the tube production, aqueous suspensions containing 50-70 wt% of 50-LSC were prepared by dispersing the powder in deionized water. Water and Darvan C© (0-10 wt% relative to the 50-LSC powder weight) were first mixed in a glass beaker prior to the addition of the 50-LSC powder. The final suspension was stirred for an additional 5-10 min, followed by an ultrasonic treatment[2] under water-cooling for 2 min at a frequency of 20.000 Hz and a transducer output power of 100 Watt. A commercial vertical centrifuge[3] with Delrin© moulds[4] was used to produce the green tubes. The inner diameter of the moulds was 1.1 cm. Their effective lengths could be adjusted between 4 and 16 cm using stoppers. Prior to filling, the mould surface was greased with a solution of Vaseline©[5] in petroleum ether (boiling range: 40-60 °C). The mould filled with the suspension was rotated for 20 min at 20.000 rpm. This speed was reached within 1 min and deceleration to standstill took slightly less than 2 min. The remaining liquid

[1]Microtrac X100, Leeds & Northrup, North Wales, USA
[2]Model 250 Sonifier, Branson Ultrasonics Corporation, Danbury, USA
[3]CEPA, GLE, Carl Padberg GmbH, Lahr, Germany
[4]DuPont de Nemours, Dordrecht, The Netherlands
[5]Elida Faberg, Bodegraven, The Netherlands

was poured out of the mould. The green compacts were dried inside the mould in a climate chamber[1] for 48 h at 30 °C and 60 % relative humidity. After drying, the green tubes were carefully removed from the mould and sintered horizontally for 10 h on a platinum support in stagnant air, at either 1150 °C or 1170 °C. The heating rate was 0.3 °C.min^{-1} and the cooling rate was either set equal or to 0.6 °C.min^{-1}. Two 1-hour dwells were introduced at 235 °C and 400 °C during heating to burn out the dispersant and relieve mechanical stress. The density of the sintered tubes was determined by the Archimedes' method using mercury. Relative densities were calculated according to a theoretical value [15] of 6.637 g.cm^{-3}.

The sintering behavior of the green tubes was studied by means of dilatometry[2]. Prior to experiment, the dispersant was removed by applying the above annealing procedure until the end of the second dwell. The tube used for the dilatometric experiment had a length of 15 mm. The heating rate was 0.3 °C.min^{-1} up to 1170 °C and the cooling rate was 0.6 °C.min^{-1}. Analysis was carried out using an air flow of 20 ml/min.

The burnout of the dispersant was investigated using combined differential scanning calorimetry (DSC) and thermogravimetric analysis (TGA)[3]. Measurements were conducted in air up to 500 °C at a heating rate of 0.3 °C/min, using a sample mass of 21.5 mg.

Oxygen permeation experiments were conducted in the range of temperature 850-950 °C. Both ends of the tube were sealed with a glass paste onto alumina tubes and inserted into the quartz glass shell of a home-made reactor. Air, with a flow rate of 98.3 ml/min, was used as the oxygen supply on the outer side of the membrane, while helium (28-277 ml/min) was used as sweeping gas on the inner side. Quantitative analysis of the permeate gas was performed using a micro-gas chromatograph[4], which also measured nitrogen in the Argon to check for gas tightness. In all cases the contribution

[1]Heraeus Vtsch, VTRK 300, Balingen, Germany

[2]Netsch Gerte GmbH, Dlmen-Merfeld, Germany

[3]Setsys 16/18, Setaram, Caluire, France

[4]CP-4900 Micro-GC, Varian Inc., Middelburg, The Netherlands

from oxygen leakage to the total oxygen flux was smaller than 0.6 %, and typically below 0.2 %.

5.3 Results and discussion

A key parameter in centrifugal casting is the stability of the suspension, which is closely related to the particle size distribution of the starting powder. Figure 5.1 shows the particle size distributions of the commercial powder for different milling times ranging from 0 (unmilled powder) to 24 h.

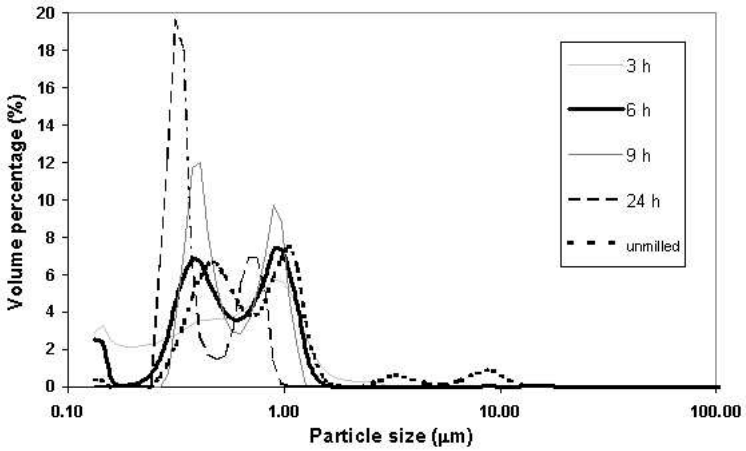

FIGURE 5.1: *Evolution of the particle size distribution of the commercial 50-LSC powder as a function of the milling time.*

The milling step is successful in removing the bigger particles (> 2 μm) present in the unmilled powder. Such a pre-treatment appeared to be necessary as the large disparity in size between the smallest and the biggest particles of the unmilled powder caused unstable suspensions. The resulting partial sedimentation generated stress during sintering and cracks were formed at both ends of the tube. As expected, the longer the milling time, the smaller the particles. It should be noted that the bi-modal distribution of the starting powder is maintained and after 24 h of milling all the particles are smaller than 1 μm.

The particle size distributions of the home-made powder for different milling times ranging from 6 to 22 h are presented in fig. 5.2.

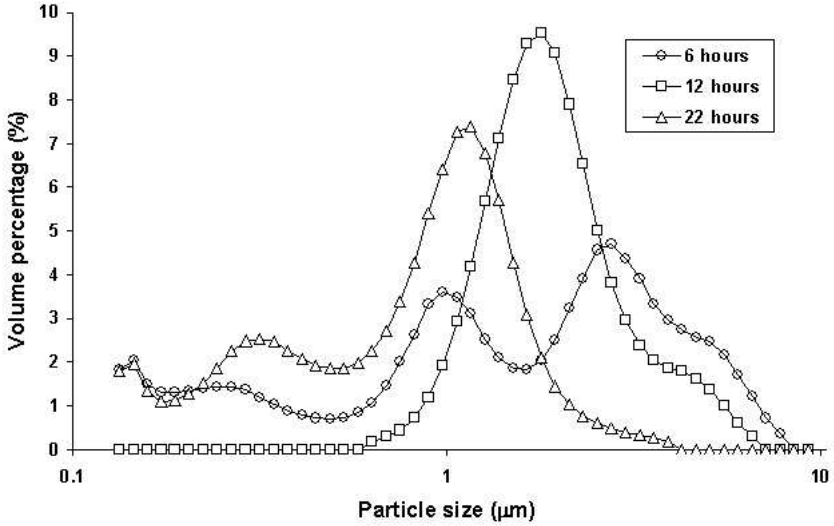

FIGURE 5.2: *Influence of the milling time on the particle size distribution of the home-made 50-LSC powder.*

After 6 h of milling the fraction of particles bigger than 1 μm is still important. Extended milling is therefore necessary but even after 22 h, big particles ($>$ 2 mm) are still present even though the highest volume percentage is obtained for particles around 1 μm.

The BET surfaces of some of the powders are presented in table 5.1.

Powder	Milling time	BET surface (m^2/g)
Home-made	6 hours	2
Commercial	-	3
Commercial	6 hours	4.5
Commercial	24 hours	6.6

TABLE 5.1: *BET surfaces of the home-made powder (milled for 6 h) and the commercial powder (milled for 0, 6 and 24 h).*

The home-made powder milled for 6 h has a BET surface which is less than half of the BET surface of the commercial powder milled for 6 h. This is a strong indication for the presence of bigger particles and/or a different morphology. Table 1 also proves that the longer the commercial powder is milled the bigger the BET surface is, meaning that the average particle size decreases.
Scanning electron microscopy was used to investigate the morphology of both powders. The almost spherical particles of fig. 5.3 belong to the commercial powder milled for 6 h.

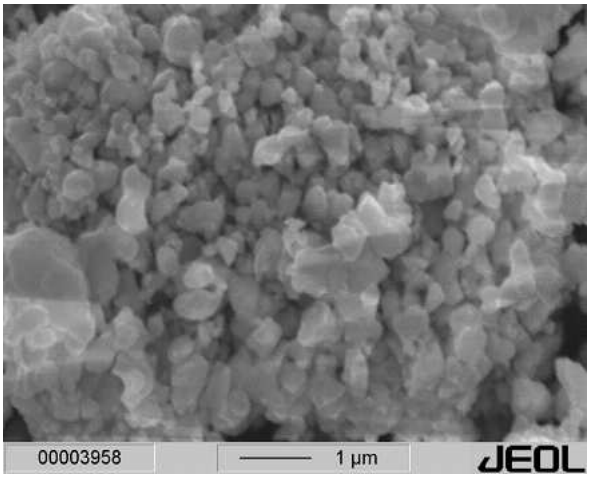

FIGURE 5.3: *SEM micrograph of the commercial powder milled for 6 h.*

This type of morphology was expected since the powder was prepared via spray pyrolysis. The particles from the home-made powder, presented in fig. 5.4, are of a different nature. They appear to be of irregular shape with many sharp edges. This could be an explanation for the difference in BET surface. The agglomeration degree for the home-made powder was also higher than that of the commercial powder.

As mentioned earlier, the stabilization of the suspension is a crucial step in centrifugal casting. In this work, two types of stabilization were investigated: pH adjustment and the addition of a stabilizer. Hydrochloric acid or ammonium hydroxide was added to a suspension containing water and the

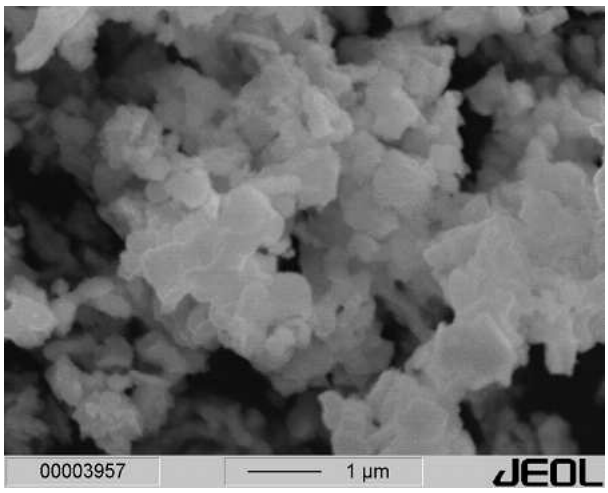

FIGURE 5.4: *SEM micrograph of the home-made powder milled for 6 h.*

commercial powder to adjust the pH to desired values. The data in fig. 5.5 show that the pH exerts only a minor influence on the stability of the suspension. This method of stabilization was therefore rejected.

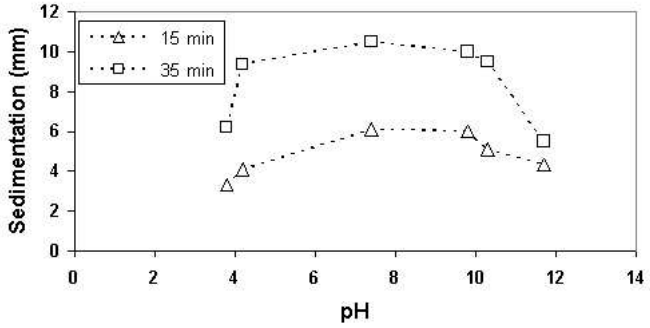

FIGURE 5.5: *Influence of the pH on the stability of a suspension made from water, powder and HCl or NH_3OH. The lines are only a guide for the eyes.*

Darvan C© (ammonium polymethacrylate) was then used as stabilizer and results of the sedimentation tests are presented in table 5.2. The first column in table 5.2 confirms that without milling pre-treatment the suspension is not stable after 15 min. When working with the 6 h milled powder, a stabilizer concentration as low as 0.5 wt% is sufficient to obtain a stable suspension

Powder	Commercial unmilled	Commercial 6 h. milled	Commercial 6 h. milled	Commercial 6 h. milled
Sedimentation measured after	*15 min.*	*15 min.*	*60 min.*	*22 h.*
No Stabiliser	43.3 mm	15.2 mm	26 mm	38 mm
0.5 wt%	-	0	0	3.5 mm
1.6 wt%	-	0	0	1.3 mm
2.1 wt%	22.1 mm	0	0	1.1 mm
7.2 wt%	18.1 mm	0	0	0

TABLE 5.2: *Results of the sedimentation test using Darvan C© as a stabilizer.*

for as long as one hour, which is longer than the time required to start the centrifuge. With a concentration of stabilizer of 7.2 wt%, the suspension is stable for as long as 22 h. At lower concentrations than 0.5 wt%, the formation of a paste was witnessed during the ultrasonic treatment, while at concentrations higher than 9 wt% green tubes cracked during the drying stage. Based on the results, it is concluded that (1) the pH of the suspension needs not to be adjusted, (2) milling beyond 6 h is not demanded for the commercial powder, (3) aqueous suspensions of 50-LSC can be stabilized using a concentration of Darvan C© in the range 0.5-7.2 wt%.

To optimize the sintering cycle, the dispersant burn out and sintering behavior of the tubes were studied. Data of combined TGA/DSC analysis are given in fig. 5.6. The TGA data show that the burnout of Darvan C© starts around 160 °C, and is complete at 220 °C, which is consistent with data provided by the manufacturer. The heat flow analysis provides less information, which relates with the slow heating rate of 0.3 °C.min^{-1} during experiment. It was chosen to be similar to the heating rate used in the sintering program. Upon increasing the heating rate to 2 °C.min^{-1} a broad exothermic peak was found with a maximum around 220 °C.

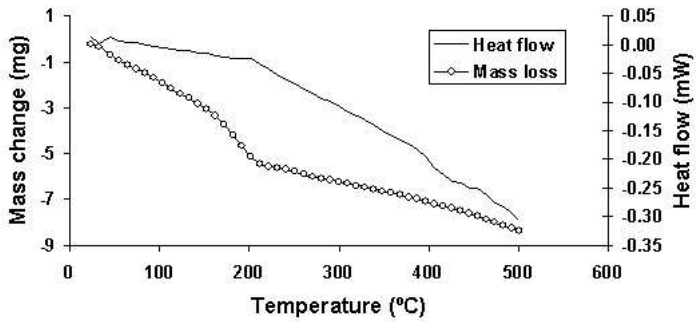

FIGURE 5.6: *TGA/DSC analysis of a piece of tube made with the commercial 50-LSC powder.*

The results of the dilatometric investigations are shown in fig. 5.7. The densification starts below 800 °C and the linear shrinkage rate advances to a maximum just before entering the dwell at 1170 °C. The density of this sample was 6.37 g.cm^{-3}, which is 96 % of the theoretical density. The density of tubes sintered at 1150 °C reached only 92 % of the theoretical density.

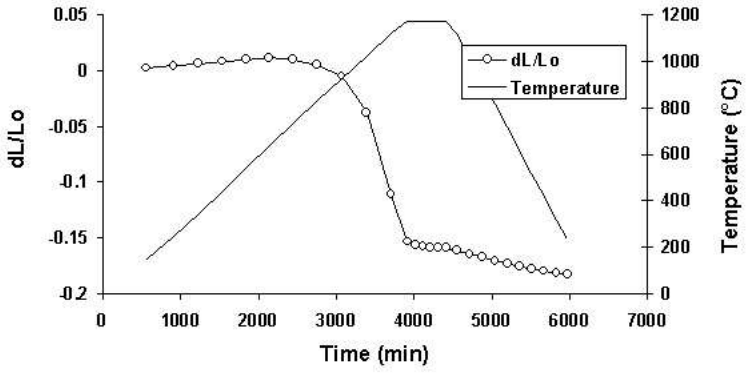

FIGURE 5.7: *Dilatometric analysis of a piece of tube made with the commercial 50-LSC powder.*

A typical example of fabricated tubes after sintering is presented in fig. 5.8. In the case shown, the length of the green tube was 16 cm. The length after sintering was 12 cm, with an outer diameter of 9 mm and a thickness of 1.3 mm. The most prominent feature of the tubes is the smoothness of

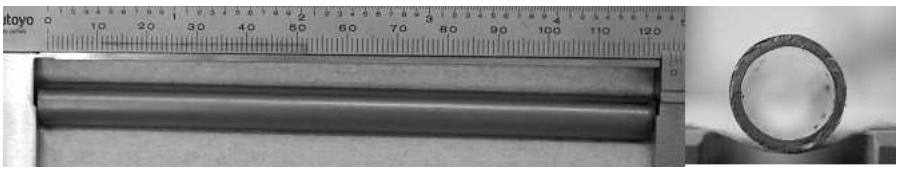

FIGURE 5.8: *Left: overview of a tube obtained with the commercial powder. Right: cross-section view of the same tube.*

their inner surfaces, looking very shiny. A slight curvature appeared after sintering, but the tubes showed perfect roundness and a uniform wall thickness. The curvature was quantified by applying a ruler against the tubes and measuring its departure from the middle point of the tube. From data of multiple experiments, it was found that the relative magnitude of the curvature (less than 1 % of the tube length) varied proportionally with the concentration of dispersant. For this reason, yet not fully understood, it is advisable to use as little stabiliser as possible. The difference in particle morphology between the two powders is also reflected in the green density and the shrinkage behavior during sintering. Tubes prepared with the home-made powder milled for 6 and 12 h showed good quality, and were indeed shorter and thicker than those prepared with the commercial powder at the same powder loading.

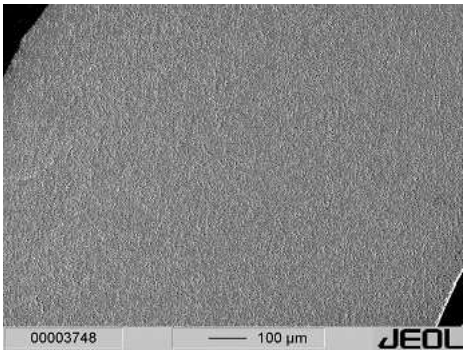

FIGURE 5.9: *SEM micrograph from the cross-section of a tube obtained with the home-made powder.*

The green length of these tubes was 4 cm. After sintering, the length was typically reduced to 30 mm, with an outer diameter of 7.5 mm and wall thickness of 1.95 mm. The density in all cases was found to be around 92 %

of the theoretical one. Using scanning electron microscopy (fig. 5.9), it was found that the density varied homogenously across the thickness of a tube specimen.
Sintered tubes with a length of 35 mm and wall thickness of 1.2 mm were tested in oxygen permeation experiments in the temperature range 850 − 950 °C. Under an air/He gradient, an oxygen flux of 0.23 sccm.cm^{-2} was measured. The activation energy was found to be 94 kJ/mol. These values are in good agreement with those found for disk-type 50-LSC membranes [16].

5.4 Conclusions

The applicability of centrifugal casting to the production of dense tubular perovskite membranes of composition $La_{0.5}Sr_{0.5}CoO_{3-\delta}$ has been demonstrated. For the tube manufacture, two powders with different particle morphologies were used. Both yield high-quality tubes, with relative densities in excess of 92 %. The difference in particle morphology was reflected in the green density and shrinkage behavior during sintering. The preferred concentration of stabilizer is less than 1 wt%. Oxygen permeation measurements were conducted in the temperature range 850-950 °C in air/He gradients. Results were found to be consistent with literature data for disk-type membranes of the same composition.

5.5 Acknowledgments

The authors would like to thank Harry G.J. Eshuis and Samuel Sánchez Ordez for assistance in the experimental work, and Louis Winnubst for several helpful and stimulating discussions.

Bibliography

[1] A. Royer, *Horizontal Centrifugation: A Technique of Foundry Well Adapted to the Processing of High Reliability Pieces*, J. Mater. Shaping Technol. 5 (1988) 197-209.

[2] Y. Fukui, *Fundamental Investigation of Functionally Gradient Material Manufacturing System using Centrifugal Force*, JSME International Journal (1991) Series III, Vol. 34, No. 1.

[3] W. Huisman, T. Graule and L.J. Gauckler, *Alumina of High Reliability by Centrifugal Casting*, J. Eur. Ceram. Soc. 15 (1995) 811-821.

[4] J.C. Chang, B.V. Velamakanni, F.F. Lange and D.S. Pearson, *Centrifugal Consolidation of Al_2O_3 and Al_2O_3/ZrO_2 Composite Slurries vs Interparticle Potentials: Particle Packing and Mass Segregation*, J. Am. Ceram. Soc. (1991) 74 [9] 2201-2204.

[5] P.M. Biesheuvel, V. Breedveld, A.P. Higler and H. Verweij, *Graded membrane supports produced by centrifugal casting of a slightly polydisperse suspension*, Chem. Eng. Sci. 56 (2001) 3517-3525.

[6] A. Nijmeijer, C. Huiskes, N.G.M. Sibelt, H. Kruidhof and H. Verweij, *Centrifugal casting of tubular membrane supports*, Am. Ceram. Soc. Bull. 77 (1998) 95-98.

[7] G.C. Steenkamp, H.W.J.P. Neomagus, H.M. Krieg and K. Keiser, *Centrifugal casting of ceramic membrane tubes and the coating with chitosan*, Sep. Purif. Technol. 25 (2001) 407-413.

[8] P.M. Biesheuvel and H. Verweij, *Calculation of the Composition Profile of a Functionally graded material Produced by Centrifugal Casting*, J. Am. Ceram. Soc. (2000) 83 [4] 743-749.

[9] P.V. Hendriksen, P.H. Larsen, M. Mogensen, F.W. Poulsen and K. Wiik, *Prospects and problems of dense oxygen permeable membranes*, Catal. Today 56 (2000) 283-295.

[10] J.R.Rostrup-Nielsen, *Syngas in perspective*, Catal. Today 71 (2002) 243-247.

[11] J.H. Lunsford, *Catalytic conversion of methane to more useful chemicals and fuels: a challenge for the 21st century*, Catal. Today 63 (2000) 165-174.

[12] P.N. Dyer, R.E. Richards, S.L. Russek and D.M. Taylor, *Ion transport membrane technology for oxygen separation and syngas production*, Solid State Ionics 134 (2000) 21-33.

[13] R.H.E. van Doorn, H. Kruidhof, A. Nijmeijer, L. Winnubst and A.J. Burggraaf, *Preparation of $La_{0.3}Sr_{0.7}CoO_{3-\delta}$ perovskite by thermal decomposition of metal-EDTA complexes*, J. Mater. Chem. 8(9) (1998) 2109-2112.

[14] S. Kaji and N. Sakamoto, *Flow properties of aquous perovskite-type oxide $La_{0.6}Sr_{0.4}CoO_{3-\delta}$ suspension*, Solid State Ionics 108 (1998) 235-240.

[15] N.M.L.N.P. Closset, R.H.E. van Doorn, H. Kruidhof and J. Boeijsma, *About the crystal structure of $La_{1-x}Sr_xCoO_{3-\delta}$ ($0 \leq x \geq 0.6$)*, Powder Diffr. 11 (1996) 31-34.

[16] H.J.M. Bouwmeester and L.M. van der Haar, *Oxygen permeation through mixed-conducting perovskite oxide membranes*, pp. 49-57 in: Materials for Electrochemical Energy Conversion and Storage, Ceramic Transactions, Vol. 127. Edited by A. Manthiram, P.N. Kumta, S.K. Sundaram and G. Ceder. The American Ceramic Society, Westerville, USA, 2002.

Chapter Six

Bi-layered membrane concept

6.1 Introduction

The thermodynamic stability of the perovskite phase is one of the major issues preventing these materials to be used in membrane reactors for the partial oxidation of methane into synthesis gas. It is recognized in literature [1–5] and shown in previous chapters that the materials exhibiting the highest oxygen fluxes are also the less stable in a reduced oxygen partial pressure environment. Therefore, the selection of a membrane material is restricted to a compromise between ionic conductivity and thermodynamic stability, essentially sacrificing one for the other.

One remedy to this problem is to protect a known high-flux perovskite phase by coating a second stable perovskite layer on top of it. This concept has been demonstrated in the past in the field of solid oxide fuel cells. Yahiro *et al.* [6] have successfully coated a thin film of stabilized zirconia on their electrolyte, $(CeO_2)_{0.9}(YO_{1.5})_{0.1}$, to protect it against reduction from hydrogen. Wachsman *et al.* [7] showed that SOFC's fabricated from a bilayered ceria/bismuth oxide electrolyte exhibit higher open-cicuit potentials than those fabricated with a single ceria layer, and are stable against reduction by hydrogen. More recently, this concept was applied for the fabrication of a bi-layered membrane for the conversion of methane into synthesis gas [8]. $La_{0.6}Sr_{0.4}Co_{0.8}Fe_{0.2}O_{3-\delta}$ was coated with $(Sm_2O_3)_{0.1}(CeO_2)_{0.9}$. While non-coated $La_{0.6}Sr_{0.4}Co_{0.8}Fe_{0.2}O_{3-\delta}$ degrades rapidly in the presence of methane, the bi-layered membrane turned out to be stable and exhibited an increased oxygen flux for more than 50 h.

The deposition of a thin film on top of a dense oxide material can be achieved via several techniques, among them RF-sputtering, screen-printing and pulse laser deposition (PLD). The main concern in this matter is the mismatch in thermal expansion coefficient between the two materials. In this study, two perovskite materials, $La_{0.8}Sr_{0.2}FeO_{3-\delta}$ (80-LSF) and $La_{0.7}Sr_{0.3}CoO_{3-\delta}$ (30-LSC) were chosen to prepare a bi-layered membrane. The difference in thermal expansion coefficient between these two materials is relatively small. This system was chosen as a proof-of-principle. A simple model is used to

described the transport of oxygen through the bi-layered membrane and a comparison between its performance and the performance of single-phase membranes in syngas generation experiments is presented.

6.2 Theoretical background

The benefit of a bilayered membrane is represented in fig. 6.1. If the material with thickness L_1 were to be used in the oxygen chemical potential gradient depicted by P'_{O_2} and P''_{O_2}, it would not be stable because P''_{O_2} is lower than $P_{O_2\ crit}$, where $P_{O_2\ crit}$ corresponds to the lowest oxygen partial pressure where the material with thickness L_1 is stable.

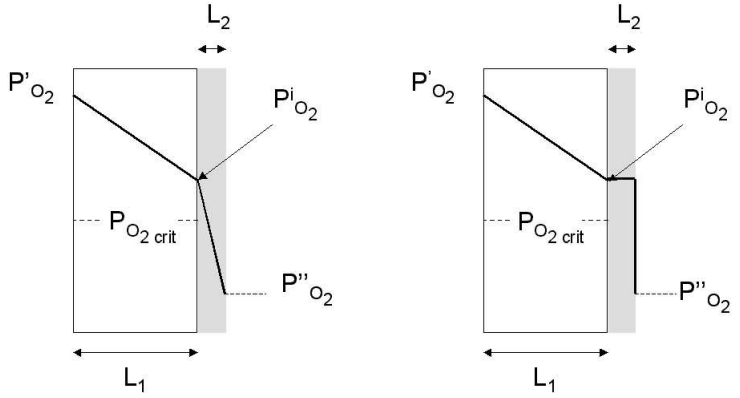

FIGURE 6.1: *Schematic representation of a bi-layered membrane in an oxygen chemical potential gradient represented by thick black lines.*

By applying a second layer of a less conductive but more stable perovskite phase, with a thickness L_2, a part of the oxygen chemical potential gradient is consumed to transport oxygen through this layer. Therefore the $P^i_{O_2}$, i.e. the virtual oxygen partial pressure at the interface, becomes higher than $P_{O_2\ crit}$. In this configuration, depicted in fig. 6.1 (left-hand), the oxygen transport is bulk-limited in the layer with thickness L_2 and the material with thickness L_1 is not exposed to an oxygen partial pressure lower than $P_{O_2\ crit}$. The balance between the two thicknesses L_1 and L_2 (to keep $P^i_{O_2}$ higher than

$P_{O_2\ crit}$) depends on the ionic conducting properties of the two perovskite phases under consideration.
On the right-hand in fig. 6.1, the surface exchange on the low-P_{O_2} side of the membrane is the rate limiting process for the transport of oxygen through the layer with thickness L_2. In this case, the rate of oxygen exchange at the surface controls the value of $P^i_{O_2}$.

6.3 Experimental

6.3.1 Material preparation

The support material $La_{0.3}Sr_{0.7}CoO_{3-\delta}$ was prepared with the previously described EDTA method [12]. The obtained ceramic samples (disc-shaped) were polished with diamant paste (3 μm). The final diameter of these supports was 15 mm with a thickness of 0.5 mm.
The material chosen for the thin film is $La_{0.8}Sr_{0.2}FeO_{3-\delta}$ and a target (PLD) from this composition was prepared with the EDTA method [12] substituting cobalt nitrate for iron nitrate. The obtained discs were polished with SiC paper (1000 mesh). The final diameter of these samples was 15 mm with a thickness of roughly 2 mm.

6.3.2 Pulsed Laser Deposition

The laser ablation experiments were carried out with a KrF laser excimer (Compex 205, Lambda Physik) with a wave length of 248 nm in a controlled oxygen environment (P_{O_2} = 0.1 mbar). The frequency was set to 10 Hz and the ablation time varied from 5 to 30 min. The beam entered the vacuum chamber at an angle of 45 ° with respect to the target normal. A mask was placed in the laser beam to reduce the spatial variation of the laser energy within the beam to less than 10 %. The energy of the laser beam behind the mask was measured as an average over multiple pulses to ensure an energy

density of 4 J.cm^{-2}. The distance from the target to the substrate was 40 mm, so that the substrates were located at the end of the visible laser plume. Three types of substrates were used:

- Commercially available yttrium stabilized zirconia (YSZ)
- Commercially available $SrTiO_{3-\delta}$ (STO)
- Home-made $La_{0.3}Sr_{0.7}CoO_{3-\delta}$ (30-LSC)

The PLD-produced thin films were characterized by X-ray diffraction (XRD). Their composition was determined by X-ray fluorescence (XRF) and X-ray photoelectron spectroscopy (XPS).

6.3.3 Oxygen permeation

Oxygen permeation experiments under air/He gradients were conducted at 900 °C with a 1.87 mm-thick membrane with composition $La_{0.8}Sr_{0.2}FeO_{3-\delta}$ following the procedure described in *Chapter 2*.
Catalytic partial oxidation experiments were conducted with a 0.5 mm-thick $La_{0.8}Sr_{0.2}FeO_{3-\delta}$ membrane and with the bi-layered membrane at 900 °C following the procedure presented in *Chapter 3*.

6.4 Results

6.4.1 Pulse laser deposiiton

YSZ substrate

$La_{0.8}Sr_{0.2}FeO_{3-\delta}$ was deposited on a c-axis oriented cubic YSZ substrate with the above mentioned parameters. YSZ was chosen instead of STO because of the similarity in crystal structure between STO and $La_{0.8}Sr_{0.2}FeO_{3-\delta}$, both having a cubic perovskite structure. The specimen was analyzed with X-ray diffraction to check the crystal structure of the deposited film. The

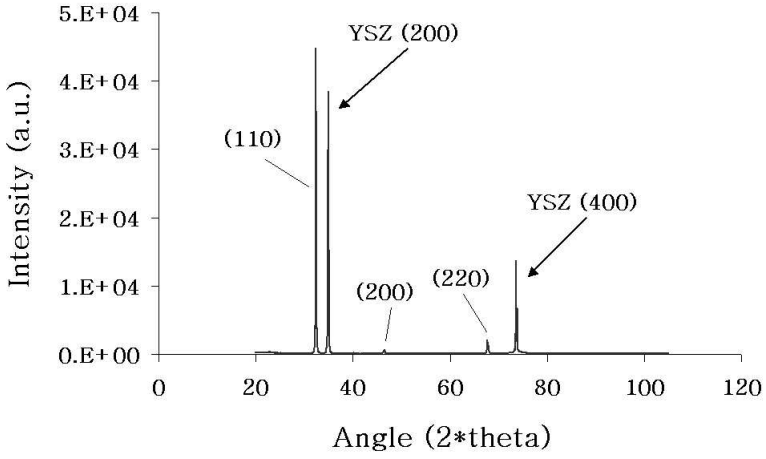

FIGURE 6.2: *Diffractogram of a thin $La_{0.8}Sr_{0.2}FeO_{3-\delta}$ film deposited on a YSZ substrate. The (hkl) values are given for each reflection.*

diffractogram is shown in fig. 6.2. The three reflections of the $La_{0.8}Sr_{0.2}FeO_{3-\delta}$ phase are characteristic of a cubic perovskite structure. It can be seen that some reflections are missing due to the preferred orientation during the growth of the film. This is probably resulting from the influence of the substrate material.

STO substrates

$La_{0.8}Sr_{0.2}FeO_{3-\delta}$ was grown on STO substrates with different deposition times to determine the growth rate of the films. The thickness together with the composition of the deposited thin films were analyzed by means of X-ray fluorescence (XRF). The results are presented in fig. 6.3. There is a good agreement between the results from the measurements on STO substrates and the one on YSZ. The composition of each deposited film is close to the expected stoichiometry of $La_{0.8}Sr_{0.2}FeO_{3-\delta}$ (calculated for $\delta = 0$). In addition, the thickness of the films varies almost linearly with the deposition time, as expected for this type of oxide materials. The estimated growth rate is 28 nm.min^{-1}.

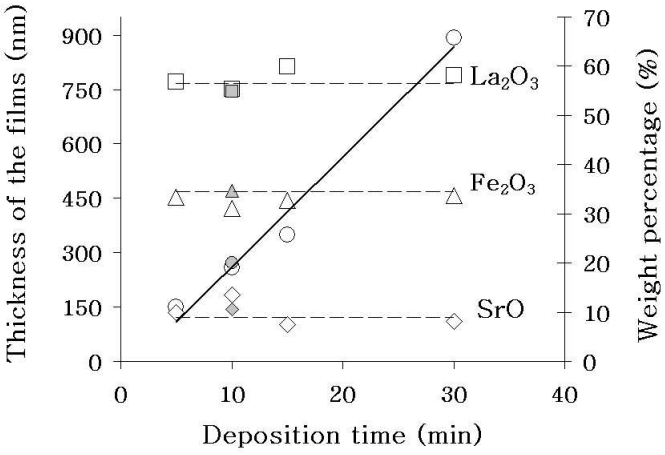

FIGURE 6.3: *Thickness (◯, left-hand axis) and composition (□ : La_2O_3, △ : Fe_2O_3, ◊ : SrO, right-hand axis) of the deposited $La_{0.8}Sr_{0.2}FeO_{3-\delta}$ films as a function of the deposition time. A linear fitting of the thickness is shown. The grey measurement points correspond to a deposition on a YSZ substrate.*

Deposition on 30−LSC

$La_{0.8}Sr_{0.2}FeO_{3-\delta}$ was deposited on to the perovskite substrate with composition $La_{0.3}Sr_{0.7}CoO_{3-\delta}$. The thickness of the films and/or their composition was measured with X-ray fluorescence and X-ray photoelectron spectroscopy. The results are shown in table 6.1 (XRF) and 6.2 (XPS).

Deposition time	La_2O_3 (wt %)	SrO (wt %)	Fe_2O_3 (wt %)	Thickness (nm)
5 min	57.8	8	34.2	173
10 min	58.5	7	34.5	275
20 min	58.8	8.2	33	507
Expected values	56.4	9	34.6	-

TABLE 6.1: *Results of the XRF analyses of the supported $La_{0.8}Sr_{0.2}FeO_{3-\delta}$ thin films. The support composition is $La_{0.3}Sr_{0.7}CoO_{3-\delta}$.*

The composition of these thin films is very close to the expected stoichiometry based on a value of δ equal to zero. The thickness values are close to the expected ones from fig. 6.3.

Deposition time	La (at. %)	Sr (at. %)	Fe (at. %)	O (at. %)	Thickness (nm)
5 min	–	–	–	–	138
10 min	25.5	4.1	26	45.4	254
Reference					
#1	26.3	4.5	22	47.13	–
#2	24.1	4.4	24.8	46.7	–

TABLE 6.2: *Results of the XPS analyzes of the supported* $La_{0.8}Sr_{0.2}FeO_{3-\delta}$ *thin films. The support composition is* $La_{0.3}Sr_{0.7}CoO_{3-\delta}$.

The composition of the film grown for 5 min was not measured with XPS, only its thickness. The film grown for 20 min was not analyzed with XPS as it is a destructive method. Two reference measurements (in table 6.2) were used for comparison with the results obtained on the film deposited for 10 min. The atomic percentage found in reference #1 and #2 are in good agreement with each other and the composition of the film matches.

6.4.2 Oxygen permeation under air/He gradients

After the deposition of a 229 nm-thick $La_{0.8}Sr_{0.2}FeO_{3-\delta}$ layer on top of a $La_{0.3}Sr_{0.7}CoO_{3-\delta}$ support, this bi-layered membrane was tested at 900 °C for the permeation of oxygen under an air/He gradient. The results are plotted in fig. 6.4. As the total flowrate increases, i.e. the flowrate of helium is increased, the oxygen partial pressure on the low-P_{O_2} side of the membrane decreases. The oxygen chemical potential gradient therefore becomes larger and the oxygen flux through the bi-layered membrane increases.

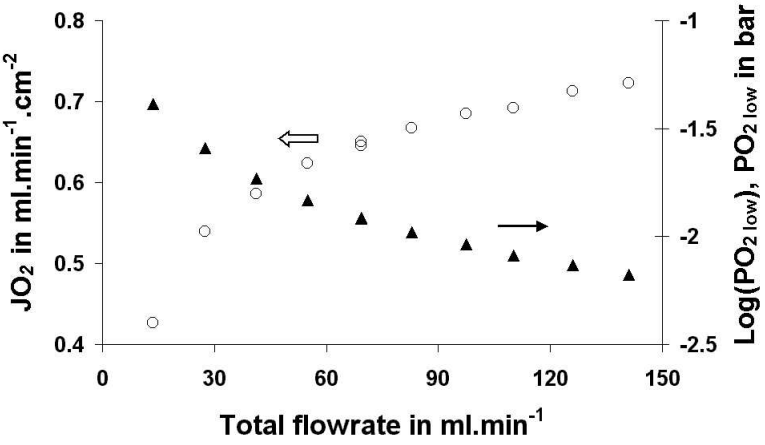

FIGURE 6.4: *Oxygen flux through a bi-layered membrane and logarithm of the $P_{O_2\,low}$ as a function of the total flowrate on the low-P_{O_2} side of the membrane.*

6.4.3 Oxygen permeation under CPO conditions

CPO with $La_{0.8}Sr_{0.2}FeO_{3-\delta}$

A 0.5 mm-thick $La_{0.8}Sr_{0.2}FeO_{3-\delta}$ membrane was tested at 900 °C for the production of syngas. The catalyst used for this experiment was prepared according to the recipe given in 3.2.2 on page 49. The results are plotted in fig. 6.5. A maximum oxygen flux of 1.7 ml.min^{-1}.cm^{-2} was obtained with a pure methane feed. The flowrate of methane was increased further but methane was then detected in the effluent gas.

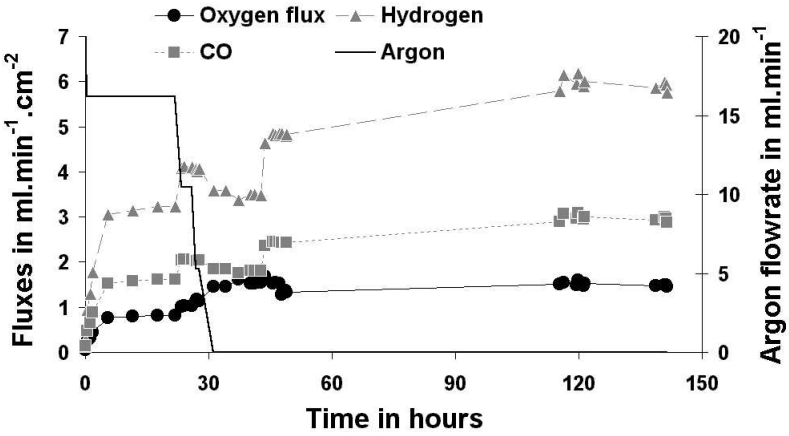

FIGURE 6.5: *Catalytic partial oxidation of methane with a 0.5 mm-thick membrane of composition $La_{0.8}Sr_{0.2}FeO_{3-\delta}$ at 900 °C.*

CPO with the bi-layered membrane

The same membrane as in 6.4.2 on page 118 was used under CPO conditions and the results are given in fig. 6.6.

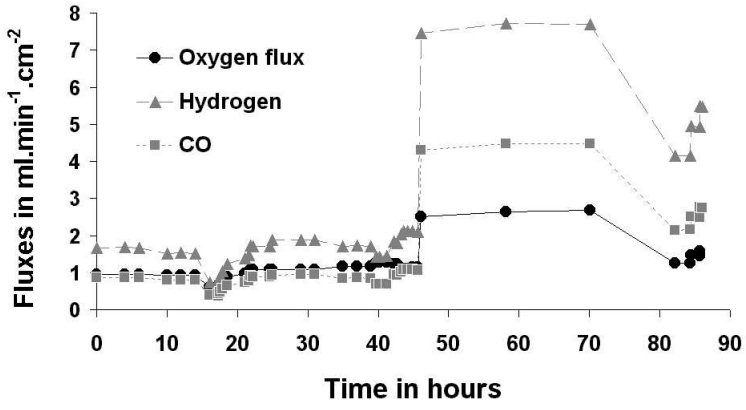

FIGURE 6.6: *Catalytic partial oxidation of methane with a bi-layered membrane ($La_{0.8}Sr_{0.2}FeO_{3-\delta}$ on top of $La_{0.3}Sr_{0.7}CoO_{3-\delta}$) at 900 °C.*

6.5 Discussion

6.5.1 Structure and growth rate of the deposited films

The results obtained with the YSZ substrate prove that the parameters of deposition are adequate to grow a thin film having the perovskite structure. This film is found to be (slightly) preferably oriented, which is assume to be a consequence of the orientation of the support itself.
The multiple depositions on STO showed that good reproducibility could be achieved for the composition of the films (cf. fig. 6.3). In addition, the thickness varies linearly with respect to the deposition time, with a growth rate estimated to be 28 nm.min^{-1}. A rough estimate of the deviation for the thickness of the films is 7 to 8 % depending on the deposition time. This value is based on the comparison of the results obtained on the film deposited in 10 min with XRF (table 6.1) and XPS (table 6.2).
The stoichiometry of the film is found to be very close to that of the target material, independently of the support material (YSZ, STO or 30-LSC). This is important for the applications envisioned because changes in the stoichiometry of the film will influence its transport properties, leading to erroneous conclusions.

6.5.2 The bi-layered membrane in air/He gradients

It is assumed that the oxygen transport through $La_{0.3}Sr_{0.7}CoO_{3-\delta}$ can be described by bulk diffusion, i.e. that the surface process on the high-P_{O_2} side of the membrane is not rate limiting. The following model was chosen to describe the ionic conductivity of this material:

$$\sigma_{ion} = \sigma^0_{ion} \cdot P^n_{O_2} \tag{6.1}$$

where P_{O_2} is the oxygen partial pressure. Based on the data collected in *Chapter 2*, the two parameters σ°_{ion} and n have a value of 30 S.m^{-1} and 0.1, respectively. For the $La_{0.8}Sr_{0.2}FeO_{3-\delta}$ material, values of 0.77 S.m^{-1} and

0.26 were chosen based on oxygen permeation measurements at 900 °C (use of eq. 2.3 on page 33). It is furthermore assumed that the interface between the two perovskite layers does not hinder the transport of oxygen.
The oxygen partial pressure at the interface of the bi-layered membrane and at the surface of the $La_{0.8}Sr_{0.2}FeO_{3-\delta}$ material was then calculated. The results obtained are presented in fig. 6.7.

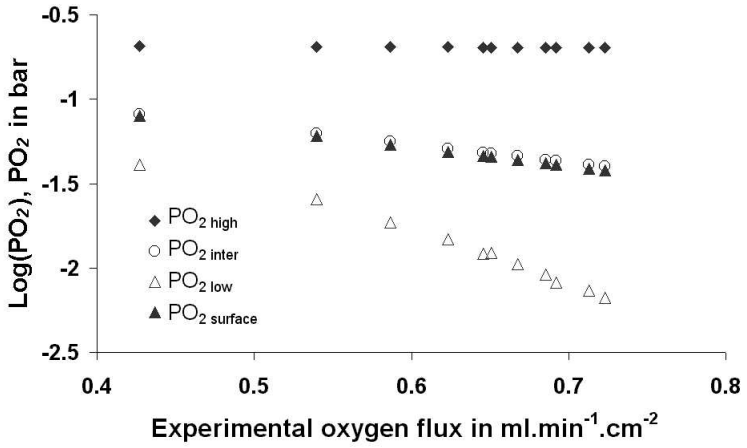

FIGURE 6.7: *Logarithm of the oxygen partial pressure on the air-side, at the interface, at the surface and on the helium-side of a bi-layered membrane at 900 °C as a function of the oxygen flux.*

As the oxygen flux through the membrane increases, i.e. the helium flowrate increases, both the $P_{O_2}^{inter}$ and the $P_{O_2}^{surface}$ are decreasing. The maximum experimental oxygen flux is 0.67 ml.min^{-1}.cm^{-2}, more than 30 times larger than for $La_{0.8}Sr_{0.2}FeO_{3-\delta}$ alone (0.02 ml.min^{-1}.cm^{-2}) and about half of the value found for $La_{0.3}Sr_{0.7}CoO_{3-\delta}$ alone (1.3 ml.min^{-1}.cm^{-2}). The values of the oxygen flux for the single-phase membranes were calculated with the values of σ_{ion}° and n given above, using the experimental values of $P_{O_2}^{high}$ and $P_{O_2}^{low}$. These results are not surprising since a part of the total driving force is consumed by the surface process on the low-P_{O_2} side of the bi-layered membrane, as can be seen in fig. 6.7. The characteristic length, as defined by Bouwmeester and Burggraaf [10], for $La_{0.9}Sr_{0.1}FeO_{3-\delta}$ and $La_{0.6}Sr_{0.4}FeO_{3-\delta}$ are estimated to be 60 μm and 500 μm, respectively, at 1000 °C [11]. The

thickness of the $La_{0.8}Sr_{0.2}FeO_{3-\delta}$ layer is less than 1 μm in all cases, therefore much smaller than the characteristic length. The bulk diffusion can be described in a similar way as for the $La_{0.3}Sr_{0.7}CoO_{3-\delta}$ layer but it is the surface oxygen exchange which is the limiting step for the transport of oxygen through this layer.

6.5.3 The bi-layered membrane under CPO conditions

The same procedure as described in 6.5.2 was used for calculating the oxygen partial pressure at the interface of the bi-layered membrane and at the surface of the $La_{0.8}Sr_{0.2}FeO_{3-\delta}$ material. The results are presented in fig. 6.8.

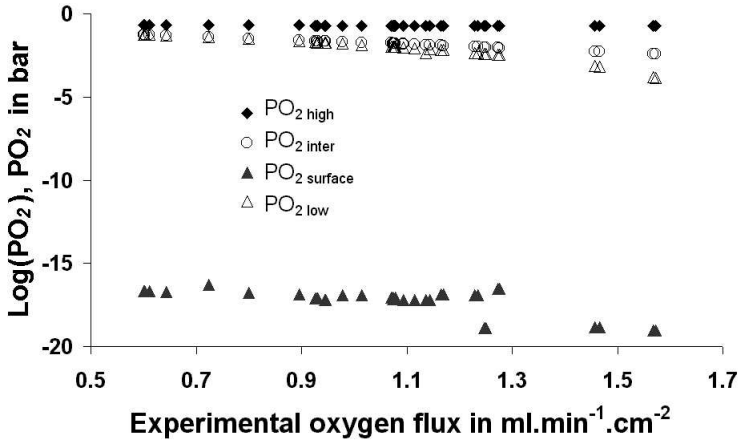

FIGURE 6.8: *Logarithm of the oxygen partial pressure on the air-side, at the interface, at the surface and on the methane-side of a bi-layered membrane at 900 °C as a function of the oxygen flux.*

The $P_{O_2}^{low}$ was estimated via a thermodynamical calculation using the different gas fluxes determined from the gas chromatograph measurements as input parameters. The trend is similar to that of fig. 6.7, both the $P_{O_2}^{inter}$ and $P_{O_2}^{surface}$ decrease with an increasing oxygen flux. A large part of the total driving force is indeed consumed through the surface exchange on the methane-side of the membrane. It can be seen that the oxygen partial pressure at the interface is always higher than $\sim 2.10^{-4}$ bar. This value is higher

than the critical P_{O_2} where the $La_{0.3}Sr_{0.7}CoO_{3-\delta}$ material starts to decompose. The bi-layered membrane is therefore stable in the reducing environment associated with the production of syngas. This also proves that the layer with the composition $La_{0.8}Sr_{0.2}FeO_{3-\delta}$ was indeed prepared dense and crack-free. It should be noted here that the material with composition $La_{0.3}Sr_{0.7}CoO_{3-\delta}$ degrades rapidly under a reducing atmosphere and membrane failure occurs.

The purpose of the thin $La_{0.8}Sr_{0.2}FeO_{3-\delta}$ layer is to protect the less stable $La_{0.3}Sr_{0.7}CoO_{3-\delta}$ material from the reducing gas. It should then consume a high enough part of the total driving force applied across the membrane to ensure that the $P_{O_2}^{inter}$ stays in a so-called friendly P_{O_2}-range for the $La_{0.3}Sr_{0.7}CoO_{3-\delta}$ material. This requirement is here fulfilled thanks to the relatively poor surface exchange properties of the $La_{0.8}Sr_{0.2}FeO_{3-\delta}$ phase.

An oxygen flux of about 1.5 ml.min^{-1}.cm^{-2} is obtained for the bi-layered membrane under CPO conditions. This is only a fraction less than that of the single-phase $La_{0.8}Sr_{0.2}FeO_{3-\delta}$ membrane. This illustrates that by fine-tuning the composition and the thickness of the thin layer (and that of the support material), it is possible to get high oxygen fluxes.

The logarithm of the oxygen flux through the bi-layered membrane as a function of the logarithm of the oxygen chemical potential difference across the $La_{0.8}Sr_{0.2}FeO_{3-\delta}$ surface is plotted in fig. 6.9. Although small errors are to be expected from the thermodynamic calculations determining the $P_{O_2}^{low}$ because of the lack of accuracy at such small oxygen partial pressures, the results of fig. 6.9 suggest a different mechanism for the surface exchange reaction in the case of an helium sweep compared with the case where methane is present (CPO conditions). It is indeed mentioned by Jiang *et al.* [13] and by Peterson *et al.* [2] that methane might react directly with lattice oxygen at the surface of the membrane.

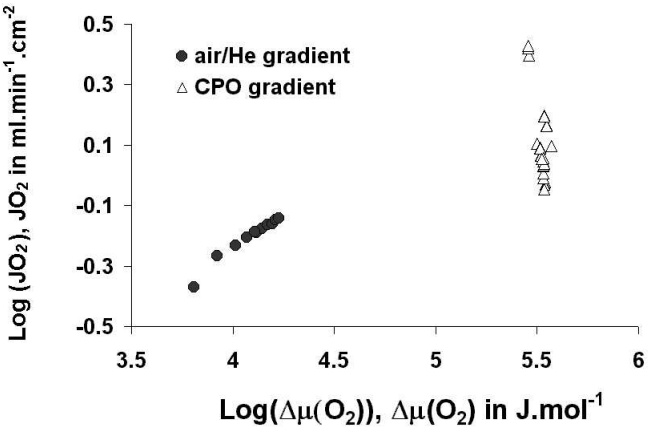

FIGURE 6.9: *Logarithm of the oxygen flux at 900 °C through a bi-layered membrane as a function of the logarithm of the oxygen chemical potential difference across the surface of the* $La_{0.8}Sr_{0.2}FeO_{3-\delta}$ *material.*

6.6 Conclusions

The deposition of a thin film of $La_{0.8}Sr_{0.2}FeO_{3-\delta}$ on top of a $La_{0.3}Sr_{0.7}CoO_{3-\delta}$ substrate with pulse laser deposition was successful. Under air/He gradients, the oxygen flux obtained at 900 °C with this bi-layered membrane is half of that obtained with the $La_{0.3}Sr_{0.7}CoO_{3-\delta}$ material with the same thickness. In CPO conditions, the oxygen flux obtained at 900 °C with the bi-layered membrane is a fraction smaller than that of the $La_{0.8}Sr_{0.2}FeO_{3-\delta}$ material with the same thickness.

It is demonstrated that a thin layer of phase I on top of a MIEC of phase II can act as a protection against reduction only if the transport properties of the material with phase I are poor, i.e. either a low ionic conductivity or poor surface kinetics. The results of this study show that with the chosen system of $La_{0.8}Sr_{0.2}FeO_{3-\delta}$ on top of $La_{0.8}Sr_{0.2}FeO_{3-\delta}$, the situation of fig. 6.1 (right-hand) occurs.

Bibliography

[1] A. Petric, P. Huang and F. Tietz, *Evaluation of La-Sr-Co-Fe-O perovskites for solid oxide fuel cells and gas separation membranes*, Solid State Ionics 135 (2000) 719-725.

[2] P.V. Hendriksen, P.H. Larsen, M. Mogensen, F.W. Poulsen and K. Wiik, *Prospects and Problems of dense oxygen permeable membranes*, Catal. Today 56 (2000) 283-295.

[3] H.J.M. Bouwmeester, *Dense ceramic membranes for methane conversion*, Catal. Today 82 (2003) 141-150.

[4] H. Ullmann, U. Guth, V.V. Vashook, M. Bulow, W. Burckhardt and R. Gotz, *Ceramic oxides with high oxygen transport*, Recent Res. Devel. Solid State Ionics, 2 (2004): ISBN: 81-7895-145-2.

[5] S. Pei, M.S. Kleefisch, T.P. Kobylinski, J. Faber, C.A. Udovich, V. Zhang-McCoy, B Dabrowski, U. Balachandran, R.L. Mieville and R.B. Poeppel, *Failure mechanisms of ceramic membrane reactors in partial oxidation of methane to synthesis gas*, Catal. Lett. 30 (1995) 201.

[6] H. Yahiro, Y. Baba, K. Eguchi and H. Arai, *High Temperature Fuel Cell with Ceria-Yttria Solid Electrolyte*, J. Electrochem. Soc. 135 (1988) 2077.

[7] E.D. Wachsman, P. Jayaweera, N. Jiang, D.M. Lowe and B.G. Pound, *Stable High Conductivity Ceria/Bismuth Oxide Bilayered Electrolytes*, J. Electrochem. Soc. 144 (1997) 233.

[8] E.D. Wachsman and T.L. Clites, *Stable Mixed-Conducting Membranes for Direct Conversion of Methane to Syngas*, J. Electrochem. Soc. 149 (2002) A242-A246.

[9] V.V. Kharton, E.N. Naumovich and A.V. Nikolaev, *A method to investigate oxide ionic transport for materials with high electronic conductivity*, Solid State Ionics 83 (1996) 301-307.

[10] H.J.M. Bouwmeester and A.J. Burggraaf, *Dense ceramic membranes for oxygen separation*, in: CRC Handbook of Solid State Electrochemistry, Eds. P.J. Gellings and H.J.M. Bouwmeester, CRC Press, Boca Raton (1997) ISBN 0-8493-8956-9.

[11] T. Ishigaki, S. Yamauchi, K. Kishio, J. Mizusaki and J. Fueki, *Diffusion of oxide ion vacancies in perovskite-type oxides*, J. Solid State Chem. 73 (1988) 179-187.

[12] R.H.E. van Doorn, H. Kruidhof, A. Nijmeijer, L. Winnubst and A.J. Burggraaf, *Preparation of $La_{0.3}Sr_{0.7}CoO_{3-\delta}$ perovskite by thermal decomposition of metal-EDTA complexes*, J. Mater. Chem. 8(9) (1998) 2109-2112.

[13] R. Jin, Y. Chen, W. Li, W. Cui, Y. Ji, C. Yu and Y. Jiang, *Mechanism for the catalytic partial oxidation of methane to syngas over a Ni/Al_2O_3 catalyst*, App. Cat. A-Gen. 201 (2000) 71-80.

[14] A.F. Sammells, M. Schwartz, R.A. Mackay, T.F. Barton and D.R. Peterson, *Catalytic membrane reactors for spontaneous synthesis gas production*, Catal. Today 56 (2000) 325-328.

Chapter Seven

Recommendations and outlook

This thesis focuses on the performance of membranes with the perovskite structure for oxygen separation. In *Chapter 2*, their behavior under mild gradients (air/He) is of interest. The oxygen flux through this type of materials is proportional to the number of oxygen vacancies. Creating more oxygen vacancies, for instance by increasing the dopant concentration on the A-site of the perovskite structure, is therefore a suitable strategy to improve the performance of the membrane in terms of magnitude of the oxygen flux. The mobility of these oxygen vacancies is also of importance, since ordering or trapping can occur. The technique used in *Chapter 2* to determine the ionic conductivity of a series of material with the composition $La_{1-x}Sr_xCoO_{3-\delta}$ (x = 0.1, 0.2, 0.5 or 0.7) is based on oxygen permeation measurements. It is a rather straightforward technique, which enables the measurement of an intrinsic transport parameter not easily accessible by means of other techniques such as impedance spectroscopy analysis with electron blocking electrodes. The discrepancy found between the expected behavior and the experimental values at high level of doping were explained by the presence of a stagnant layer on the permeate side of the membrane. The Achilles heel of this interpretation is the difficulty to find a suitable model for the oxygen flux, which model integrates both bulk diffusion and transport through the stagnant layer. Further research should focus on separating both contributions to study the possibility of preventing/suppressing ordering effects by co-doping on the B-site of the perovskite structure. Similar reasoning could be applied to other type of materials with the perovskite structure, for instance the ones used under larger oxygen chemical potential gradients as in catalytic membrane reactors.

Chapter 3 and *4* deal with the use of membranes with the perovskite structure in a catalytic membrane reactor for the partial oxidation of methane to synthesis gas. A large number of materials were tested and the results show a number of trends. The influence of barium (A-site) and chromium (B-site) has been clearly established: both dopants are detrimental to the oxygen flux and beneficial to the stability of these materials under the operating

conditions associated with the production of syngas. The best candidate, $La_{0.7}Sr_{0.3}Fe_{0.7}Ga_{0.3}O_{3-\delta}$, exhibits an oxygen flux of 5.1 ml.min^{-1}.cm^{-2} at 900 °C for a membrane thickness of 0.5 mm. Materials exhibiting higher oxygen flux, such as $Ba_{0.5}Sr_{0.5}Co_{0.8}Fe_{0.2}O_{3-\delta}$, are unstable in a reducing environment. Gallium-based materials seem to be a promising direction for further research although cost considerations may prevent them to be widely used. Parameters such as the influence of the Fe/Ga ratio and the type of dopant used on the A- and B-site should be investigated. Long-term measurements could help understand the reason for the strontium segregation revealed in *Chapter 4*.

For industrial applications, a tubular geometry is favored because of the ease of sealing tubes into small volume modules (high surface area). The possibility of producing dense tubular membranes with centrifugal casting has been investigated in *Chapter 5* with the composition $La_{0.5}Sr_{0.5}CoO_{3-\delta}$. The tubes obtained are of very high quality with a smooth inner surface and perfect roundness. The developed procedure requires a few adjustments when other perovskite compositions are used, for instance the rotation speed and time or the ratio powder:stabilizer, but it is possible to produce dense tubular membrane of good quality with centrifugal casting. Further study is needed to take full advantage of the properties of centrifugal casting such as the possibility of producing a membrane with a graded composition (ref. to *Chapter 6*) or a graded porosity (with an inner thin dense layer). The particle size, the particle size distribution and the sintering conditions are example of the key parameters to obtain such systems.

In *Chapter 6*, the concept of a dense bi-layered membrane is presented. A few attempts have been reported in preparing a thin dense film supported on a porous material but a few difficulties render this approach rather laborious. The expansion coefficient of the support and the thin film should match to avoid stress and consequently membrane failure. A solution is to prepare the support of the same material as the thin film but there are only a few reported attempts at preparing a porous support material with the

perovskite composition since it proved to be a difficult task. The solution proposed in *Chapter 6* is to use two dense layers of different (but compatible) perovskite structures. The proof-of-principle system, $La_{0.8}Sr_{0.2}FeO_{3-\delta}$ on $La_{0.3}Sr_{0.7}CoO_{3-\delta}$, gives promising results in CPO experiments. Higher oxygen fluxes could be achieved with fine-tuning both the thickness and the composition of the two layers. Nevertheless, this type of system will be limited by the need of (thermal and chemical) expansion compatibility. The behavior at the interface is so far unknown but at the envisioned temperatures of operation, inter-diffusion will certainly occur and it will affect the overall performance of a bi-layered membrane.

The End